

STUDIES ON FLUXON DYNAMICS IN COUPLED JOSEPHSON JUNCTIONS

**Thesis submitted
in partial fulfilment of the requirements
for the award of the DEGREE of**

DOCTOR OF PHILOSOPHY

P. D. SHAJU

**DEPARTMENT OF PHYSICS
COCHIN UNIVERSITY OF SCIENCE AND TECHNOLOGY
KOCHI-22, KERALA
INDIA**

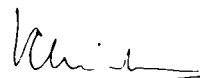
2002

CERTIFICATE

Certified that the thesis entitled **Studies on fluxon dynamics in coupled Josephson junctions** is a bonafied record of the research carried out by Mr. P. D. Shaju, under my supervision in the Department of Physics, Cochin University of Science and Technology, Kochi, in partial fulfilment of the requirements for the award of the Degree of Doctor of Philosophy and no part of it has been included in any other thesis submitted previously for the award of any degree of any other university.

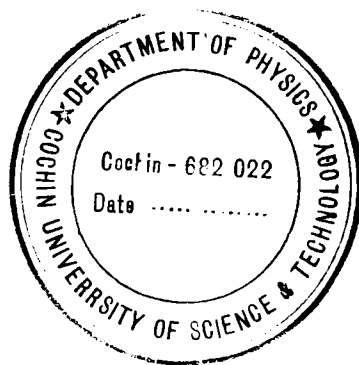
Cochin

1 November 2002



Prof. V. C. Kuriakose

(Supervising Guide)



PREFACE

The work presented in this thesis has been carried out by the author at the Department of Physics, Cochin University of Science and Technology during the period 1995 to 2002.

Fluxon dynamics in coupled Josephson junctions have recently become the subject of intensive theoretical and experimental investigations. Coupled junctions attract much attention because they are promising objects for application in cryoelectronics and they exhibit a variety of interesting physical phenomena. Systems of many closely coupled long Josephson junctions (LJJ) are being considered for many applications of superconducting electronics. They are widely used in the voltage standard applications, in microwave generators and in Josephson computing elements. The discovery of intrinsic Josephson effects in some high-temperature superconductors such as $Bi_2Sr_2CaCu_2O_x$ convincingly showed that these materials are essentially natural superlattice of Josephson junction formed on the atomic scale. The layered high- T_c superconductors can be described as intrinsic stacks of Josephson junctions. Therefore study of fluxon dynamics in artificial stacks can help to understand the phenomena that take place in high- T_c superconductors. Another importance of the study of coupled junctions is in the fact that, it is often possible to multiply a physical effect achieved in one junction by the number of junctions in a stack. This can be exploited for fabrication of many solid-state devices. In addition, multilayered solid-state systems show some peculiar phenomena which result from the interaction between individual layers.

Long Josephson junctions possess an extremely rich spectrum of linear and nonlinear electromagnetic excitations. Josephson junctions are unique nonlinear systems which offer the possibility of studying quantized magnetic flux (fluxon) moving along the dielectric barrier. The stable and undistorted propagation of fluxons in the junction manifests the interplay between dissipation and nonlinearity in the superconducting tunnel junction.

The thesis deals with a detailed theoretical analysis of fluxon dynamics in single and in coupled Josephson junctions of different geometries under various internal and external conditions. Two new geometries *viz.* semiannular and quarter annular geometries are proposed and fluxon dynamics in these junctions are also studied and they find important applications in making some new superconducting devices.

Fluxon dynamics in Josephson junctions has been an active subject ever since the epoch-making discovery of Josephson effects in superconductor-insulator-superconductor junctions by Josephson in 1962. Intensive research in this field contributed various types of superconducting quantum devices and paved way to a new branch of science known as superconducting quantum electronics. The surprising discoveries of superconductivity at temperatures above 100K in some layered cuprate based ceramics and the parallel advancements in low temperature engineering and lithography have instigated extensive research to make Josephson devices a practical reality. Rapid developments in this field are viewed with greater curiosity as these small sized, ultrafast, high performance devices have the potential to replace the existing semiconductor devices.

Josephson junctions are endowed with remarkable properties such as Cooper-pair tunneling, *dc* and *ac* Josephson effects, flux quantization, superconducting quantum interferences etc., which are the basic principles behind the widely used high sensitive devices like the SQUID magnetometers, superconductor-insulator-superconductor mixers, constant voltage standards and the hot-electron bolometer etc. The realization that the unattainable goals of the semiconductor digital devices can be met with the superconducting components make Josephson junction devices a competitive contender in fabricating high performance digital devices. The recent innovative developments in Rapid Single Flux Quantum (RSFQ) circuits are expected to give a new dimension to the current digital device technology. Low capacitance Josephson junctions offer a promising way to

realize quantum bits (both voltage based and flux based qubits have been proposed) for quantum information processing, which is expected to give solutions to the present day computational crisis.

Fluxon dynamics in the junction is described by the well-known one-dimensional sG nonlinear partial differential equation. A sG equation possesses a series of remarkable features including solitary wave solutions with particle-like properties. A soliton is a localized wave which has the fantastic ability to propagate undistorted over long distances and to remain unaffected after collision with each other. Quantized flux propagation in long Josephson junction is associated with a voltage pulse, which can be detected across the junction. In this solid state system, a dc bias current applied to the junction exerts a Lorentz force on the fluxons and drives them through the junction. The velocity of a fluxon is proportional to the voltage and average velocity determines the current-voltage characteristics of the junction. Fluxon dynamics in LJJs is employed as a mechanism in the construction of flux-flow oscillators, logic gates, voltage rectifiers etc.

To overcome the limitations of single junctions, vertically stacked junctions are used. Apart from the basic knowledge of the physical phenomena-taking place in different layers of the junctions, coupled junctions offer various configurations of the fluxons suitable for specific applications. Intensive research is done in stacked Josephson junctions to find applications of these junctions in superconducting electronic devices. All these developments demand further investigations to explore all possible mechanisms and to exploit them for implementing commercially viable high performance devices. Innovative mathematical models are required to take into account all physical properties and geometrical configurations of the junctions.

The thesis deals with a detailed theoretical analysis of fluxon dynamics in single and in coupled Josephson junctions of different geometries under various internal and external conditions. The main objectives of the present work are to

investigate the properties of narrow LJJ's and to discuss the intriguing physics. The main results are subdivided into the following chapters.

In Chapter I, a general introduction underlying the basic properties of Josephson junction are presented giving emphasis to nonlinear properties of the junction. Derivations of the basic equations of fluxon dynamics in single and coupled junctions are also presented. Basic theoretical and technical aspects of studying fluxon dynamics in various geometries are reviewed.

Fluxon dynamics in the presence of various types of perturbing agents have been an interesting topic and are studied to make some practical applications out of it. When fluxons are accelerated through a spatially periodic potential various internal fluxon configurations arises resulting in fluxon creation or annihilation process. In Chapter II, a detailed study is undertaken to understand the fluxon creation and annihilation phenomena. Under some special conditions, fluxons of the same polarity can bunch together in spite of the repulsive interaction between them. Fluxon bunching can greatly increase the stability of fluxon propagation in the junction and is highly useful in high voltage applications. Extensive numerical analysis is done to determine the parameter regimes of the bunching process. Basic ideas of numerical simulation procedure is presented. These studies have important practical applications in the construction of logic gates and in implementing certain digital devices.

Fluxon dynamics becomes complicated when junctions of different physical properties are vertically stacked. Motion of fluxons in one junction influences the motion of fluxons in the other junctions. In Chapter III, vertically stacked, inductively coupled junctions are studied to construct fluxon based logic gates. Josephson junctions of different geometries with various internal conditions are studied in the past to make small sized, less dissipative ultrafast logic gates. Extensive numerical simulations are carried out on two and three inductively coupled, vertically stacked Josephson junctions for realizing ultrafast digital switches

and logic gates. Using fluxons as information bits, the interactive dynamics is pursued and identified the possible configurations of structural and dissipative parameters in implementing the elementary logic gates AND, OR and XOR.

Long Josephson junctions of various geometries with different boundary conditions are investigated in the past to realize specialized applications from them. In particular long linear overlap junctions and annular junctions are studied in detail. In linear junctions fluxons make successive reflections at the edges and give periodic pulse forms at the edges of the junction. Annular junctions make reflectionless motion of fluxons in the junction. In Chapter IV, a new geometry - a semiannular geometry - is proposed for making fluxon based diodes. Analytical and numerical studies on semiannular junction show that an external static magnetic field applied parallel to the dielectric barrier interacts through the interior of the junction and produces a tilted potential which pushes out trapped fluxons from the interior of the junction and flux-free state exists in the junction in the absence of an external bias current. Due to the semiannular shape, the effective field at the ends of the junction has opposite polarities which supports penetration of opposite polarity fluxons into the junction in the presence of a forward biased dc current. When the direction of the dc current is reversed, flux penetration is not possible and flux-free state exists in the junction. Thus, this geometry can be used in implementing a fluxon based diode. The rectification properties of the junction are demonstrated using square waves, triangular waves, and sinusoidal ac signals. In the forward biased state, fluxons and anti-fluxons enter the junction and move in opposite directions. Using this property, a novel bidirectional flux-flow oscillator with a distinct operational mechanism is demonstrated. When an rf magnetic field is applied, flux linked with the ends of the junction reverse polarity in alternate half cycles. Under a constant dc bias, flux penetration is possible only in alternate half cycles. Using this property, rectification of rf magnetic fields is demonstrated.

A new geometry with a better performance is proposed for Josephson junctions to construct fluxon based diodes in Chapter V. It is found that a quarter annular Josephson junction terminated with a load resistor at one end behaves as a diode under a homogeneous static magnetic field applied parallel to the dielectric barrier. The external field creates asymmetric boundary conditions and because of that fluxon penetration is possible only from one end of the junction under a properly biased dc current. If the direction of the current is reversed, fluxon penetration and propagation is not possible and flux-free state exists in the junction. This unique phenomenon is specific to this geometry and is extremely useful in making quantum diodes for rectification of ac signals. An rf magnetic field applied to the junction has opposite polarities at one end in alternate half cycles. Under a constant dc bias, flux penetration is possible only in alternate half cycles. Using this property rectification of rf magnetic fields are demonstrated in junctions of different geometrical and dissipative parameters.

In Chapter VI, quarter annular geometry for making a Josephson flux-flow oscillator is studied and theoretically demonstrated that quarter annular geometry provides several advantages for making Josephson flux-flow oscillator over rectangular geometry. An external static magnetic field applied parallel to the dielectric barrier of a quarter annular junction has asymmetric boundary conditions that make a preferential direction for flux-flow even in the absence of a dc bias. When the applied field is increased above a threshold level, static field distribution becomes unstable and gives rise to a train of fluxons moving unidirectionally from one end to the other end of the junction. The speed and density of the flux-flow can be controlled by controlling the field or using a small dc bias transverse to the junction. The output power of the oscillator is found to be directly proportional to the applied field. Low power consumption, increased output power, higher tunability and decreased line-width are some of the advantages of the proposed oscillator. This proposed device would be useful in millimeter and sub-millimeter

wave experiments. To get increased output power, two vertically stacked inductively coupled junctions are studied. Analysis shows that in-phase flux-flow mode in coupled junctions increases the output power and stability of the oscillator.

Flux quantization and superconducting quantum interference have been employed to make ultra-sensitive magnetic field sensors. SQUID magnetometers are capable of detecting even the feeble magnetic fields of the biological cells. Various superconducting materials with different geometrical configurations are proposed to detect magnetic fields of different intensity levels. In Chapter VII, using the quarter annular geometry, a new fluxon based sensor is proposed for an extremely sensitive measurement of the magnetic field, which is higher than the first critical field of the Josephson junction. An exponentially tapered dielectric barrier is introduced in the junction to facilitate unidirectional flow of fluxons. The tapering provides a geometrical force for the fluxons. It is found that above a threshold value of the applied field, static flux distribution in the junction becomes unstable and gives rise to a train of fluxons moving in the junction. The asymmetric boundary conditions associated with an external field make penetration of fluxons from one end of the junction even in the absence of a *dc* bias. The proposed sensor is found to be effective in detecting static magnetic fields and time varying *rf* fields.

Conclusions and results presented in the thesis are summarized in Chapter VIII.

A part of these investigations has appeared in the form of the following published/submitted papers

1. Soliton creation and annihilation in Josephson junctions in the presence of periodic perturbations, *Mod. Phys. Lett. B* **12**, 1217 (1998)
2. Logic gates using stacked Josephson junctions
Physica C **322**, 163 (1999)
3. Logic gates using three coupled Josephson junctions

- Phys. Lett. A* **267**, 420 (2000)
4. Semicircular Josephson junction embedded in a magnetic field
Phys. Rev. B, **65**, 214508 (2002)
 5. Magnetic field driven fluxons in semicircular Josephson junctions
Physica Scripta, **65**, 545 (2002)
 6. Fluxon diode using semicircular Josephson junction
Phys. Lett. A. **299**, 628 (2002)
 7. Magnetic field rectifiers using semicircular Josephson junctions
Pri'sma Zh. Eksp. Teor. Phsik, **76**, 14 (2002) (*JETP Sov. Phys.*)
 8. Josephson junction diode
Supercond. Sci. Technol. (*in press*)
 9. Rectification of harmonically oscillating magnetic fields using quarter circular Josephson junctions, *Physica C* (*in press*)
 10. Quarter circular Josephson flux-flow oscillator
JETP (*submitted*)
 11. A fluxon based magnetic field sensor using exponentially tapered quarter circular Josephson junction, *Supercond. Sci. Technol.* (*submitted*)

Contents

Preface	i
1 Fundamentals of Josephson junctions	1
1.1 The Josephson junction	2
1.2 The Josephson effect	3
1.3 Shapiro steps	4
1.4 Magnetic field effects	4
1.5 Static phase distribution in a small junction	5
1.6 Dynamics of a small junction	6
1.7 The long Josephson junction(LJJ)	7
1.8 The sine-Gordon equation	7
1.8.1 Boundary conditions	10
1.9 Lagrangian and Hamiltonian functions	10
1.10 Excitations of the sine-Gordon system	12
1.10.1 Soliton solutions	12
1.10.2 Fluxons and Antifluxons	13
1.10.3 Breather solution	14
1.10.4 Plasmons	14
1.11 Perturbative analysis	14
1.12 Coupled Josephson junctions	16
1.12.1 Two coupled junctions	20
1.13 Regimes of fluxon dynamics	20
1.13.1 Zero Field Steps (ZFS)	20
1.13.2 Fiske Steps (FS)	21
1.13.3 Flux-Flow Steps (FFS)	21
1.14 Annular junctions	21
1.15 Conclusions	22
2 Fluxon creation and annihilation in Josephson junctions	29
2.1 Introduction	29
2.2 Model equations	30
2.2.1 Bunching effects	31
2.3 Numerical methods	33

2.4	Demonstration of fluxon creation and annihilation	35
2.4.1	First ZFS	35
2.4.2	Second ZFS	36
2.4.3	Third ZFS	36
2.5	Conclusions	36
3	Logic gates using coupled Josephson junctions	39
3.1	Introduction	39
3.2	Logic gates using three coupled Josephson junctions	41
3.2.1	Theoretical model	41
3.2.2	Design aspects	43
3.2.3	OR gate	44
3.2.4	XOR gate	45
3.2.5	AND gate	46
3.3	Logic gates using two coupled Josephson junctions	47
3.3.1	AND gate	48
3.3.2	OR gate	48
3.3.3	XOR gate	48
3.4	Conclusions	49
4	Semiannular Josephson junctions	53
4.1	Introduction	54
4.2	Derivation of the model equations	55
4.2.1	Lagrangian and Hamiltonian functions	59
4.3	General properties of the junction	61
4.3.1	Properties of the junction under a <i>dc</i> bias	61
4.3.2	Properties of the junction under a static field	62
4.4	Demonstration as a fluxon diode	63
4.4.1	Rectification of a square wave	64
4.4.2	Rectification of a sine wave	65
4.5	Flux-flow state - demonstration as a bidirectional flux-flow oscillator	65
4.6	<i>rf</i> field rectification	68
4.6.1	Introduction	68
4.6.2	Theoretical model	69
4.6.3	IVC in <i>rf</i> fields	72
4.6.4	Rectification of alternating fields	72
4.7	Conclusions	73
5	Quarter annular Josephson junctions	81
5.1	Theoretical model	81
5.2	General Properties of the junction	83
5.2.1	<i>dc</i> current voltage characteristics	83
5.2.2	Critical current versus magnetic field	84

5.3	<i>ac</i> bias - demonstration as a diode	85
5.3.1	Rectification of a sine wave	85
5.3.2	Rectification of a square wave	86
5.4	Rectification of <i>rf</i> fields	86
5.4.1	Theoretical model	86
5.4.2	Current voltage characteristics	89
5.5	Rectification of alternating fields	89
5.6	Conclusions	90
6	Quarter annular Josephson flux-flow oscillator	95
6.1	Introduction	96
6.2	Theoretical aspects	97
6.2.1	Static and dynamic solutions	97
6.2.2	Fluxon-fluxon repulsive force	98
6.2.3	Laminar flux-flow - Energetic analysis	99
6.3	General properties of the junction	100
6.3.1	<i>dc</i> IVC of the oscillator	100
6.3.2	Magnetic field - voltage characteristics	101
6.4	Flux-flow characteristics	102
6.4.1	Spatial and temporal behavior	102
6.4.2	Output power	103
6.5	Two coupled flux-flow oscillator	104
6.5.1	Theoretical model	105
6.5.2	Numerical results	106
6.6	Conclusions	106
7	Magnetic field sensors using exponentially tapered quarter annular Josephson junctions	111
7.1	Introduction	111
7.2	Theoretical model	112
7.3	Static field detection properties	115
7.4	<i>rf</i> field detection	116
7.5	Conclusions	117
8	Results and conclusions	120
I	Appendix	123
	Bibliography	128

Chapter 1

Fundamentals of Josephson junctions

Josephson junction based devices making use of many closely coupled junctions are being considered for making reliable high- T_c superconducting electronic devices. Coupled Josephson junctions are used in the fabrication of Josephson voltage standards, in the microwave generators based on the coherent action of many junctions, and in Josephson computer elements. Large networks of Josephson junctions also received much attention as model systems for phase transition studies. The layered high- T_c superconducting materials show properties of many layered closely coupled vertically stacked junctions. Therefore studies of the dynamical properties of coupled Josephson junctions can help to understand the properties of the layered superconducting materials.

In this chapter the Josephson effect is introduced and the dynamics of the charges and the electromagnetic fields in short and long Josephson junctions are related to the phase difference between the order parameter describing the Cooper pairs in each superconducting electrodes. The fundamental nonlinear properties of Josephson junctions are briefly reviewed giving emphasis to the basic equations governing fluxon dynamics in single long junctions and in coupled junctions. The basic equations governing fluxon dynamics in two-coupled junctions are derived. Various types of electromagnetic excitations in Josephson junctions are reviewed

and various regimes of fluxon dynamics is presented.

1.1 The Josephson junction

Josephson junctions are systems in which two superconductors are weakly coupled to one another as shown in Fig.1.1 [1, 2]. In each of the two superconductors the conduction electrons are interacting with phonons of the crystal lattice. At low temperatures this effect gives rise to an effective interaction between the electrons which then forms pairs of opposite spin and angular momentum. Such pairs are called Cooper pairs and are the carriers of the charge in the superconductor. Due to the anti-parallel spin and the angular momenta of the electrons in each pair, the total angular momentum vanishes and the Cooper pairs have Boson character. At zero temperature, all Cooper pairs are Bose-condensed into the electronic ground state of the superconductor. All excited quasiparticles states are separated by an energy gap Δ , which is proportional to the effective binding energy of the Cooper pair, from the superconducting ground state. The superconducting state can be described by an effective macroscopic wave function with an amplitude proportional to the density of Cooper pairs ρ_i and a phase θ_i

$$\Psi_i = \sqrt{\rho_i} \exp(i\theta_i) \quad (1.1)$$

where Ψ is the superconducting order parameter.

The two superconductors are weakly coupled with one another due to small overlap of the macroscopic wave functions. The overlapping of the wave functions is shown in Fig.1.1b. Different types of weak links are discussed in literature[3, 4, 5, 6, 7]. Coupling of two superconductors via a thin insulating barrier is a common type junction and such a system is called a superconductor-insulator-superconductor (SIS) tunnel junction.

The typical tunneling current-voltage characteristics of an SIS Josephson tunnel junction is depicted in Fig.1.2a. Four different tunneling regimes as shown in

Fig.1.2a-e can be observed in this characteristics. At zero voltage, Cooper pairs tunnel through the barrier ($S \rightarrow S$), giving rise to a non-dissipative current. At voltages $0 < V < 2\Delta/e$, quasiparticles tunnel through the barrier giving rise to the quasiparticle subgap current ($Q \rightarrow Q$). The voltage $V_g = 2\Delta/e$ is called the gap voltage. At voltages $V \geq 2\Delta/e$, Cooper pairs are broken up and quasiparticles tunnel ($S \rightarrow Q$) through the barrier. All the three processes follow the linear branch of normal electron tunneling ($n \rightarrow n$) at voltages $V > V_g$.

1.2 † The Josephson effect

The tunneling of Cooper pairs through the insulating barrier of an SIS type junction was predicted by Josephson in 1962[1] and experimentally observed for the first time by Anderson and Rowell in 1963[7]. Solving the quantum mechanical problem of the tunneling of Cooper pairs across a potential barrier in a point like junction, Josephson found that the local superconducting tunnel current density at zero voltage is given by

$$j = j_0 \sin \phi \quad (1.2)$$

where $\phi = \theta_1 - \theta_2$ is the difference in phase between the order parameters of the two superconducting junctions. This equation describes the *dc* Josephson effect, *i.e.*, a nonlinear current flow across the junction in the absence of an applied voltage across the junction. The maximum supercurrent current density j_0 of the junction, calculated from macroscopic theory by Ambegaoker and Baratoff [8] is given by

$$j_0 = \frac{\pi}{4} \frac{2\Delta(T)}{\rho e} \tanh\left(\frac{\Delta(T)}{2k_b T}\right) \quad (1.3)$$

where $\Delta(T)$ is the temperature dependent energy gap of the superconductor and ρ is the normal tunnel resistance of the junction per unit area. The electron charge is denoted by e and k_b is the Boltzmann constant. Applying a constant *dc* voltage across the junction, the phase difference ϕ evolves in time according

to the *ac* Josephson equation

$$V = \frac{\Phi_0}{2\pi} \frac{d\phi}{dt} \quad (1.4)$$

where $\Phi_0 = h/2e = 2.07 \times 10^{-15} \text{Wb}$ is the flux quantum. At the constant voltage V , the supercurrent through the junction oscillates with the characteristic frequency

$$\frac{d\phi}{dt} \frac{1}{2\pi V} = \frac{1}{\Phi_0} = 483.6 \text{ MHz}/\mu\text{V} \quad (1.5)$$

Thus Josephson junctions acts as a frequency to voltage standard.

1.3 Shapiro steps

Shapiro steps are constant voltage steps on the current-voltage characteristics of the junction when the junction is irradiated with an electromagnetic radiation. It was first observed by Shapiro in 1963[9]. In a voltage biased junction, due to the influence of the external field of frequency f_1 , the effective voltage becomes

$$V = V_0 + V_1 \cos(2\pi f_1 t)$$

Therefore the phase changes as $\varphi = \int \frac{2\pi}{\Phi_0} V dt$. Substituting in Eq. (1.2), we get the expression for the supercurrent as

$$I_s = I_c \sin\left[\varphi_0 + \frac{2\pi}{\Phi_0} V_0 t + \frac{V_1}{\Phi_0 f_1} \sin(2\pi f_1 t)\right]$$

simplifying the above expression, we see that, a time-independent (*dc*) current distribution occurs at $\frac{2\pi}{\Phi_0} V_0 = 2\pi n f_1$ at the *dc* voltage $V_0 = n f_1 \Phi_0$, $n = 0, \pm 1, \pm 2, \dots$. Typical applications of this effect need large number of junctions in series to get 1V.

1.4 Magnetic field effects

When a magnetic field is applied to a short Josephson junction, the corresponding phase difference across the junction can be shown to be[3]

$$\phi = \theta_2 - \theta_1 + \frac{2\pi}{\Phi_0} \int \bar{A} d\bar{l} \quad (1.6)$$

where \bar{A} is the electromagnetic vector potential. Considering a junction as shown in Fig.1.3a, the difference in phase ϕ between the two coordinates P and Q chosen at different points along the junction is given by

$$\phi(Q) - \phi(P) = \frac{2\pi}{\Phi_0} \left[\int_{P_1}^{P_2} \bar{A}(P) d\bar{l} - \int_{Q_1}^{Q_2} \bar{A}(Q) d\bar{l} \right] \quad (1.7)$$

If an external magnetic field \bar{H} is applied in the plane of the junction, the flux enclosed in the contour is given by

$$\Phi = \int_s \mu_0 \bar{H} d\bar{S} = \oint \bar{A} d\bar{l} \quad (1.8)$$

$$= \int_{Q_1}^{Q_2} \bar{A} d\bar{l} + \int_{P_1}^{P_2} \bar{A} d\bar{l} + \int_{P_2}^{P_1} \bar{A} d\bar{l} + \int_{P_1}^{Q_1} \bar{A} d\bar{l} \quad (1.9)$$

The second and fourth terms in above equation vanish if the closed path is chosen considerably deeper in the superconductor than the London penetration depth λ_J , which is the characteristic screening length of the magnetic field in a superconductor. Thus, equating Eqs. (1.9) and (1.7) and considering the flux enclosed in the differential small section dx of the junction, we get

$$\frac{\phi(Q) - \phi(P)}{dx} = \frac{2\pi}{\Phi_0} \Lambda \mu_0 H \quad (1.10)$$

where μ_0 is the permeability of free space, $\Lambda = t_j + 2\lambda_L$ is the magnetic thickness of the junction and t_j is the thickness of the tunnel barrier. $\Lambda \mu_0 H$ is the magnetic flux per unit length penetrating into a junction taking into account the screening of the magnetic field due to the superconductors (Fig.1.3b). Thus the gradient of ϕ can be expressed as

$$\nabla\phi = \frac{2\pi}{\Phi_0} \Lambda \mu_0 \bar{H} \times \hat{z} \quad (1.11)$$

where \hat{z} is the unit vector normal to the plane.

1.5 Static phase distribution in a small junction

The total supercurrent carried by a Josephson junction depends on the applied external magnetic field H . According to Eq. (1.11), the field induces a constant

gradient of the phase difference across the junction. Thus, the local Josephson current oscillates sinusoidally with the coordinate perpendicular to the field. The total supercurrent is given by[3, 6]

$$I_c = \int_A j_c \sin(2\pi \frac{\mu_0 \Lambda H x}{\Phi_0}) dA \quad (1.12)$$

over the junction area A , where we assume a spatially homogeneous critical-current density j_c . If a rectangular junction is considered the integral can be solved explicitly as

$$I_c(H) = I_c(0) \frac{\sin(\pi \Phi / \Phi_0)}{\pi \Phi / \Phi_0} \quad (1.13)$$

where $\Phi = \mu_0 \Lambda H w$ is the total flux threading the junction length. This expression is called the critical-current diffraction pattern of a rectangular junction and is shown in Fig.1.3c.

1.6 Dynamics of a small junction

If the length of the junction is smaller than λ_J , the electrostatics of the junction can be described by neglecting the variation of the phase difference across the junction area. In this case, the junction looks like as in Fig.1.4a and can be described by the equivalent electrical circuit shown in Fig.1.4b. This model is called the resistively and capacitively shunted junction (RCSJ) model[3, 6]. Using Kirchoff's laws, the total current through the junction is given by

$$I = I_c \sin \phi + \frac{V}{R} + C \frac{dV}{dt} \quad (1.14)$$

Introducing the superconducting phase difference across the barrier, the above equation forms

$$I = I_c \sin \phi + \frac{\Phi_0}{2\pi R} \frac{d\phi}{dt} + \frac{\Phi_0 C}{2\pi} \frac{d^2\phi}{dt^2} \quad (1.15)$$

This equation is equivalent to a driven and damped pendulum or equivalently the viscous motion of a particle in a tilted potential (washboard potential).

1.7 The long Josephson junction(LJJ)

LJJs possess an extremely rich spectrum of linear and nonlinear electromagnetic excitations[10]. In large area Josephson junction, the phase difference ϕ between the top and bottom electrodes may vary in space. The spatial extension of the junction gives rise to the existence of solitons (fluxons) [4, 11], breathers and other nonlinear and linear excitations. In such junctions, the characteristic length scale of the spatial variation of ϕ is called the Josephson length λ_J . If the length of the junction is much larger than the Josephson length ($l \gg \lambda_J$), then the junction is called a long Josephson junction. Flux dynamics in LJJ can be described by the well-known sine-Gordon equation and Josephson junction forms one of the outstanding physical systems in which nonlinear properties can be studied experimentally.

1.8 The sine-Gordon equation

The sine-Gordon equation describing flux dynamics in a LJJ can be derived from the equivalent electrical circuit describing the junction. A LJJ and its equivalent discrete model in an external homogeneous magnetic field H applied parallel to the dielectric barrier is given in Fig.1.5. In this model the junction is described by a parallel connection of small RCSJ like Josephson junctions interconnected by a parallel connection of an inductance and a resistance[12, 13]. An external bias current I_k is injected in each node k and the external flux Φ_{ext} threading each cell is taken into account. In this model, the wave equation is derived considering the flux quantization

$$\phi_{k+1} - \phi_k = \frac{2\pi}{\Phi_0}(\Phi_{ext} - LI_k^L) \quad (1.16)$$

where the flux threading the loop k due to an externally applied field can be expressed as $d\Phi_{ext} = \mu_0 \wedge H \Delta x$. The Kirchoff law at the node $k + 1$ is given by

$$I_k^{Rs} + I_k^L + I_{k+1} = I_{k+1}^L + I_{k+1}^{Rs} + I_{k+1}^{RCSJ} \quad (1.17)$$

Thus considering a small section Δx of the long junction we can write down the continuous limit of the above equations as

$$\frac{\phi_{k+1} - \phi_k}{\Delta x} = \frac{\partial \phi}{\partial x} = \frac{2\pi}{\Phi_0} (\mu_0 \Lambda H - L^* I^L) \quad (1.18)$$

$$\frac{\partial I^L}{\partial x} = j - j^{RCSJ} - \frac{\partial I^{R_s}}{\partial x} \quad (1.19)$$

with $L^* = L/\Delta x$, $j = I/\Delta x$ and $j^{RCSJ} = I^{RCSJ}/\Delta x$. Differentiating Eq. (1.18) with respect to space we find

$$\frac{\partial^2 \phi}{\partial x^2} = \frac{2\pi}{\Phi_0} \left(\mu_0 \Lambda \frac{\partial H}{\partial x} - L^* \frac{\partial I^L}{\partial x} \right) \quad (1.20)$$

substituting Eq. (1.19) with $I^{R_s} = -1/\rho_s \partial V/\partial x$ and the RCSJ current density (1.15) into Eq. (1.20) and considering a homogeneous external magnetic field ($\partial H/\partial x = 0$), we get the above equation as

$$\frac{\Phi_0}{2\pi L^*} \frac{\partial^2 \phi}{\partial x^2} = -j + j_c \sin \phi + \frac{V}{\rho} + C^* \frac{\partial V}{\partial t} - \frac{1}{\rho_s} \frac{\partial^2 V}{\partial x^2} \quad (1.21)$$

where $C^* = C/\Delta x$, $\rho = R\Delta x$ and $\rho_s = R_s \Delta x$. Expressing the voltages using the equation $V = (\Phi_0/2\pi) \partial \phi/\partial t$ and using the *ac* Josephson relation, we get the perturbed one-dimensional wave equation for the superconducting phase difference $\phi(x, t)$ called the perturbed sine-Gordon equation

$$\frac{\Phi_0}{2\pi L^*} \frac{\partial^2 \phi}{\partial x^2} - \frac{\Phi_0 C^*}{2\pi} \frac{\partial^2 \phi}{\partial t^2} - j_c \sin \phi = -j + \frac{\Phi_0}{2\pi \rho} \frac{\partial \phi}{\partial t} - \frac{\Phi_0}{2\pi \rho_s} \frac{\partial^3 \phi}{\partial x^2 \partial t} \quad (1.22)$$

where L^* is the specific inductance of the junction, C^* is the specific capacitance of the junction, ρ is the quasiparticle resistance per unit length and ρ_s is the surface resistance of the superconducting electrodes per unit length. The electric and magnetic fields are related to the phase difference ϕ in the following way:

$$E = \frac{V}{t_j} = \frac{1}{t_j} \frac{\Phi_0}{2\pi} \frac{\partial \phi}{\partial t} \quad (1.23)$$

$$H = \frac{1}{L^*} \frac{\Phi_0}{2\pi} \frac{\partial \phi}{\partial x} \quad (1.24)$$

The specific inductance and capacitance of the junction are given by $L^* = \mu_0 d'$ and $C^* = \frac{\epsilon_0 \epsilon_j}{t_j}$, where ϵ_j is the relative dielectric constant of the junction barrier, t_j is the thickness and d' is the magnetic thickness. In the limit of the thick electrodes ($d > \lambda_L$), d' is given by $d' = 2\lambda_L + t_j$. Dividing Eq. (1.22) by j_c and introducing the Josephson length λ_J and the plasma frequency ω_p

$$\lambda_J = \sqrt{\frac{\Phi_0}{2\pi L^* j_c}} \quad (1.25)$$

$$\omega_p = \sqrt{\frac{2\pi j_c}{\Phi_0 C^*}} \quad (1.26)$$

Eq. (1.22) can be expressed as

$$\lambda_J^2 \phi_{xx} - \frac{1}{\omega_p^2} \phi_{tt} - \sin \phi = -\frac{j}{j_c} + \frac{1}{\omega_p^2 C^* \rho} \phi_t - \frac{\lambda_J^2 L^*}{\rho_s} \phi_{xxt} \quad (1.27)$$

From the above equation, the phase velocity of linear waves in the system is given by

$$c_0 = \omega_p \lambda_J = c \sqrt{\frac{t_j}{\epsilon_j d'}} \quad (1.28)$$

where c_0 is termed as the Swihart velocity[14] and c is the velocity of light in vacuum. In long junctions, the Swihart velocity is typically only a few percent of c because the magnetic field penetrates into the superconductor on a length scale d' , while the electric field is localized only in the junction barrier of thickness $t_j \ll d'$. Normalizing the time with plasma frequency and space with the Josephson penetration depth, $\tilde{t} = \omega_p t$ and $\tilde{x} = x/\lambda_J$, the perturbed equation becomes

$$\phi_{\tilde{t}\tilde{t}} - \phi_{\tilde{x}\tilde{x}} + \sin \phi = -\alpha \phi_{\tilde{t}} + \beta \phi_{\tilde{x}\tilde{x}\tilde{t}} + \gamma \quad (1.29)$$

The perturbation terms in the right hand side of the above equation are defined as

$$\gamma = \frac{j}{j_c} \quad (1.30)$$

$$\alpha = \sqrt{\frac{\Phi_0}{2\pi j_c \rho^2 C^*}} = \frac{1}{\rho C^* \omega_p}, \quad \beta = \sqrt{\frac{2\pi j_c L^{*2}}{\Phi_0 C^* \rho_s^2}} = \frac{\omega_p L^*}{\rho_s} \quad (1.31)$$

where the first term is the normalized bias current, the second term is the damping term due to quasiparticle resistance and the third term corresponds to the damping due to the surface impedance of the superconducting electrodes. The terms $\alpha\phi_i$ and $\beta\phi_{\bar{x}\bar{x}\bar{t}}$ represent normal electron current flow across and along the junction respectively (shunt and longitudinal losses).

1.8.1 Boundary conditions

The boundary conditions of a long overlap junction of normalized length l in the absence of an external magnetic field is given by $\phi_{\bar{x}}(0, \bar{t}) = 0 = \phi_{\bar{x}}(l, \bar{t})$. In this case, any trapped fluxons in the junction executes oscillatory motion in the junction and they cannot escape from the junction due to the impedance mismatch. When an external magnetic field is applied parallel to the dielectric barrier of the junction, then the corresponding boundary conditions become $\phi_{\bar{x}}(0, \bar{t}) = \bar{H} = \phi_{\bar{x}}(l, \bar{t})$. Where $\bar{H} = \frac{2\pi}{\Phi_0} \mu_0 \Lambda H \lambda_J$ is the **normalized** magnetic field. In this case, fluxons are nucleated at one end of the junction and they are driven to the opposite end by the bias current. When the fluxons reach the opposite end of the junction they are pushed out from the junction.

1.9 Lagrangian and Hamiltonian functions

To calculate the energy of the system it is useful to introduce the Lagrangian and Hamiltonian of the system. To determine the Lagrangian, the energies of the electromagnetic fields and the Josephson coupling are to be considered. Combining the kinetic energy T_{kin} associated with the energy density of the electric field and the potential energy U_{pot} associated with the energy density of the magnetic field and the Josephson coupling, we obtain the Lagrangian $L = T_{kin} - U_{pot}$ by integrating over the junction volume V

$$L = \int_v \left[\frac{1}{2} \varepsilon_0 \varepsilon_j E^2 - \frac{1}{2} \mu_0 \mu_r H^2 - \delta(z) \frac{\Phi_0}{2\pi} j_c (1 - \cos \phi) \right] dV \quad (1.32)$$

Expressing the electromagnetic field by the phase difference ϕ according to Eq. (1.23) and (1.24) and rewriting their coefficients in terms of λ_J and ω_p we find

$$L = \int_0^l \int_0^w \left\{ \int_{-t_j/2}^{t_j/2} \left[\frac{1}{2} \frac{j_c^2}{\epsilon_0 \epsilon_j} \left(\frac{1}{\omega_p^2} \phi_t \right)^2 \right] dz - \int_{-d/2}^{d/2} \left[\frac{1}{2} \mu_0 \mu_r j_c^2 (\lambda_J^2 \phi_x)^2 \right] dz - \frac{\Phi_0}{2\pi} j_c (1 - \cos \phi) \right\} dy dx \quad (1.33)$$

upon rearranging the coefficients and performing the integration over the width of the junction w and perpendicular to the junction plane and considering the different penetration depths of the electric and magnetic fields into the junction barrier, we find the Lagrangian

$$L = \frac{\Phi_0}{2\pi} j_c w \int_0^l \left[\frac{1}{2} \frac{1}{\omega_p^2} \phi_t^2 - \frac{1}{2} \lambda_J^2 \phi_x^2 - (1 - \cos \phi) \right] dx \quad (1.34)$$

The normalized Lagrangian is

$$L = \frac{L}{\Xi_0} = \int_0^l \left[\frac{1}{2} \phi_t^2 - \frac{1}{2} \phi_x^2 - (1 - \cos \phi) \right] d\tilde{x} \quad (1.35)$$

with the characteristic energy scale of the junction $\Xi_0 = \frac{\Phi_0}{2\pi} j_c w \lambda_J$. Here $l = L/\lambda_J$ is the normalized junction length. Making use of the Lagrangian formalism, the sine-Gordon equation is obtained by calculating the equation of motion

$$\frac{d}{dt} \frac{\partial L}{\partial \phi_t} + \frac{d}{dx} \frac{\partial L}{\partial \phi_x} - \frac{\partial L}{\partial \phi} \quad (1.36)$$

The Hamiltonian, determining the total energy of a LJJ is given by $H = H^{sG} + H^P$. Where H^{sG} is Hamiltonian of the unperturbed sG equation given by[15]

$$H^{sG} = \int_0^l \left(\frac{1}{2} \phi_t^2 + \frac{1}{2} \phi_x^2 + 1 - \cos \phi \right) d\tilde{x} \quad (1.37)$$

It contain the magnetic energy ($\propto \phi_x^2$), the electric energy ($\propto \phi_t^2$) and the Josephson coupling energy ($\propto 1 - \cos \phi$). H^P is the contribution to the total energy due to the perturbation terms.

1.10 Excitations of the sine-Gordon system

In a sG system, a large variety of linear and in particular nonlinear excitations like solitons, anti-solitons, breathers and plasmons etc. do exist. The unperturbed sG equation is known to possess the Painlevé property[16] and is completely integrable. However perturbation terms make it nonintegrable. There are several different approaches to the analytical description of soliton dynamics in nonintegrable systems. The most powerful perturbative technique is based on the inverse scattering transform (IST). IST was introduced by Gardner *et al.*[17]. Lax[18], Zakharov and Shabat[19] and Ablowitz *et al.* [20, 21, 22] developed it further. The method is well explained and details of the method can be found in a number of books[23, 24, 25]. Equations exactly integrable by the IST possess many remarkable properties such as Backlund transforms[26], the Painlevé property, the possibility of representation in the Hirota bilinear form[27] and so on.

1.10.1 Soliton solutions

Neglecting all terms in the right hand side of the perturbed equation, Eq. (1.29), the unperturbed sG equation is given by

$$\phi_{\tilde{t}\tilde{t}} - \phi_{\tilde{z}\tilde{z}} + \sin \phi = 0$$

This equation represents a dispersive nonlinear wave equation which can be solved exactly giving the soliton solution[28, 29]

$$\phi(\tilde{x}, \tilde{t}) = 4 \arctan \left[\exp \left(\sigma \frac{\tilde{x} - u\tilde{t} - x_0}{\sqrt{1-u^2}} \right) \right] \quad (1.38)$$

Depending on the polarity σ , ϕ describes a kink (for $\sigma = +1$) or an antikink (for $\sigma = -1$) in the phase difference ϕ moving at a normalized velocity $0 \leq u \leq 1$. The kink corresponds to a jump of ϕ from 0 to 2π (or 2π to 0 for an antikink). The supercurrent distribution ($j \propto \sin \phi$) associated with this excitation changes sign around the center of the kink. Solitary waves exist in systems in which

dispersion, which leads to the spreading of the energy of the wave form in space, and the nonlinear effects compensate each other. As a result, a stable solitary wave may propagate in a nonlinear medium while its energy remains localized in space. The kink in a sine-Gordon system is a topological soliton and there is no dynamical restriction on its existence.

1.10.2 Fluxons and Antifluxons

In the superconducting state only quantized flux can enter the junction. A quantum of flux with the magnetic field value $\Phi_0 = h/2e = 2.07 \times 10^{-15} \text{Wb}$ has the properties of a particle and behaves as a soliton in the junction. The solution of the unperturbed sG equation (with $\sigma = +1$ in Eq. 1.38) represents a fluxon if the total phase difference (ϕ) along the junction varies from 0 to 2π as x varies from $-\infty$ to $+\infty$. Fig.1.6a shows this phase variation and represents a kink soliton or a fluxon. Thus a quantum of flux which produces a phase variation from 0 to 2π along the junction is called a fluxon.

If the flux quantum makes a phase variation from 2π to 0 along the junction as x varies from $-\infty$ to $+\infty$, then it is called an antifluxon (antikink). The phase variation (Eq. 1.38 with $\sigma = -1$) corresponding to an antikink is shown in Fig.1.6b. Thus fluxons and antifluxons have the same magnetic field value and differs in polarity[30].

The supercurrent associated with the fluxon ($j \propto \sin \phi$) flows in closed form across the junction. The supercurrent flows horizontally within a penetration depth λ inside the superconductor[4]. These current loops encircle the flux and the resulting configuration is called a Josephson vortex. Since the supercurrent density is zero at the center, there is no core for the Josephson vortex[31]. The supercurrent direction associated with the antifluxon is in opposite direction to that of a fluxon as shown in Fig.1.6c. Fluxons of the same polarity repels each other while fluxons of opposite polarity attracts each other.

1.10.3 Breather solution

Under certain conditions, a kink and an antikink may form a bound pair called breather[32]. Thus a breather corresponds to a bound state of a soliton and an antisoliton which oscillates around the center of mass. The solution can be written in the form

$$\phi_{br}(\bar{x}, \bar{t}) = 4 \arctan \left[\tan \theta \frac{\sin(\bar{t} \cos \theta)}{\cosh(\bar{x} \sin \theta)} \right]$$

Breathers are unstable with respect to perturbations and decay after some transient time.

1.10.4 Plasmons

In a LJJ, linear small amplitude excitations of φ do exist. These can be modelled by the linearized sG equation

$$\varphi_{\bar{t}\bar{t}} - \varphi_{\bar{x}\bar{x}} + \varphi = 0$$

which has linear wave solution of the form

$$\varphi(\bar{x}, \bar{t}) = \varphi_0 \exp(ik\bar{x} - i\omega\bar{t})$$

with a spectrum $\omega(k) = \sqrt{1 + k^2}$ [32], where k is the wave number of the mode and ω is the frequency. There is a gap of $\Delta\omega = 1$ in the excitation spectrum. These linear excitations of the LJJ are called plasmons.

1.11 Perturbative analysis

In LJJ, fluxons can be driven by external forces, *i.e.*, using a current bias applied to the junction. The bias current gives rise to a Lorentz-Magnus force acting on the charge carriers of the vortex, resulting in the propagation of the fluxon along the junction. Due to the presence of dissipation, driving forces and damping forces are balanced for a certain fluxon velocity, leading to a steady motion of

the fluxon. McLaughlin and Scott [15] showed that the dynamics of the fluxon can be described by the lowest order perturbation theory. In this approximation, the effect of the perturbations is assumed to influence only the dynamics of the center of mass coordinate of the fluxon but not its shape. Substituting the soliton solution, Eq. (1.38), into the unperturbed sine-Gordon Hamiltonian, the normalized energy of the fluxon moving with the velocity u can be obtained as

$$H^{sG} = \frac{8}{\sqrt{1-u^2}} \quad (1.39)$$

thus we can see that the rest energy of the soliton is 8, which is equal to the normalized rest mass of the fluxon. The change of the fluxon energy with time is given by

$$\frac{d}{dt}H^{sG} = \frac{8u}{(1-u^2)^{3/2}} \frac{du}{dt} \quad (1.40)$$

The perturbational parameters modulate the velocity of the solitons and may dissipate energy. The rate of dissipation is calculated from the expression

$$\frac{d}{dt}H^P = - \int_{-\infty}^{\infty} (\alpha\phi_t^2 + \beta\phi_{xt}^2 + \gamma\phi_t) dx \quad (1.41)$$

where H^P is the Hamiltonian of the perturbation terms. The first and second terms represents the dissipation due to quasiparticle tunneling and due to the surface impedance while the third term represents the power supplied to the junction from the bias current. Substituting the soliton solution, Eq. (1.38), to the above equation and integrating, we get

$$\frac{d}{dt}H^P = -8\alpha \frac{u^2}{\sqrt{1-u^2}} - \frac{8\beta}{3} \frac{u^2}{(1-u^2)^{3/2}} + 2\pi\gamma u \quad (1.42)$$

At equilibrium condition at which the energy supplied to the system is equal to the energy dissipated, we get

$$8\frac{du}{dt} + 8\alpha u(1-u^2) + \frac{8\beta u}{3} + 2\pi\gamma(1-u^2)^{3/2} = 0 \quad (1.43)$$

neglecting the surface damping term the equilibrium velocity can be obtained as

$$u = \pm \left[1 + \left(\frac{4\alpha}{\pi\gamma} \right)^2 \right]^{-1/2} \quad (1.44)$$

In Fig.1.7a typical normalized current-voltage characteristics is plotted. On increasing the bias current, fluxon velocity approaches the maximum velocity. At the maximum velocity relativistic effects are observed. The unperturbed sG equation is invariant with respect to Lorentz transformations. Thus solitons undergo Lorentz contraction. Therefore the field profile changes with the velocity. Fig.1.7b shows the variation of the field profile of a fluxon.

1.12 Coupled Josephson junctions

There has recently been considerable interests in coupled LJJ due to a variety of applications[33, 34]. Using low- T_c superconductors stacks can be formed by layers of $(Nb/AlO_x)_xNb$. For anisotropic layered high- T_c superconductors, such as $Bi_2Sr_2CaCu_2O_x$ and $Tl_2Ba_2Ca_2Cu_3O_x$, it has been demonstrated that the crystal itself shows the features of stacked LJJs. An important case occurs when the thickness of the superconducting layer is comparable to or less than the magnetic penetration depth of the superconducting layer. In such cases strong inductive coupling can be expected among the LJJs making the stack. In the case of high- T_c intrinsic Josephson junction stacks, inductive coupling is extremely strong. In multilayers, due to the close spacing of the superconductor-insulator lattice, the superconducting screening currents range across many layers and induce a coupling between individual junctions. The coupling of the junction can be adjusted by varying the thickness of the superconducting films. An external field parallel to the layers penetrates stacked junction in the form of fluxons. In multilayers, the magnetic field associated with the fluxons spread over many layers. Josephson junction multilayers are good candidates for high power flux-flow oscillators at THz frequencies.

A coupled junction consists of multiple thin films of the superconductor (*eg.* Nb) which are weakly linked in the vertical direction through insulating (*eg.* Al/AlO_x) layers. Fig.1.8 shows a stack of overlap Josephson junctions. To

bias the junction stack a vertical current is applied across the junction. The width of the system is made much smaller than the length of the junction. A schematic representation of the various layers and dimensions of the stack is shown in Fig.1.8a. The film thickness plays an essential role, as it determines the strength of the coupling between the stacked junctions[35, 36, 37, 38, 39, 40].

The mathematical model used to describe the system was first proposed by Sakai, Bodin and Pedersen[41]. The importance of the model is that all parameters such as characteristic lengths, frequencies and coupling parameters can be calculated from the system's physical properties such as the critical current density, junction conductance and capacitance.

When an external magnetic field is applied to stacked Josephson junctions in the direction of the y -axis or when currents flow in the system, magnetic flux penetrates into the Josephson layers and gives rise to the field distribution shown in Fig.1.9. The straight forward approach to model the coupling between the superconducting layers is thus based on the vector potential and the currents associated with it. Consider the flux Φ enclosed in the path $P_1P_2Q_2Q_1$

$$\Phi = \int \bar{B}_i \cdot d\bar{S} = \oint \bar{A} \cdot d\bar{l} \quad (1.45)$$

Using the quantum mechanical definition of the current density

$$\bar{j} = -\frac{1}{2e\mu_0\lambda^2}(\hbar\nabla\theta + 2e\bar{A})$$

and integrating along the paths parallel to the layers

$$\int_{Q_2}^{P_2} \bar{j}_i^L \cdot d\bar{l} = -\frac{\hbar}{2e\mu_0\lambda_i^2}(\theta_{P_1} - \theta_{Q_1}) - \frac{1}{\mu_0\lambda_i^2} \int_{Q_1}^{P_1} \bar{A} \cdot d\bar{l} \quad (1.46)$$

$$\int_{Q_1}^{P_1} \bar{j}_{i-1}^U \cdot d\bar{l} = -\frac{\hbar}{2e\mu_0\lambda_{i-1}^2}(\theta_{P_2} - \theta_{Q_2}) - \frac{1}{\mu_0\lambda_{i-1}^2} \int_{Q_2}^{P_2} \bar{A} \cdot d\bar{l} \quad (1.47)$$

The superindices U and L indicate the currents flowing in the top and bottom of a superconducting film. Assuming the density of the surface currents \bar{j}_i^L and \bar{j}_{i-1}^U

and the magnetic field \bar{B} constant over the short distance dx and then adding the above equations and using the phase difference expression

$$\phi = \theta_{Q_2} - \theta_{Q_1} + \frac{2e}{\hbar} \int_{Q_1}^{Q_2} \bar{A} \cdot d\bar{l} \quad (1.48)$$

along with Eq. (1.45), we get

$$\frac{\hbar}{2e} \partial_x \phi_l = \mu_0 \lambda_{l-1}^2 \bar{j}_{l-1}^U - \mu_0 \lambda_l^2 \bar{j}_l^L - d_l B_l \quad (1.49)$$

To calculate the surface currents we rewrite the second London equation, $\partial_{xx} \bar{B} = \frac{1}{\lambda_l^2} \bar{B}$, and solve it for the superconducting layer l with the appropriate magnetic fields as boundary conditions

$$B(z) = \frac{B_{l+1} \sinh(z/\lambda_l) - B_l \sinh((z - t_l)/\lambda_l)}{\sinh(t_l/\lambda_l)} \quad (1.50)$$

Using Ampere's law $\nabla \times \bar{B} = \mu_0 \bar{j}$, for the geometry we get

$$j_l^L = \frac{B_l \cosh(t_l/\lambda_l) - B_{l+1}}{\mu_0 \lambda_l \sinh(t_l/\lambda_l)}$$

$$j_{l-1}^U = \frac{B_{l-1} - B_l \cosh(t_{l-1}/\lambda_{l-1})}{\mu_0 \lambda_{l-1} \sinh(t_{l-1}/\lambda_{l-1})}$$

Inserting the result into Eq. (1.49), it becomes

$$-\frac{\hbar}{2e} \partial_x \phi_l = s_{l-1} B_{l-1} + s_l B_{l+1} + d'_l B_l \quad (1.51)$$

where the effective magnetic thickness d'_l and the coupling parameter s_l are defined by

$$d'_l = d_l + \lambda_l \coth\left(\frac{t_l}{\lambda_l}\right) + \lambda_{l-1} \coth\left(\frac{t_{l-1}}{\lambda_{l-1}}\right)$$

$$s_l = -\frac{\lambda_l}{\sinh\left(\frac{t_l}{\lambda_l}\right)} \quad (1.52)$$

Inserting Ampere's law for the z -component of the current $\mu_0 j^z = \partial_x B(x)$ and taking the current densities that are described by the resistively and capacitively shunted Josephson junction

$$j_l^z = \frac{\hbar}{2e} C_l \partial_{tt} \phi_l + \frac{\hbar}{2e} G_l \partial_t \phi_l + J_l \sin \phi_l - I_l \quad (1.53)$$

we can write the Eq. (1.51) in the matrix form

$$\frac{\hbar}{2e\mu_0} \partial_{xx} \begin{pmatrix} \phi_1 \\ \phi_2 \\ \dots \\ \phi_N \end{pmatrix} = \begin{pmatrix} d'_1 & s_1 & \dots & & 0 \\ s_1 & d'_2 & s_2 & \dots & \dots \\ 0 & s_2 & d'_3 & s_1 & 0 \\ \dots & \dots & \dots & \dots & \dots \\ \dots & \dots & 0 & s_{N-1} & d'_N \end{pmatrix} \begin{pmatrix} j_1^z \\ j_2^z \\ \dots \\ j_N^z \end{pmatrix} \quad (1.54)$$

The effective Josephson penetration depth becomes

$$\lambda_J^{(2)} = \left(\frac{\hbar}{2e\mu_0 (d' + s)} \right)^{1/2}$$

and the velocity of light in the barrier becomes

$$\bar{c}^{(2)} = \frac{1}{\sqrt{\epsilon \mu_0}} \left(\frac{d}{d' + s} \right)^{1/2}$$

compared to a single-junction soliton case we note that

$$\frac{\lambda_J^{(2)}}{\lambda_J^{(1)}} = \frac{\bar{c}^{(2)}}{\bar{c}^{(1)}} = \left(\frac{d'}{d' + s} \right)^{1/2}$$

since $s < 0$, $\bar{c}^{(2)}$ is larger than $\bar{c}^{(1)}$. Thus in stacked junctions, velocity of light exceed the velocity of light in single junction case. In normalized units the above equation becomes

$$\partial_{\bar{x}\bar{x}} \begin{pmatrix} \phi_1 \\ \phi_2 \\ \dots \\ \phi_{N-1} \\ \phi_N \end{pmatrix} = \begin{pmatrix} 1 & \sigma & \dots & \dots & 0 \\ \sigma & 1 & \sigma & \dots & \dots \\ \dots & \dots & \dots & \dots & \dots \\ \dots & \dots & \sigma & 1 & \sigma \\ \dots & \dots & 0 & \sigma & 1 \end{pmatrix} \begin{pmatrix} \partial_{\bar{t}\bar{t}}\phi_1 + \alpha\partial_{\bar{t}}\phi_1 + \sin\phi_1 - \gamma \\ \partial_{\bar{t}\bar{t}}\phi_2 + \alpha\partial_{\bar{t}}\phi_2 + \sin\phi_2 - \gamma \\ \dots \\ \partial_{\bar{t}\bar{t}}\phi_{N-1} + \alpha\partial_{\bar{t}}\phi_{N-1} + \sin\phi_{N-1} - \gamma \\ \partial_{\bar{t}\bar{t}}\phi_N + \alpha\partial_{\bar{t}}\phi_N + \sin\phi_N - \gamma \end{pmatrix} \quad (1.55)$$

where $\sigma = \frac{s}{d'}$. The external magnetic field does not influence the dynamics of the stack if the top and bottom electrodes are thicker than λ . The boundary conditions when an external magnetic field is applied to the junction are

$$\frac{\hbar}{2e\mu_0} \partial_x \begin{pmatrix} \phi_1 \\ \dots \\ \phi_l \\ \dots \\ \phi_N \end{pmatrix} = B_{ext} \begin{pmatrix} d_1^z + s_1 + s_0 \\ \dots \\ d_l^z + s_l + s_{l-1} \\ \dots \\ d_N^z + s_N + s_{N-1} \end{pmatrix} \quad (1.56)$$

The derivative of the phase difference at the edges of the stack is called the open boundary conditions. In this case, flux can enter end exit the junctions.

1.12.1 Two coupled junctions

A two coupled stack is an important configuration for both theoretical and experimental studies. In this case, fluxon dynamics can be described using the system of equations[41]

$$\begin{aligned}\phi_{tt} - \frac{1}{1-S^2}\phi_{xx} + \sin\phi &= -\alpha\phi_t - \gamma - \frac{S}{1-S^2}\psi_{xx} \\ \psi_{tt} - \frac{1}{1-S^2}\psi_{xx} + \sin\psi &= -\alpha\psi_t - \gamma - \frac{S}{1-S^2}\phi_{xx}\end{aligned}\tag{1.57}$$

where ϕ is the phase difference of the eigen functions of the first junction and ψ is the phase difference of the eigen functions of the second junction. S ($S < 0$) is the normalized coupling constant. A two coupled stack supports two types of fluxon motion in it. Both in-phase and out-of-phase locked modes of fluxon motion can be observed. It has been predicted that the in-phase flux-flow mode multiplies the power of flux-flow oscillator whereas the out-of-phase mode doubles the main radiation frequency of the oscillator. The out-of-phase flow of fluxons in a two-fold stack is shown in Fig.1.10a and in-phase flow of fluxons is shown in Fig.1.10b.

1.13 Regimes of fluxon dynamics

Josephson junction with open boundary condition will interact with the environment not only through the bias current but also through the external magnetic field at the boundaries. Therefore the dynamics in LJJ with open boundary conditions is complex. Three major regimes of fluxon motion can be observed in single long junctions as well as in stacks.

1.13.1 Zero Field Steps (ZFS)

In the absence of magnetic field the current voltage characteristics (IVC) of a long junction shows a family of so-called zero field steps. In this state one or more fluxons or antifluxons propagate in the junction, driven by the bias current.

At the junction boundaries they are reflected with the opposite polarity[42, 43]. The reflection at the boundaries gives rise to microwave emission. The maximum voltage of these steps is then calculated as $V_{\max} = \Phi_0 \frac{n\bar{c}}{L}$.

1.13.2 Fiske Steps (FS)

When a magnetic field is applied to the junction, the field penetrates partially into the junction and will decrease the fluxon energy at one side and increase it at the other side of the junction. At magnetic fields larger than a certain threshold value, fluxons are nucleated at one end of a current biased junction and is annihilated at the other end. In the process of annihilation, plasmons are emitted, which resonate with the junction cavity. In this case the IVC shows steps called the Fiske steps. The maximum voltage of the Fiske steps can be calculated as $V_{\max} = \Phi_0 \frac{n\bar{c}}{2L}$. This is valid only in a limited range of magnetic field values. Fiske steps are cavity resonances in LJJ[44].

1.13.3 Flux-Flow Steps (FFS)

In the high field limit of the Fiske modes, dynamics is dominated by the flow of fluxons. These are nucleated at one junction edge and viscously flow in a dense chain through the junction to exit at the other end. This effect is effectively utilized in the flux-flow oscillator. The maximum voltage of the flux-flow step is $V_{\max} = H \Lambda \bar{c}$, where H is the applied field, Λ is the magnetic thickness and \bar{c} is the Swihart velocity. This relation is valid for superconducting electrodes thicker than the London penetration depth[45].

1.14 Annular junctions

Different geometries are proposed for LJJ to study the fluxon dynamics and among them, annular geometries offer the advantage of reflectionless motion of fluxons and is studied extensively theoretically and experimentally[11, 46, 47,

48]. The annular geometry is of particular importance for the experimental and theoretical investigation of non-linear properties of LJJ. An annular LJJ tunnel junction is formed by two ring shaped superconducting electrodes separated by a thin tunnel barrier as shown in Fig.1.11. The electrostatics of a junction of length l is described by the perturbed sG equation with the periodic boundary conditions

$$\varphi(x = 0) = \varphi(x = l) - 2\pi n$$

$$\frac{\partial\varphi}{\partial x}(x = 0) = \frac{\partial\varphi}{\partial x}(x = l)$$

The number of kinks initially present in the annular junction is conserved due to the closed topology. Experimentally, annular junctions are prepared in states with n topologically trapped Josephson vortices by cooling the junction from the normal to the superconducting state in a small applied field. Alternately, vortices may be trapped in the junction by locally heating up one of the electrodes in an external field using an electron or laser beam in a low temperature scanning microscope. The number of the flux-quanta trapped in the junction can be determined from the IVC of the junction.

1.15 Conclusions

In short, LJJ offer the possibility of studying solitons that account for the magnetic flux-quanta (fluxon) moving along the tunnel barrier. A fluxon is basically a quantum of magnetic field which can be used for transmission of information or can be an object based on which certain novel Josephson devices such as flux-flow oscillators, voltage rectifiers, logic gates, magnetic field rectifiers, field sensors, etc. can be implemented. Fluxons can be trapped in the junction either during the normal-superconducting transition or by applying an external magnetic field parallel to the junction. In the superconducting state only fluxons or antfluxons can exist in the junction and they are driven by the Lorentz force associated with a dc current. In the absence of an external magnetic field, trapped

fluxons cannot escape from a linear junction and they make successive reflections at the edges of the junction. Progressive fluxon motion in LJJ is associated with a *dc* voltage which can be detected across the junction.

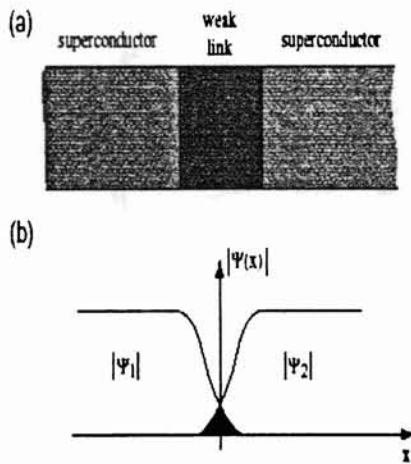


Fig.1.1(a) Two superconductors weakly coupled to one another. (b) Amplitude of the macroscopic wave function of the two superconductors.

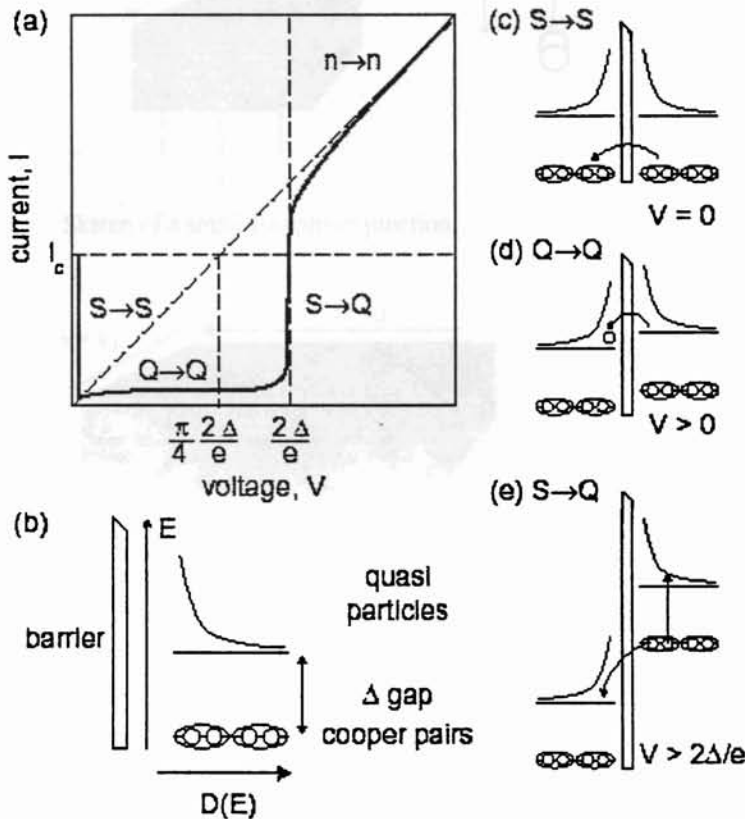


Fig.1.2 (a) Current voltage characteristics of a Josephson tunnel junction. (b) Bose representation of the electron density of states of the superconductor. (c) Josephson tunneling process. (d) quasiparticle tunneling process. (e) Cooper pair dissociation and tunneling into quasiparticle states.

Chapter 1. Figures

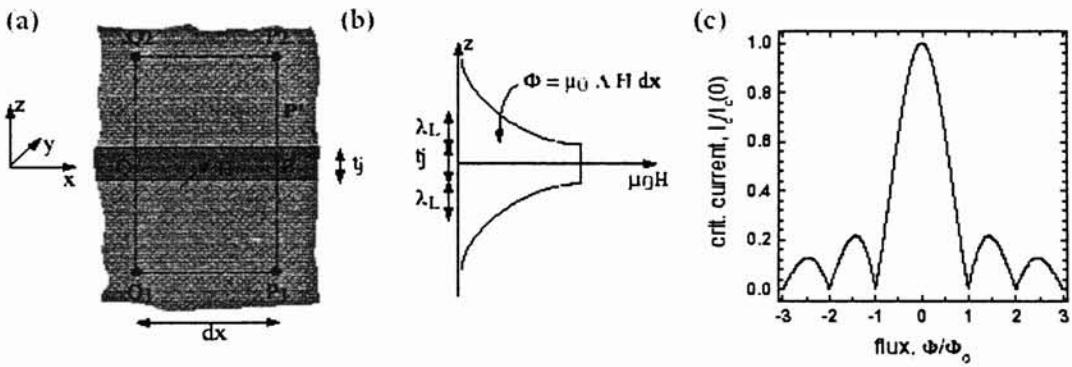


Fig.1.3 (a) Closed path across the barrier of a Josephson junction. (b) Magnetic field penetration into the superconductor. (c) Critical current diffraction pattern of a small rectangular junction.

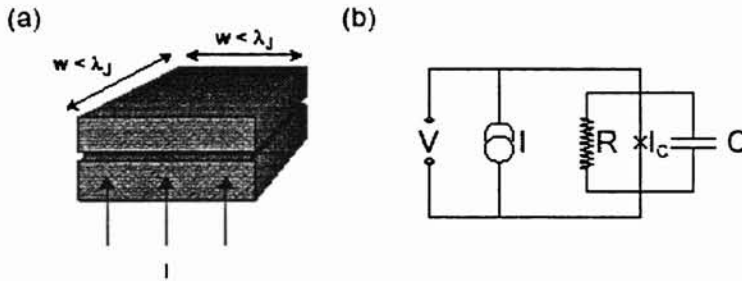


Fig.1.4 (a) Sketch of a small Josephson junction. (b) Discrete circuit model of a small junction.

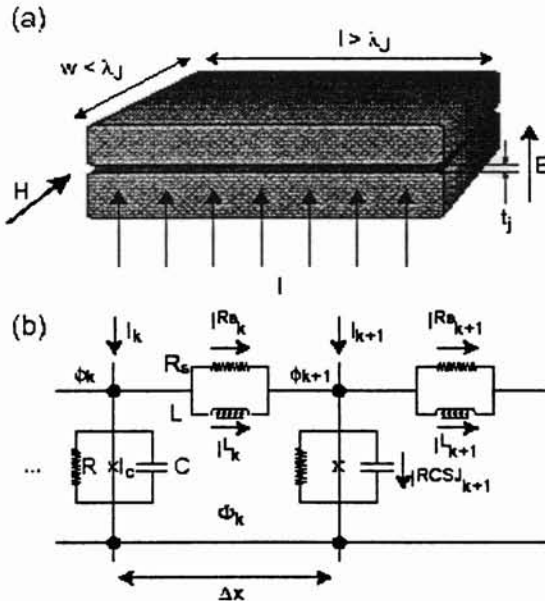


Fig.1.5 (a) Sketch of a LJJ. (b) The equivalent discrete model of the LJJ. The phase difference across the junction at node k is given by ϕ_k . The current through the RCSJ junction is I^{RCSJ} .

Chapter 1. Figures

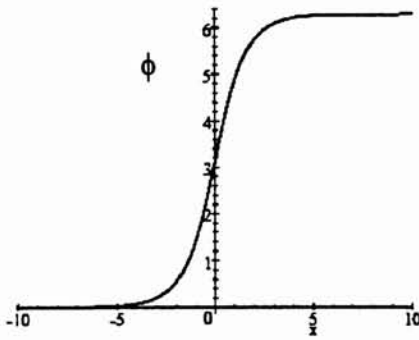


Fig.1.6a The kink solution of the sG equation.

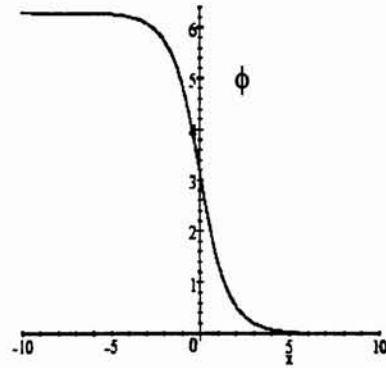


Fig.1.6b The antikink solution of the sG equation.

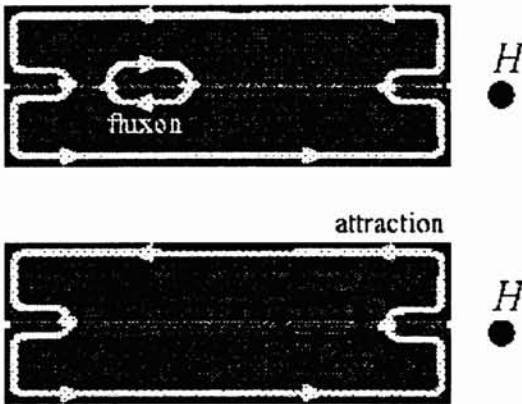


Fig.1.6c The supercurrent encircling a fluxon and an antifluxon in a rectangular junction. The applied field H parallel to the dielectric barrier induces a screening current and the field penetrates the junction over a distance λ_j .

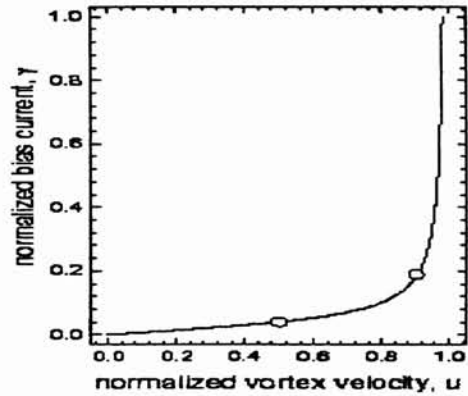


Fig.1.7a Normalized bias current vs. fluxon velocity

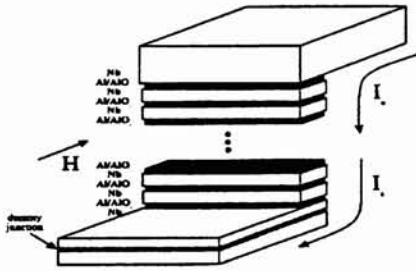


Fig.1.8 A stack of inductively coupled overlap Josephson junctions in an applied magnetic field H . A bias current is applied from the top electrode to the bottom electrode.

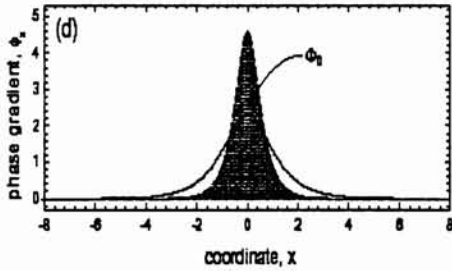


Fig.1.7b Gradient of the phase proportional to the magnetic field threading the junction. Total flux associated with the kink in the phase is Φ_0 .

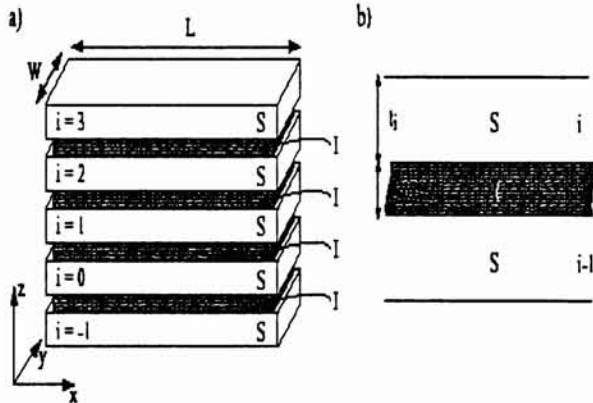


Fig.1.8a Schematic representation of the various layers and dimensions of the stack.

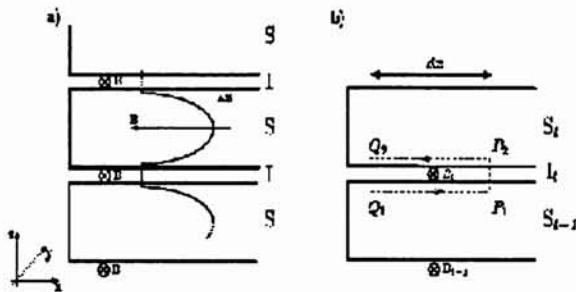


Fig.1.9 (a) Field penetration inside a stack. (b) Closed integration path across the barrier.

out-of-phase



Fig.1.10a Out-of-phase flow of fluxons in a two coupled junction

in-phase

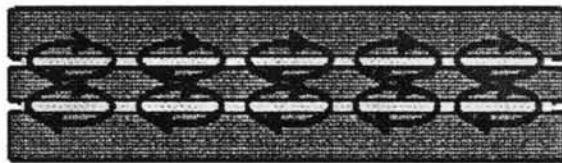


Fig.1.10b In-phase flow of fluxons in a two coupled junction

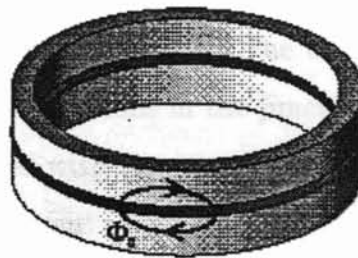


Fig.1.11 An annular long LJJ. The current distribution associated with a fluxon is indicated with the closed arrow mark.

Chapter 2

Fluxon creation and annihilation in Josephson junctions

The fluxon creation and annihilation processes are demonstrated numerically, in the LJJ in the first, second and third zero-field step cases, using the perturbed sine-Gordon equation in the presence of periodic point-like weak inhomogeneities. In all the zero-field cases, the created fluxon is found to be in a bunched (congealed) mode with the other fluxons. The current-voltage characteristics, depicting stable dynamics of fluxons in the junction in the absence of the periodic perturbation is compared with the current-voltage characteristics in the presence of the periodic perturbation.

2.1 Introduction

The dynamical properties of magnetic flux quanta are critical in the fabrication of high-speed, high-density and low power memory and logic devices. The fluxon (soliton) motion in a nonlinear medium is drastically modified by the presence of periodic spatial inhomogeneities[49, 50]. The collision of solitons with localized obstacles can produce different outcomes like emission of linear waves, creation or annihilation of solitons etc.[51, 52]. The threshold for the soliton creation in sG system is calculated analytically in Ref.[53]. The soliton creation or annihilation in the presence of periodic perturbation under the action of a pulse-like biasing

current is studied in Ref.[54].

Fulton and Dynes[42, 55] conceived the idea that the LJJ could support the resonant propagation of fluxons trapped in the junction, the fluxon being a 2π jump in the phase difference (ϕ) across the insulating barrier which separates the two superconductors. The oscillatory motion of a fluxon in the junction is manifested in the IVC by the steps at multiples of the voltage $V_n = n\Phi_0\bar{c}/L$, where $\Phi_0 = h/2e = 2.064 \times 10^{-15}$ Wb is the flux quantum, \bar{c} is the Swihart velocity, L is the length of the junction and n is the number of fluxons in the junction[56]. Analog and numerical studies have shown that fluxon can execute two types of oscillatory motions (i) a bunched (congealed) mode with the fundamental frequency f and (ii) a symmetric mode which on the N^{th} ZFS have the frequency Nf [12].

2.2 Model equations

Perturbed sine-Gordon (sG) equation takes into account the dissipation and inhomogeneities of the physical systems (*cf.* Sec.1.8). The fluxon dynamics in LJJ with periodically installed microresistors can be modelled with the perturbed sG equation

$$\phi_{tt} - \phi_{xx} + \sin \phi = -\alpha\phi_t + \beta\phi_{xxt} + \sum_{i=1}^N \mu\delta(x - a_i) \sin \phi - \gamma \quad (2.1)$$

with the boundary condition (in the absence of an external magnetic field)

$$\phi_x(0, t) = \phi_x(l, t) = 0 \quad (2.2)$$

where $\phi(x, t)$ is the superconducting phase difference between the electrodes of the junction. x and t are the normalized distance and time. The term $\sum_{i=1}^N \mu\delta(x - a_i) \sin \phi$ represents periodic local regions of low Josephson current (microresistors). The parameter μ is the strength of the localized inhomogeneity. A fluxon when passing through the microresistors loses energy. Thus due to the

periodic microresistors, the dispersion of the system increases so that the effective nonlinearity of the system decreases. The boundary condition indicates that the fluxon will be reflected at the end of the junction as an antfluxon.

In the absence of perturbations, ($\alpha = \beta = \gamma = \mu = 0$), Eq. (2.1) becomes the sG equation which is a conservative, nonlinear dispersive wave equation that supports special solutions called solitons. A sG soliton is a localized wave that is analytically described by the formula Eq. (1.38). The perturbational parameter terms α and β cause both the fluxons and the antfluxons to slow down, while γ term drives the fluxons to the left and the antfluxons to the right. At small values of γ , the fluxon will lose all its kinetic energy (KE) before passing the microshort and will be reflected back. At sufficiently higher values of γ , the fluxon will slow down near the inhomogeneity and loses some of its KE.

At $\alpha \neq 0$ and $\gamma \neq 0$, the fluxon moves under the action of a friction force $F_\alpha = -8\alpha \frac{d\xi}{dt}$ and a driving force $F_\gamma = 2\pi\gamma$. A fluxon is pinned by the microresistor if $\gamma < \gamma_{thr} = \frac{4}{\sqrt{\pi}}\alpha^{3/4}(2\mu)^{1/4}$. At higher bias, fluxons are depinned and the depinning current can be calculated as $\gamma > \gamma_c = \frac{4}{\sqrt{3\pi^3}}|\mu|$ [15]. In the presence of the periodic perturbation $\sum_{i=1}^N \mu\delta(x - a_i) \sin \phi$ the fluxon moves in an effective potential

$$U(\xi) = -2\mu \sum_{i=1}^N \text{sech}^2(\xi - a_i) - 2\pi\gamma\xi \quad (2.3)$$

where ξ is the center-of-mass coordinate of the fluxons. The modified Hamiltonian is

$$H = H^{sG} - \sum_{i=1}^N \mu\delta(x - a_i) (1 - \cos \phi) \quad (2.4)$$

2.2.1 Bunching effects

At higher velocities the surface-loss term β produces a spatially oscillating trailing tail behind a moving fluxon which may create a bunched (bound) mode oscillations in the junction. Bunching effects may occur between moving fluxons of the same polarity. At sufficiently high velocity they can overcome the repulsive

force and can form a bound state. Bunching effects break the symmetry and helps the chain to overcome dissipative losses. A fast moving fluxon on hitting a microresistor dissipates energy. A small amplitude wave is created and the small amplitude waves add up in energy to form a soliton[51, 52, 57, 58].

A solution of the perturbed sG equation can be obtained in the following form. Let $\xi = x + vt$, then the sG equation become

$$(1 - v^2)\phi_{\xi\xi} - \sin\phi = \alpha\phi_\xi - \beta\phi_{\xi\xi\xi} - \gamma \quad (2.5)$$

now, we will search for a solution which consists of a fluxon with an oscillating tail of the form

$$\phi(\xi) = \phi_0(\xi) + \phi_1 \exp(\rho\xi) \quad (2.6)$$

where $|\phi_1| \ll 1$. since $\sin\phi_0 \simeq \gamma$ and $\cos(\phi_1 \exp(\rho\xi)) \simeq 1$, we get, $\sin(\phi_0 + \phi_1) = \gamma + \phi_1\sqrt{1 - \gamma^2}$. Substituting in Eq. (2.5), we get

$$(1 - v^2)\rho^2 - \sqrt{1 - \gamma^2} - \alpha\rho + \beta\rho^3 = 0 \quad (2.7)$$

In the case $v < 1$ and $\gamma^2 < 1$, we get

$$\beta\rho^3 + (1 - v^2)\rho^2 - \alpha\rho - 1 = 0 \quad (2.8)$$

Eq. (2.8) always has a positive real root and either two negative real roots or two complex conjugate roots with negative real part (trailing fluxon tail). Setting $\alpha = 0$, Eq. (2.8) has a pair of complex roots at $(1 - v^2) < (1 - v_0^2) = 3(\frac{\beta}{2})^{2/3}$.

At the onset of the oscillating tail, at $v = v_0$, bunching is not possible since $\rho < |\rho_{2,3}|$, the repulsive tail is stronger. Bunching becomes possible at $v = v_1$ given by

$$(1 - v^2) < (1 - v_1^2) = (\frac{\beta^2}{2})^{1/3} \quad (2.9)$$

In this case roots can be calculated as $\rho_1 = (2\beta)^{-1/3}$ and $\rho_2 = \rho_3 = (-1 \pm i)\rho_1$, *i.e.*, the repulsive and oscillating tail have the same decay length[12, 59, 60, 61, 62, 63].

2.3 Numerical methods

To solve Eq. (2.1) and (2.2), we use an explicit method treating φ_{xx} with a six point, φ_{tt} with a three point and φ_t with a two point symmetric finite-difference method[64]. An implicit finite-difference method is used to solve the equation. Representing the phase $\phi(x, t)$ to a square mesh by $\phi_i^n = \phi(ih, nk)$, the following approximate forms of the derivatives are obtained[12]:

$$\phi_t = \frac{1}{2k}(\phi_i^{n+1} - \phi_i^{n-1})$$

$$\phi_x = \frac{1}{2h}(\phi_{i+1}^n - \phi_{i-1}^n)$$

$$\phi_{tt} = \frac{1}{k^2}(\phi_i^{n+1} - 2\phi_i^n + \phi_i^{n-1})$$

$$\phi_{xx} = \frac{1}{2h^2}(\phi_{i+1}^{n+1} - 2\phi_i^{n+1} + \phi_{i-1}^{n+1} + \phi_{i+1}^{n-1} - 2\phi_i^{n-1} + \phi_{i-1}^{n-1})$$

$$\phi_{xxt} = \frac{1}{2kh^2}(\phi_{i+1}^{n+1} - 2\phi_i^{n+1} + \phi_{i-1}^{n+1} - \phi_{i+1}^{n-1} + 2\phi_i^{n-1} - \phi_{i-1}^{n-1})$$

Substituting these equations in Eq. (1.29), we get the following system of equations:

$$c_1\phi_{i+1}^{n+1} + c_2\phi_i^{n+1} + c_3\phi_{i-1}^{n+1} = c_3(\phi_{i+1}^{n-1} + \phi_{i-1}^{n-1}) - c_4\phi_i^{n-1} + c_5\phi_i^n + c_6(\sin \phi_i^n - \gamma)$$

$$i = 1, 2, \dots, N, \quad n = 0, 1, \dots,$$

These system of equations are solved by means of iteration by using a tridiagonal matrix algorithm. Where the constants are given by $c_1 = \beta + k$, $c_2 = -(\alpha h^2 + 2h^2/k + 2\beta + 2k)$, $c_3 = \beta - k$, $c_4 = (\alpha h^2 - 2h^2/k + 2\beta - 2k)$, $c_5 = -4h^2/k$, and $c_6 = 2h^2k$.

The boundary conditions are treated by the introduction of imaginary points (*i.e.*, $\varphi(-x, t) = \varphi(x, t)$). The nonlinear term is evaluated using a predictor-corrector loop. A time step of 0.0125 and a space step of 0.025 is used for the discretization. Calculations are re-checked by systematically halving and doubling the time and space steps. Details of the simulation procedure are given in Appendix. After the simulation of the phase dynamics for a transient time,

we calculate the average voltage V for a time interval T as

$$V = \frac{1}{T} \int_0^T \varphi_t dt = \frac{\varphi(T) - \varphi(0)}{T} \quad (2.10)$$

for faster convergence of our averaging procedure, we additionally averaged the phases $\varphi(x)$ in Eq. (2.10) over the length of the junction. Once the voltage averaging for a current γ is complete, the current γ is increased by a small amount $\delta\gamma = 0.01$ to calculate the voltage at the next point of the IVC. We use a distribution of the phases and their derivatives achieved in the previous point of the IVC as the initial distribution for the following point. The average velocity of the fluxons can be calculated from the average voltage using the relation $u = V \frac{l}{2\pi}$. Thus the mean voltage in the junction is proportional to the average velocity of the fluxons. The instantaneous voltage pulse form across the junction is calculated using

$$V(t) = \frac{1}{l} \int_0^l \varphi_t dx \quad (2.11)$$

where we have averaged the voltage pulses over the length of the junction.

Numerical simulations are carried out on a LJJ of normalized length $l = 6$. We have installed five inhomogeneities (one each in each Josephson length λ_J) of strength $\mu = 0.5$. The δ function in Eq. (2.1) is approximated by a smooth hyperbolic function as represented in Fig.2.1[65]

$$g(x) \equiv \mu\delta(x - a_i) \approx \left[1 - \tanh^2 \frac{2(x - a_i)}{\mu} \right] \quad (2.12)$$

The junction parameters used in the simulations are $\alpha = 0.05$, $\beta = 0.02$, $\mu = 0.5$ and $N = 5$. The numerical integration was continued till the first three Fourier components of $\phi_t(l, t)$ remained constant to within 2%. The zero order Fourier component (average value) of ϕ_t corresponds to the *dc* junction voltage through the equation

$$V = (\Phi_0\omega_0/2\pi)\phi_t \equiv V_N\phi_t \quad (2.13)$$

Thus, a plot of $V_N \langle \phi_t \rangle$ versus the applied bias current γ corresponds to the IVC of the junction. In Fig.2.2 the IVC, depicting stable dynamics of fluxons in the

2.4.2 Second ZFS

In the second ZFS case, two fluxons are launched from locations $x_1 = 1$ and $x_2 = 3$. At the bias value $\gamma = 0.26$, an additional fluxon is created and the created fluxon is found to be in a bunched mode with the other two fluxons and found to be stable upto a bias value $\gamma = 0.40$. Fig.2.4 shows a three fluxon bunched mode in the junction. In the annihilation process, a fluxon is destroyed at $\gamma = 0.20$ and a single fluxon is found to be in a stable oscillatory state. Fig.2.5 shows this annihilation process.

2.4.3 Third ZFS

In this case, three fluxons are launched from locations $x_1 = 1, x_2 = 1.5$ and $x_3 = 2$. One additional fluxon is created at $\gamma = 0.3$ and the created fluxon is observed in a bunched mode with other three fluxons. Fig.2.6 shows this phenomenon. In the annihilation process a fluxon is destroyed and the remaining two fluxons are seen in a bunched mode at the bias value $\gamma = 0.2$. This is displayed in Fig.2.7. The voltage pulse form corresponding to this mode is shown in Fig.2.8.

2.5 Conclusions

The fluxon creation and annihilation process are crucial for the understanding of the internal dynamics of the junctions. These phenomena will have important applications in the design and fabrication of superconducting digital devices like logic gates. It will be interesting to check the creation and annihilation process in annular junctions. Coupled junctions are another important area where these phenomena can be demonstrated.

Chapter 2. Figures

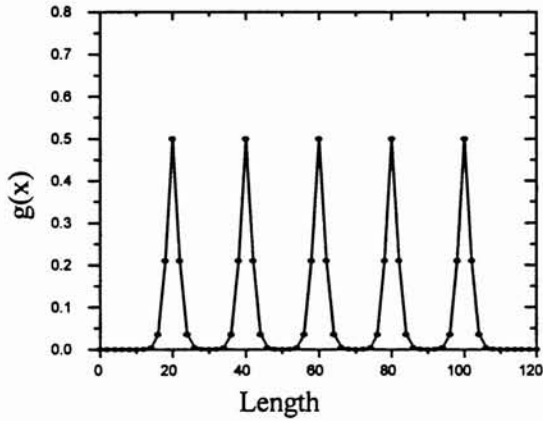


Fig.2.1. The profile of the spatial modulation produced by the periodic inhomogeneities in the junction

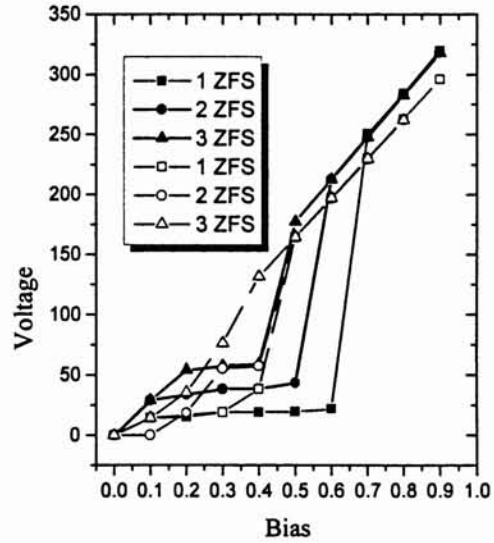


Fig.2.2 The numerically calculated I-V characteristics in the 1ZFS, 2ZFS and 3ZFS cases. The solid symbols corresponds to stable oscillatory motion of the fluxons in the absence of the periodic perturbations and open symbols represents IVC in the presence of perturbations.

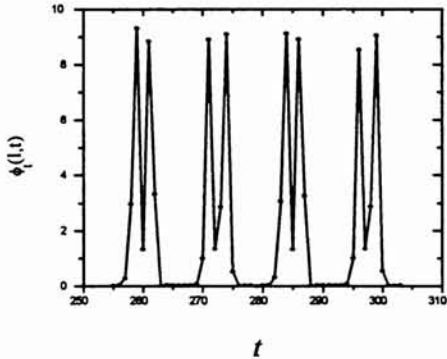


Fig.2.3. The Voltage pulse on the 1ZFS at one end of the junction for 50 time units with the bias value $\gamma = 0.41$ with $\alpha = 0.05$, $\beta = 0.02$.

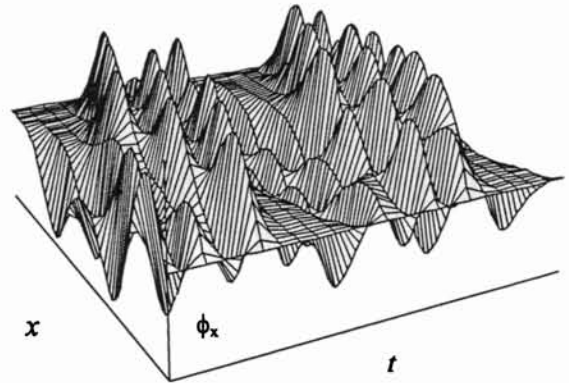


Fig.2.4. Three fluxon bunched mode on the 2ZFS in terms of $\phi_x(x,t)$ for 25 time units with $x_1=1$, $x_2=3$, $v = 0.8$, $\alpha = 0.05$, $\beta = 0.02$ and $\gamma = 0.26$.

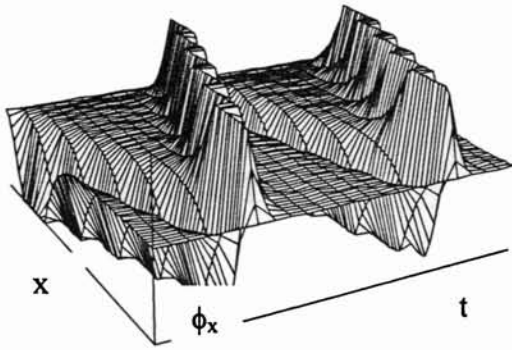


Fig.2.5. Single fluxon oscillatory motion created on the 2ZFS in terms of $\phi_x(x,t)$ for 25 time units with $\gamma = 0.20$, $x_1 = 1$, $x_2 = 3$, $v = 0.80$, $\alpha = 0.05$ and $\beta = 0.02$.

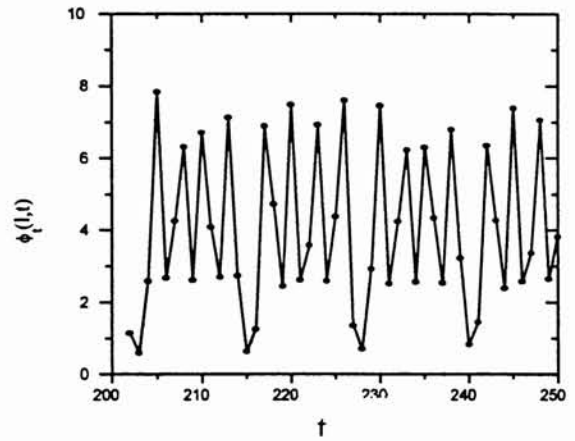


Fig.2.6. The voltage form corresponding to the four soliton bunched mode on the 3ZFS with $\gamma = 0.3$ for 50 time units.

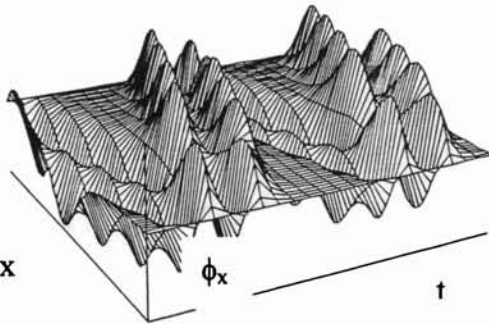


Fig.2.7. Two soliton bunched mode on the 3ZFS in terms of $\phi_x(x,t)$ for 25 time units with $x_1 = 1$, $x_2 = 1.5$, $x_3 = 2$, $v = 0.90$, $\alpha = 0.05$, $\beta = 0.02$ and $\gamma = 0.2$.

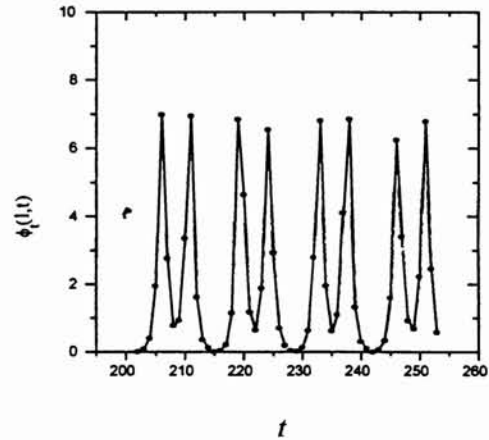


Fig.2.8. Voltage pulse form in the 3ZFS showing two bunched mode at $\alpha = 0.05$, $\beta = 0.02$ and $\gamma = 0.2$.

Chapter 3

Logic gates using coupled Josephson junctions

The possibility of making ultrafast superconducting logic gates, using multi-stacked Josephson junctions are investigated. Employing flux quanta as information bits, the functions of the logic gates AND, OR and XOR are implemented. Other logic functions and memory elements can be made by properly configuring these elementary logic gates. Design of these devices exhibits wide tolerance and flexibility in selecting the geometrical and electrical parameters.

3.1 Introduction

Investigations of fluxon dynamics in multilayered superconducting junctions have great importance both in theoretical and practical aspects. The Lawrence-Doniach model[66] of high temperature layered superconductors shows strong resemblance with stacked Josephson junctions and therefore is best understood in terms of Josephson tunneling. Intrinsic Josephson effects inherent in these superconductors are key factors in realizing tunneling-junction devices. High-speed switching devices making use of intrinsic Josephson junctions are indispensable in oscillators, digital signal processing circuits and in high-speed communication systems. Vertical stacking of the junctions provide an effective means of inductive coupling between them and create a high degree of integration between the junctions. Ul-

trafast logic operations require small sized, high-speed switching components. High packing density of these components are essential to reduce delay when information is transmitted between individual elements in the circuit. The low power dissipation and faster switching capability of LJJ devices makes them ideal for making logic gates. With the rapid growing superconducting technology, it is possible to make micron or submicron devices with high critical current densities bringing down the switching times to subpico second values and the energy dissipation to much lower than 10^{-18} J/operation.

Recent reports of the existence of bistable states and soliton switching in non-linear directional couplers[67, 68] and in multicored optic fiber waveguides[69, 70] have invited attention to soliton switching in multilayered Josephson stacks[71]. Stable and sharper switching exhibited by the high-sensitive superconducting quantum devices[72] with extremely low dissipation in the subpico-second time regime have the capability of revolutionizing the computing industries and hence are getting crucial roles in high-tech data processing and information storage devices. Various geometrical structures with different coupling mechanisms are tested experimentally[73], analytically[41] and numerically[74] towards this objective.

Fluxon dynamics in LJJ's have been investigated for information processing and computing applications by many in the past[42]. The basic Josephson junction property that is useful for computing applications is the quantification of the magnetic flux which appears in units of the flux quantum Φ_0 . In the quantum flux shuttle discussed by Fulton *et al.*[55], each fluxon carries one bit of information through a shift register. The Josephson memory element proposed by Gueret[75] uses a small segment of Josephson transmission line to store a single bit in the form of a fluxon and the computing network designed by Nakajima *et al.* [76, 77] employs interaction between fluxons to realize the logic functions: OR, AND and NOT.

3.2 Logic gates using three coupled Josephson junctions

In a perfect sG system solitons will not interact even upon direct collision and such systems are ideal for information transmission applications. But in real systems dissipative effects and structural irregularities are always present so solitons do interact when they collide. Strong perturbations, both internal and external, will alter the speeds and locations of the solitons and may create or destroy solitons[78]. It is necessary to establish design control over such interactions if the above mentioned applications of the junctions are to be realized.

In this section, we investigate the possibility of making logic gates using three inductively coupled vertically stacked Josephson junctions. Truth tables of all these gates are verified using different combinations of input excitations. The high and low states of the logic functions at the output is shown in terms of the amplitude of the soliton profile. Energy and momentum values in both states are compared to confirm the observations. Maximum tolerance in the device parameters are analysed and we present parametric plots showing acceptable regions of coupling coefficients for different values of the bias current.

3.2.1 Theoretical model

Our analysis is based on three inductively coupled vertically stacked Josephson junctions. Fluxon dynamics in these quasi-one dimensional junctions are described with the following set of coupled, perturbed sG partial differential equations[41, 79, 80, 81]

$$\begin{aligned}\phi_{1,tt} - \phi_{1,xx} + \sin \phi_1 &= -\alpha_1 \phi_{1,t} + \beta_1 \phi_{1,txt} - \gamma + \epsilon_1 \phi_{2,xx} \\ \phi_{2,tt} - \phi_{2,xx} + \sin \phi_2 &= -\alpha_2 \phi_{2,t} + \beta_2 \phi_{2,txt} - \gamma + \epsilon_1 \phi_{1,xx} + \epsilon_2 \phi_{3,xx} \\ \phi_{3,tt} - \phi_{3,xx} + \sin \phi_3 &= -\alpha_3 \phi_{3,t} + \beta_3 \phi_{3,txt} - \gamma + \epsilon_2 \phi_{2,xx}\end{aligned}\tag{3.1}$$

In the absence of external fields, boundary conditions of these overlap junctions are

$$\phi_{i,x}(0, t) = \phi_{i,x}(l, t) = 0 \quad i = 1, 2, 3 \quad (3.2)$$

where $\phi_i(x, t)$ are the quantum phase shifts of the superconducting order parameters across the junctions. Strength of the inductive coupling between the first and second junction is taken as ϵ_1 and between second and third junction is taken as ϵ_2 .

In the absence of perturbations ($\alpha_i = \beta_i = \gamma = \epsilon_i = 0$), the system of equations become uncoupled exactly integrable sG equations having soliton solutions given by Eq. (1.38). The momentum of the system is defined as

$$P_i = - \int_{-\infty}^{+\infty} \phi_{i,x} \phi_{i,t} dx \quad (3.3)$$

Inserting the unperturbed solution Eq. (1.38), in Eq. (3.3), we get

$$P_i = \frac{8v_i}{(1 - v_i^2)^{\frac{1}{2}}} \quad (3.4)$$

Total energy of the system is

$$H = \sum_{i=1}^3 (H_i^{sG} + H_i^p + H^f) \quad (3.5)$$

Energy of the unperturbed sG system is

$$H^{sG} = \int_{-\infty}^{+\infty} \left[\frac{1}{2} (\phi_{1,t}^2 + \phi_{2,t}^2 + \phi_{3,t}^2 + \phi_{1,x}^2 + \phi_{2,x}^2 + \phi_{3,x}^2) + 3 - \cos \phi_1 - \cos \phi_2 - \cos \phi_3 \right] dx \quad (3.6)$$

Perturbational parameters modulate the velocity of the solitons and may cause fluxons to dissipate energy. The rate of dissipation is calculated by computing

$$\frac{d}{dt} (H^p) = - \int_{-\infty}^{+\infty} [(\alpha_1 \phi_{1,t}^2 + \beta_1 \phi_{1,xt}^2 + \gamma \phi_{1,t}) + (\alpha_2 \phi_{2,t}^2 + \beta_2 \phi_{2,xt}^2 + \gamma \phi_{2,t}) + (\alpha_3 \phi_{3,t}^2 + \beta_3 \phi_{3,xt}^2 + \gamma \phi_{3,t})] dx \quad (3.7)$$

In the present model the output is taken from the central junction and we consider a situation where the fluxons in the central junction interact with those in the

outer junctions. Hence the interaction energy is responsible for the formation of fluxon states in the central junction and can be calculated using the equation:

$$H^I = \epsilon_1 \int_{-\infty}^{+\infty} \phi_{1,x} \phi_{2,x} dx + \epsilon_2 \int_{-\infty}^{+\infty} \phi_{2,x} \phi_{3,x} dx. \quad (3.8)$$

In the steady-state condition, *i.e.*, power input to the soliton is balanced due to dissipation, we compute the energy associated with the unperturbed sG fluxon moving with equilibrium velocity in the middle junction as

$$E = \int_{-\infty}^{+\infty} \left[\frac{1}{2} (\phi_{2,t}^2 + \phi_{2,x}^2) + 1 - \cos \phi_2 \right] dx \quad (3.9)$$

Inserting Eq. (1.38) in above, we get the energy possessed by a single fluxon moving with the velocity v as $E = \frac{8}{\sqrt{1-v^2}}$. From these analysis it is observed that the rest energy of the fluxon is $E = 8.0$ with zero momentum. For $E < 8.0$, fluxon propagation is not favorable in the junctions and hence fluxons will be dissipated. For $E > 8.0$, fluxon motion can exist in the middle junction. We use this criterion to establish the two different states in the junction.

3.2.2 Design aspects

Elementary logic gates are designed with two input ports and one output port. Different distributions of input fluxons are inserted from the left end in top and bottom dielectric layers. After a transient time output is measured from the right end of the central junction. The high and low states at the output can be demonstrated either in terms of voltage across the junctions or in terms of energy associated with the propagating solitons or in terms of the amplitude evolution of the soliton profile in the junctions. In the simulations, the amplitude evolution of the solitons is considered to distinguish the high and low states. In all the figures, distance 0 – 30 represent top junction, 30 – 60 represent middle junction and 60 – 90 represent bottom junction. A soliton profile (2π kink of Eq. (1.38)) inserted in the left end corresponds to an input excitation of high-state and a zero soliton profile corresponds to a low-state. Similarly a soliton profile at the output

indicates a high-state and a phase-diffused profile indicates a low-state. Functions of AND and XOR are highly sensitive to the time lag between the inputs and is based on the coincidence of the input excitations. Sakai and Samuelsen[54] reported that a bias pulse of triangular form can be used to produce fluxons in Josephson junctions and it is possible to inject these fluxons through the edges. By applying bias pulses of same amplitude and phase in homogeneous coupled junctions, two fluxons of the same velocity and phase can be injected and these fluxons can be used as input excitations.

3.2.3 OR gate

Bistable states exhibited by coupled junctions and switching between the states are trivial factors in the making of digital devices. An OR gate is constructed by taking a stack of length $l = 5$. Other considered parameters of the stack are $\alpha_1 = \alpha_2 = \alpha_3 = 0.03, \beta_1 = \beta_2 = \beta_3 = 0.01, \gamma = 0.18$ and $\epsilon_1 = \epsilon_2 = 0.1$. High and low states at the output are established in terms of the amplitude profile of the solitons along the junctions. We verify the truth tables by plotting the spatio-temporal evolutions of the soliton profile in the dielectric layers in the initial and final states. To verify OR truth table we insert one fluxon each in top and bottom dielectric layers ($a_1 = 1$ and $a_2 = 1$). After a transient time fluxon evolution is observed in the central junction ($a_3 = 1$) which indicates that output is high when both inputs are high. Fig.3.1(a) represents the dynamics corresponding to this Boolean operation. Using Eqs.(3.3) and (3.9) the average momentum and energy of the soliton are calculated. The calculated average energy value $E = 39.5$ and momentum $P = 38.25$ confirms solitonic propagation in the central junction. If any one input port is excited ($a_1 = 1$ and $a_2 = 0$ or $a_1 = 0$ and $a_2 = 1$) then also we get a high output state $a_3 = 1$. Figs.3.1(b) and 3.1(c) represent these states. Mean energy corresponding to these two cases are found to be equal to 24.0 with momentum value 22.0. If both inputs are low then we get the trivial

low-state output.

The above mentioned logic gate exhibits wide tolerance in selecting geometrical, electrical and dissipative parameters. So fabrication of this device is characterized by several degrees of freedom that the designer must optimize. Thus it is essential to find the limits of variability for such parameters compatible with the achievement of the desired logic function. By fixing the device length and dissipative parameters, we compute the tolerance limits of the coupling factor ϵ and show the regions of acceptability in a bidimensional representation. Fig.3.2 shows the parametric plot (ϵ versus γ) of the OR logic gate. To draw this graph, we fix the parameters $l = 5, \alpha_1 = \alpha_2 = \alpha_3 = 0.03, \beta_1 = \beta_2 = \beta_3 = 0.01$ and compute the coupling factor for different values of the bias current satisfying the desired OR function. From the plot it is observed that for a particular bias value $\gamma = 0.18$, coupling factor can range from $\epsilon = 0.1$ to $\epsilon = 0.4$. On the other hand, for a fixed coupling factor $\epsilon = 0.2$ the bias value can range from $\gamma = 0.1$ to $\gamma = 0.24$.

3.2.4 XOR gate

We use a stack with $l = 4, \alpha_1 = \alpha_2 = \alpha_3 = 0.03, \beta_1 = \beta_2 = \beta_3 = 0.02, \gamma = 0.14$ and $\epsilon_1 = \epsilon_2 = 0.2$ to implement the XOR gate. When both input ports are excited ($a_1 = 1$ and $a_2 = 1$) the amplitude of fluxon profile in the central junction is below the threshold to be detected ($a_3 = 0, E < 1$ and $P = 0$). The inserted fluxons are annihilated due to dissipative interaction. Fig.3.3 shows this logic operation. If any one input is excited ($a_1 = 1$ and $a_2 = 0$ or $a_1 = 0$ and $a_2 = 1$) we get a high state ($a_3 = 1$)(*cf.* Figs. 3.1(b) and 3.1(c)). Energy in this case is found to be equal to 24.5 with an average of 22.3 momentum value. Finally we observe the trivial low-state when inputs are not excited. So we conclude that the designed structure can act as a XOR gate. Several other configurations can be identified to produce the same results. Here, we like to emphasize that the graphs presented

do not refer to limit cases. We report only those combinations which are highly stable and show wide margins of tolerance in the design. Fig.3.4 shows the ϵ versus γ plot of this XOR gate. The two shaded regions indicate the possible regimes of the coupling factor. From these regions it is clear that for a particular bias value $\gamma = 0.15$, the coupling factor can vary from $\epsilon = 0.15$ to $\epsilon = 0.21$ and from $\epsilon = 0.38$ to $\epsilon = 0.52$.

3.2.5 AND gate

For constructing an AND gate, we consider a stack of normalized length $l = 4$. Other parameters are taken as $\alpha_1 = \alpha_3 = 0.04, \alpha_2 = 0.03, \beta_1 = \beta_3 = 0.02, \beta_2 = 0.01, \gamma = 0.15$ and $\epsilon_1 = \epsilon_2 = 0.3$. AND's truth table predicts a high-state at the output if both inputs are high. To verify AND's truth table we insert one fluxon each in the input ports ($a_1 = 1$ and $a_2 = 1$). A well defined soliton profile is evolved in the central junction indicating the high state. With the excitation ($a_1 = 1$ and $a_2 = 0$ or $a_1 = 0$ and $a_2 = 1$), the amplitude profile at the output port is found to be in a phase-diffused state to conclude that output is low ($a_3 = 0$). Figs.3.5(a) and 3.5(b) show these dynamics leading to diffused states. Energy value in this state is found to be less than one with zero momentum. Which confirms that fluxon motion cannot exist in this case. For completeness we must check the AND's truth table with no excitation in both input ports ($a_1 = 0$ and $a_2 = 0$) which, however, produces the trivial low-state: no fluxon propagation exists in the junction in the absence of input fluxons. Simulations show that functions of AND gate is satisfied only in a narrow range of bias values.

Detailed analysis of the stacked junctions revealed that coupling factor alone can change the logic function. So we extend our computations on a stack with the parameters $l = 6, \alpha_1 = \alpha_2 = \alpha_3 = 0.05, \beta_1 = \beta_2 = \beta_3 = 0.02$ to determine the limits of ϵ which changes one logic function to another. The ϵ versus γ plot of this structure is shown in Fig.3.6. It is found that in the region between $\epsilon = 0.05$

and $\epsilon = 0.2$ the stack behaves as an OR gate. Between $\epsilon = 0.22$ and $\epsilon = 0.28$ it changes into XOR gate. Above $\epsilon = 0.3$, at some isolated critical points it acts as an AND gate.

3.3 Logic gates using two coupled Josephson junctions

In this section, construction of logic gates using two vertically coupled Josephson junctions are discussed. Vortex dynamics in two inductively coupled vertically stacked LJJs is described with the system of coupled, perturbed sine-Gordon (sG) partial differential equations[82, 32]

$$\phi_{tt} - \phi_{xx} + \sin \phi = -\alpha_1 \phi_t + \beta_1 \phi_{xxt} - \gamma + \epsilon \psi_{xx} \quad (3.10)$$

$$\psi_{tt} - \psi_{xx} + \sin \psi = -\alpha_2 \psi_t + \beta_2 \psi_{xxt} - \gamma + \epsilon \phi_{xx} \quad (3.11)$$

In the absence of external fields, boundary conditions of the overlap junctions are

$$\phi_x(0, t) = \phi_x(l, t) = 0 = \psi_x(0, t) = \psi_x(l, t) \quad (3.12)$$

where $\phi(x, t)$ and $\psi(x, t)$ are the phase differences between the eigen functions of the superconductors of the junctions. Strength of the inductive coupling between the junctions is taken as ϵ . In the absence of perturbations ($\alpha_i = \beta_i = \gamma = \epsilon = 0$), the system of equations become uncoupled exactly integrable sG equations having soliton solutions (Eq. (1.38)).

The theory of devices that we propose is based on two inductively coupled vertically stacked overlap Josephson junctions. Elementary logic gates are designed with two input ports and one output port[83, 84]. Input ports are placed at $x = 0$ (left end) in each dielectric layers. Output port is placed at $x = l$ (right end) across the two dielectric layers. Different distributions of input fluxons are inserted from the left end and after a transient time wave form is checked at the right end. Simulations are carried out by solving the full partial differential

Eqs. (3.10) and (3.11) with the boundary conditions (3.12) using an implicit finite-difference method mentioned in Chapter 2.

3.3.1 AND gate

For constructing an AND gate, we consider a two coupled Josephson stack of normalized length $l = 4$. Other parameters are taken as $\alpha_1 = \alpha_2 = 0.04$, $\beta_1 = \beta_2 = 0.01$, $\gamma = 0.10$ and $\epsilon = 0.5$. A fluxon profile in the junction corresponds to the binary bit 1 and a phase-diffused profile corresponds to the bit 0. The high and low states at the output can be established either in terms of amplitudes of the fluxons, or in terms of voltage across the junctions. For clarity, we verify the truth tables by plotting the spatio-temporal evolutions of the fluxon profile in the dielectric in the initial and final states (*cf.* Sec.3.2.5).

3.3.2 OR gate

An OR gate is constructed by taking a stack of length $l = 4$. Other parameters of the stack are $\alpha_1 = \alpha_2 = 0.04$, $\beta_1 = 0.02$, $\beta_2 = 0.03$, $\gamma = 0.11$ and $\epsilon = 0.4$. Truth table is verified by inserting different combinations of fluxons in the input ports (*cf.* Sec.3.2.3).

3.3.3 XOR gate

We use a stack with $l = 4$, $\alpha_1 = \alpha_2 = 0.05$, $\beta_1 = 0.03$, $\beta_2 = 0.03$, $\gamma = 0.10$ and $\epsilon = 0.4$ to implement the XOR gate. Fluxons are used for input excitations. Various other combinations of device parameters can be used to make the above mentioned XOR gate. For example, the set of values $l = 4$, $\alpha_1 = \alpha_2 = 0.012$, $\beta_1 = \beta_2 = 0.03$, $\gamma = 0.20$ and $\epsilon = 0.5$ will give the same result as above (*cf.* Sec.3.2.4).

3.4 Conclusions

Design aspects of superconducting LJJ logic gates by exploiting spatial solitons interactions in nonlinear dielectric structures are studied and truth table of some elementary logic gates are verified. Both three coupled and two coupled vertically stacked junctions are studied. By proper design of the stacked junctions it is possible to fabricate other logic gates such as NAND, NOR, NOT etc. Design of these devices exhibits wide tolerance in the assumption of device lengths, dissipative properties, coupling coefficients and input power levels. Highly complicated devices and memory elements can be created if these analysis are extended to an array of stacked junctions with multiple fluxons. The remarkable reproducibility observed in the simulations indicate wide tolerance in the assumption of device lengths, dissipative parameters, coupling coefficients and input power levels.

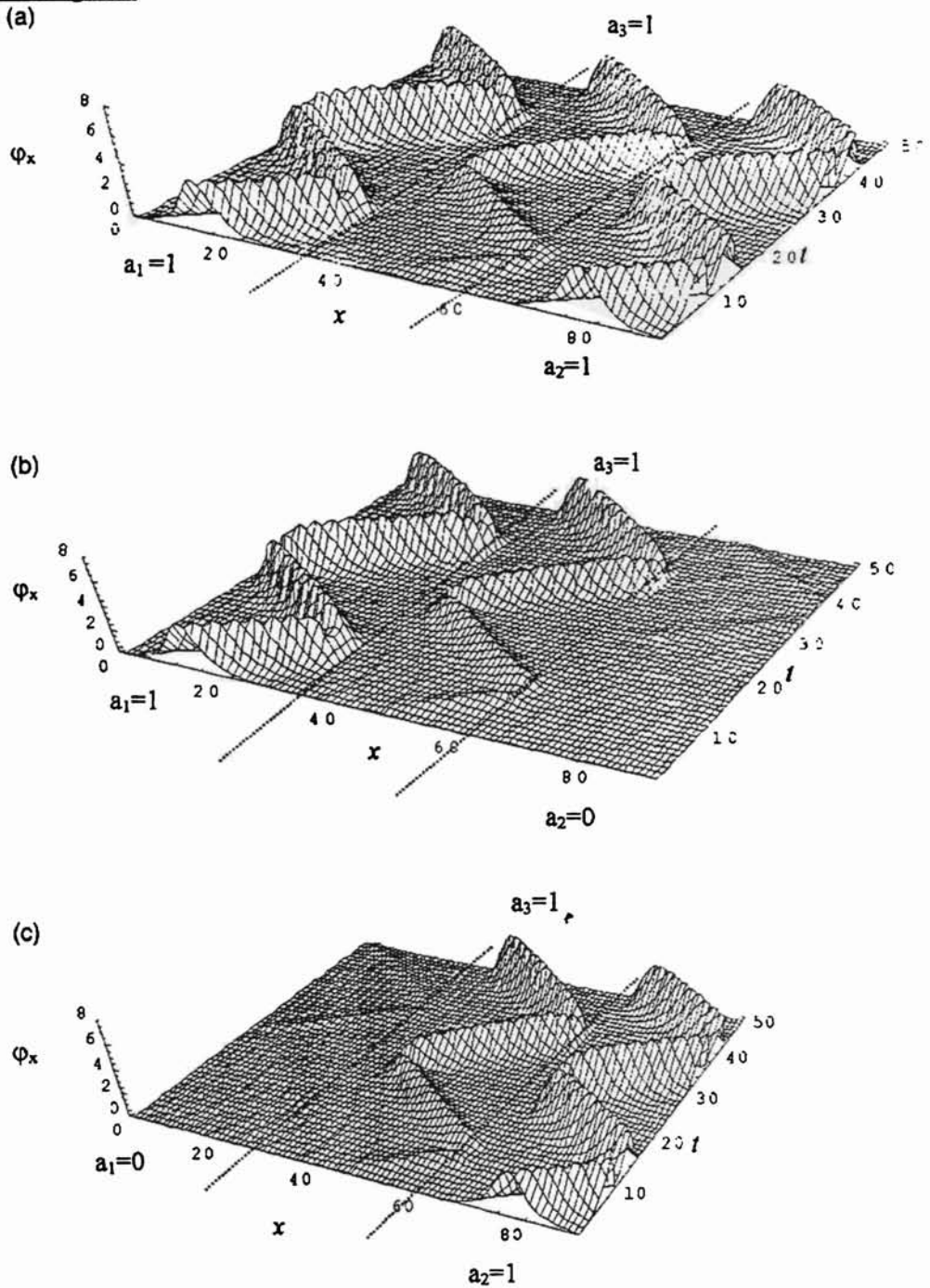


Fig.3.1 (a) Amplitude evolution of fluxons in the vertically stacked junctions corresponding to input Excitations $a_1=1$, $a_2=1$ and output $a_3=1$ of an OR gate. (b) Dynamics of fluxons in the stacked junctions corresponding to input excitations $a_1=1$ and $a_2=0$ and output $a_3=1$ of the OR gate. (c) truth table equivalent of the OR logic gate with $a_1=0$ and $a_2=1$ and output $a_3=1$

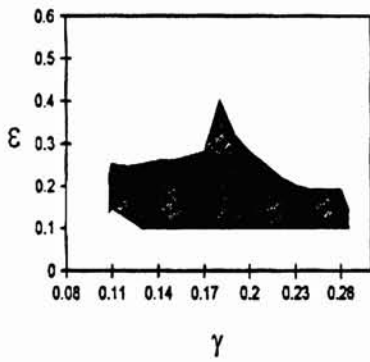


Fig.3.2 Parametric plot showing ϵ versus γ of the OR gate

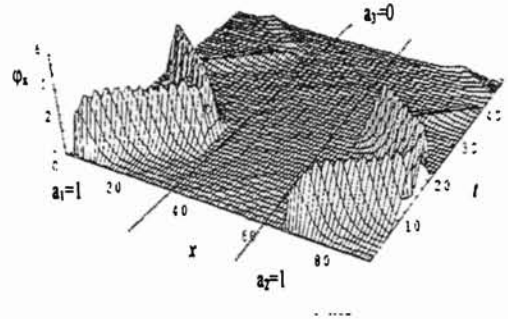


Fig.3.3 Annihilation of solitons in the junction showing Boolean operation of a XOR gate corresponding to the input $a_1=1$ and $a_2=1$.

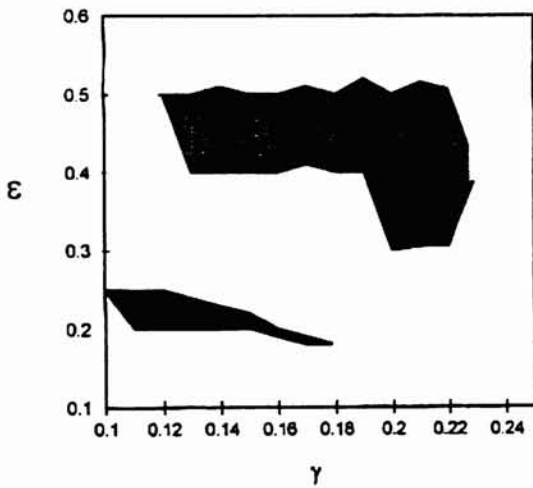


Fig.3.4. Parametric plot indicating the regions of the coupling factor for different biases of the XOR gate

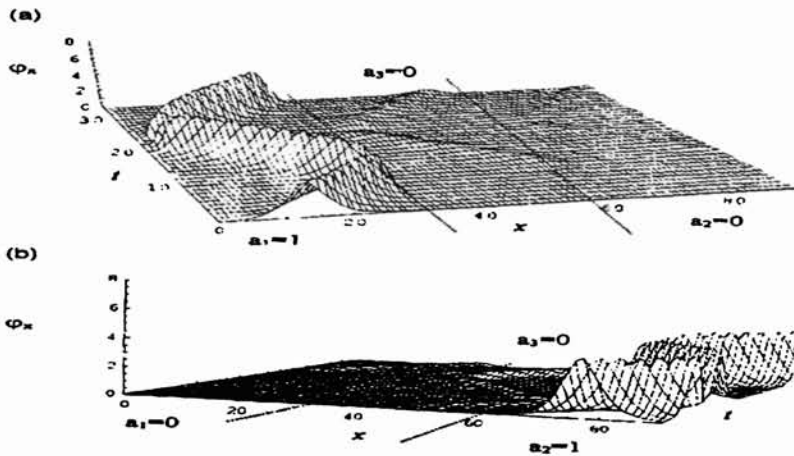


Fig.3.5. (a) AND's truth table corresponding to inputs $a_1=1$ and $a_2=0$ and output $a_3=0$
 (b) AND's truth table corresponding to inputs $a_1=0$ and $a_2=1$ and output $a_3=0$

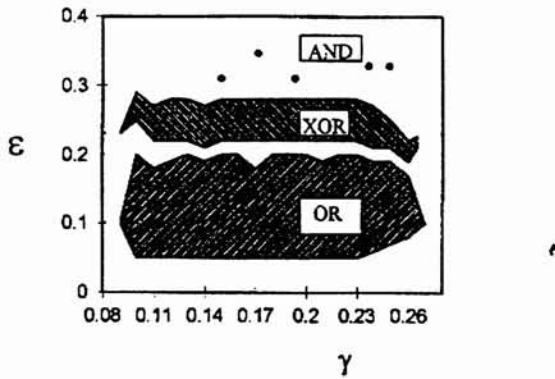


Fig.3.6. Parametric plot of the stacked junctions showing different logic gate functions at different regimes of coupling factor.

Chapter 4

Semiannular Josephson junctions

A semiannular geometry is proposed for Josephson junction and analytical and numerical studies show that an external static magnetic field applied parallel to the dielectric barrier interacts through the interior of the junction and produce a tilted potential which pushes out trapped fluxons from the interior of the junction and flux-free state exists in the junction in the absence of an external bias. Due to the semiannular shape, the effective field at the ends of the junction has opposite polarities which supports penetration of opposite polarity fluxons into the junction in the presence of a forward biased dc current. When the direction of the dc current is reversed, flux penetration is not possible and flux-free state exists in the junction. Thus this geometry can be used in implementing fluxon based diodes. The rectification property of the junction is demonstrated using square wave signals and sinusoidal ac signals. It is found that the junction is extremely useful in rectifying rf magnetic fields. In the forward biased state, fluxons and antifluxons enter the junction and move in opposite directions. Using this property, we propose and demonstrate a novel bidirectional flux-flow oscillator.

4.1 Introduction

Fluxon dynamics in nonrectangular LJJ attracted much attention in recent years. The nonrectangular shape creates nonuniformity in the junction which can be advantageously employed in certain Josephson devices. In flux-flow oscillators (FFO), nonuniformity is used to reduce self-field effects and to facilitate unidirectional fluxon motion[85]. In Josephson trigger circuits, nonuniformity is employed to make a special dependence of the critical current upon the magnetic field[86]. Nonuniformity may mean unequal conditions for Josephson vortices in different parts of the junction. It may be due to nonuniform spatial distribution of critical and bias currents[3], temperature gradient effects[87], or due to many other reasons.

Recently fluxon dynamics in some unconventional structures like the multistacked junctions (both linear[36] and annular[88]), non-symmetric and non-uniform junctions[89] etc. are being carried out by a number of authors. A static magnetic field applied parallel to the barrier in a linear LJJ has no effect in the interior part of the junction and the small perturbation produced is through the open boundary[12, 49]. The effect of a spatially homogeneous static magnetic field on annular LJJ has undergone various theoretical and experimental studies[90, 91]. The external field produces periodic potential in the annular junction which can be used to trap the fluxons[92].

In the present work, we investigate the effects of an external homogeneous static magnetic field on the propagation of fluxons in a dissipative LJJ having a semiannular shape. Analytical and numerical studies show that the field interacts through the interior of the junction as well as through the boundary conditions and can exert a driving force supporting transitory motion (from one end to the other end) for any trapped static flux-quanta inside the junction. Thus under static conditions, flux-free state exists in the junction. The main advantage of this geometry is in the fact that it allows opposite polarity fluxons to enter the

junction from opposite ends only if the junction is biased in one direction (forward bias). If the direction of the bias is reversed (reverse bias), fluxons cannot enter the junction due to the repulsive Lorentz force and flux-free state exists in the junction. Thus the junction exhibits the basic properties of a diode. By controlling the strength of the magnetic field, it is possible to get a single fluxon and a single antifluxon configuration in the junction. Detailed analysis show that this single fluxon-antifluxon state ($(\uparrow\downarrow)$) is highly stable against fluctuations. The stable dynamics exhibited by this fluxon-antifluxon pair is utilized in constructing a fluxon based diode. It is found that even in the forward biased state, there is a threshold value of the current below which fluxons cannot enter the junction. The damping effects of an external magnetic field on the motion of a single trapped fluxon in the junction is also studied. Using the semiannular junction, rectification of alternating magnetic fields is demonstrated. A novel bidirectional flux-flow oscillator is also constructed using the device.

4.2 Derivation of the model equations

An overlap LJJ with a semiannular shape is considered as shown in Fig.4.1(a) with the discrete model shown in Fig.4.1(b). An external static magnetic field applied parallel to the dielectric barrier interacts nonuniformly and produces a spatially varying perturbation. The Kirchoff equations for the Josephson phases in the cell and for the currents in one of the nodes are

$$\varphi(X + dX) - \varphi(X) = \frac{2\pi}{\Phi_0} (d\Phi_e(X) - L^p I_L(X)) \quad (4.1)$$

$$I_L(X - dX) - I_L(X) = I(X) - I_e(X) \quad (4.2)$$

where $\varphi(X)$ is the Josephson phase at the point X of the junction, $d\Phi_e(X)$ is the component of the external magnetic flux linked with the cell of length dX , L^p is the inductance of the piece of the junction electrodes between X and

$X + dX$. $I_L(X)$ is the current through the inductance, $I_e(X)$ is the externally applied current, $I(X)$ is the current through the Josephson junction.

The external magnetic field \hat{B} interacts with the interior of the junction and the component of the external flux in the plane of the junction over an infinitesimal interval dX is calculated as [91, 90, 92, 93]

$$d\Phi_e(X) = \Delta (\hat{B} \cdot \hat{n}) dX = \Delta B \cos(KX) dX \quad (4.3)$$

where Δ is the coupling of the external magnetic field with the junction, \hat{n} is the unit vector normal to the propagation direction and in the plane of the junction. Thus a homogeneous static field makes an effective nonhomogeneous field inside the junction. From Eq. (4.3), it is clear that for a linear junction (*i.e.*, if \hat{n} is independent of X) in a homogeneous magnetic field there will be no perturbation from the magnetic field to the interior of the junction. In this case there would only be interaction through the open boundary conditions. However, if the junction is in semiannular shape or in any other curved shape, \hat{n} depends on X and there is perturbation to the interior of the junction.

Using the relations

$$L^p = L' dX; I(X) = j(X) dX; I_e(X) = -j_e(X) dX \quad (4.4)$$

and substituting Eqs. (4.3) into Eqs. (4.1) and (4.2), we write the later in the following form.

$$\frac{\partial I_L(X)}{\partial X} = -\frac{\Phi_0}{2\pi L'} \frac{\partial^2 \varphi}{\partial X^2} - \frac{\Delta B K}{L'} \sin(KX) \quad (4.5)$$

$$\frac{\partial I_L(X)}{\partial X} = -j_e(X) - j(X) \quad (4.6)$$

where L' is the inductance per unit length of the junction, $K = \frac{\pi}{L}$ is the spatial periodicity of the field inside the junction and L is the length of the junction.

We assume that the dielectric is spatially uniform so that Δ and L' are independent of X . In the case of simple resistively shunted junction (RSJ) model, the supercurrent density $j(X)$ is the sum of the supercurrent, normal (quasi particle) current and displacement current densities,

$$j(X) = j_0 \sin \varphi + \frac{\Phi_0}{2\pi R} \varphi_T + \frac{C \Phi_0}{2\pi} \varphi_{TT} \quad (4.7)$$

here j_0, R, C are the critical current density, specific resistance and specific capacitance of the junction, respectively. Using Eqs.(4.5), (4.6) and (4.7) we get the sG equation

$$\frac{C \Phi_0}{2\pi} \varphi_{TT} - \frac{\Phi_0}{2\pi L'} \frac{\partial^2 \varphi}{\partial X^2} + j_0 \sin \varphi = -\frac{\Phi_0}{2\pi R} \varphi_T + \frac{\Delta B K}{L'} \sin(KX) - j_e(X) \quad (4.8)$$

The component of the external flux over an infinitesimal distance dX of the unit cell in terms of the quantized unit is

$$d\varphi(X) = \frac{2\pi}{\Phi_0} d\Phi_e(X) = \frac{2\pi}{\Phi_0} \Delta B \cos(KX) dX \quad (4.9)$$

The effect of an applied magnetic field on the junction is to induce currents in closed form across the junction. So the net current when integrated over the junction should be zero. Due to the semiannular shape, the external field induces a varying surface current along the junction. Since the spatial derivative of the superconducting phase is equivalent to the induced surface current, we get

$$\frac{d\varphi(X)}{dX} = \frac{2\pi}{\Phi_0} \Delta B \cos(KX) \quad (4.10)$$

This equation can be used to obtain the boundary conditions of the junction. Using the normalized quantities, $T = \frac{t}{\omega_0}$, $X = x \lambda_J$, $\lambda_J = \left(\frac{\Phi_0}{2\pi L' j_0}\right)^{\frac{1}{2}}$, $\omega_0 = \left(\frac{2\pi j_0}{C \Phi_0}\right)^{\frac{1}{2}}$ in Eq. (4.8) we get the general perturbed sG partial differential equation

$$\varphi_{tt} - \varphi_{xx} + \sin \varphi = -\alpha \varphi_t + b \sin(kx) - \gamma \quad (4.11)$$

where $\varphi(x, t)$ is the superconducting phase difference between the electrodes of the junction, $k = \frac{\pi}{l}$ and $b = \frac{2\pi \lambda_j \Delta B k}{\Phi_0} = 2 k \frac{B}{B_{c1}}$. Where $B_{c1} = \frac{\Phi_0}{\pi \Delta \lambda_j}$ is the first critical field of the superconductor.

Compared with the standard sine-Gordon model for Josephson junction, this equation has an extra term, $b \sin(kx)$, which corresponds to a force driving fluxons towards left and antifluxons towards right. Therefore any static trapped fluxon present in the junction will be removed and flux-free state exists in the junction in the absence of an external bias. Thus the effect of the external field is to act like a bias current $\gamma_b(x) = b \sin(kx)$, which has non-zero average in space. This bias current stops penetration of fluxon from the left end and penetration of antifluxons from the right end. So the junction does not support any fluxons in the static conditions. This non-zero average current induces a non-periodic field (potential) inside the junction.

From Eq. (4.10), we get the corresponding boundary conditions of the junction as

$$\begin{aligned} \varphi_x(0, t) &= \frac{b}{k} \\ \varphi_x(l, t) &= -\frac{b}{k} \end{aligned} \quad (4.12)$$

This boundary condition is consistent with the fact that effective field linked with the junction has opposite polarities at the ends of the junction. So only fluxons can enter from the left end ($x = 0$) and antifluxons from the right end ($x = l$) in a properly biased junction. From Eq. (4.12), we see that fluxons can enter from the left end and antifluxons can enter from the right end of the junction for positive values of γ (forward biased state). Negative values of γ drives fluxons towards left and antifluxons towards right and fluxon penetration becomes impossible (reverse biased state). Eq. (4.11) with boundary conditions Eq. (4.12) represent a semiannular LJJ in a homogeneous static magnetic field.

4.2.1 Lagrangian and Hamiltonian functions

Lagrangian density of Eq. (4.11) with $\alpha = \gamma = 0$ is

$$\mathbf{L} = \left\{ \frac{\varphi_t^2}{2} - \frac{1}{2} \left(\varphi_x - \frac{b}{k} \cos(kx) \right)^2 - (1 - \cos \varphi) \right\} \quad (4.13)$$

Therefore the corresponding potential energy density is (second term of the above equation)

$$\mathbf{U}(x) = \frac{1}{2} \left\{ \varphi_x^2 - \frac{2b}{k} \cos(kx) \varphi_x + \left(\frac{b}{k} \cos(kx) \right)^2 \right\} \quad (4.14)$$

The first term is independent of the applied field and the third term is a constant which is independent of the flux motion in the junction. Therefore the change in the potential due to the applied field can be determined from the second term as:

$$U(x) = -\frac{b}{k} \int_{-\infty}^{+\infty} \varphi_x \cos(kx) dx \quad (4.15)$$

Substituting Eq. (1.38) in (4.15) and integrating, we get

$$U(x_0) = -2bl \operatorname{sech} \left(\frac{\pi^2}{2l} \sqrt{1-u^2} \right) \cos(kx_0) \quad (4.16)$$

For long junctions and at relativistic velocities, $u \sim 1$, Eq. (4.16) becomes

$$U(x_0) = -C \cos(kx_0) \quad (4.17)$$

where $C = 2bl$ is a constant. Eq. (4.17) shows that the potential is tilted by the applied field. The potential is plotted in Fig.4.2. Tilting is either to the left side or to the right side of the junction depending on the direction of the field. This tilt in the potential causes trapped static fluxons and antifluxons to move in the opposite directions and thus the junction remain flux-free under static conditions. Thus any trapped flux can be removed from the junction by applying a static magnetic field.

Energy of the unperturbed sG system is given by Eq. (1.37). Perturbational parameters modulate the velocity of the solitons and may cause to dissipate energy. The rate of dissipation is calculated by computing

$$\frac{d}{dt}(H^P) = [\varphi_x \varphi_t]_0^l + \int_0^l [-\alpha \varphi_t^2 + (b \sin(kx) - \gamma) \varphi_t] dx \quad (4.18)$$

where the first term on the right side account for the boundary conditions. From Eq. (1.38), we get $\varphi_t = -u \varphi_x$ and from Eq. (4.12), we get $\varphi_x^2(0, t) = \varphi_x^2(l, t)$ (symmetric boundary conditions). Substituting these expressions, we find that the first term in the right hand side of the above equation vanishes - a symmetric boundary condition does not change average energy value of a fluxon. Inserting Eq. (1.38) in Eqs. (4.18) and following perturbative analysis[15], we get

$$(1 - u^2)^{-\frac{3}{2}} \frac{du}{dt} = -\alpha \frac{u}{\sqrt{1 - u^2}} - \frac{\pi}{4} \left\{ b \operatorname{sech} \left[\frac{\pi^2 \sqrt{1 - u^2}}{2l} \right] \sin(kx_0) - \gamma \right\} \quad (4.19)$$

This expression describes the effect of perturbations on the fluxon velocity. In the absence of *dc* bias (*i.e.*, $\gamma = 0$), from Eq. (4.19), we get the threshold value of the magnetic field for producing equilibrium velocity (*i.e.*, at $\frac{du}{dt} = 0$) on a trapped fluxon as

$$b = -\frac{4\alpha}{\pi} \frac{u_0}{\sqrt{1 - u_0^2}} \frac{1}{\operatorname{sech} \left[\frac{\pi^2 \sqrt{1 - u_0^2}}{2l} \right] \sin(kx_0)} \quad (4.20)$$

For a long junction, $\frac{\pi^2}{2l} \ll 1$, we obtain the approximate equilibrium velocity of the fluxon when $u_0 \sim 1$ with $x'_0 = \frac{l}{2}$ as

$$u_0 \simeq \pm \left[1 + \left(\frac{4\alpha}{\pi b} \right)^2 \right]^{-1/2} \quad (4.21)$$

This equilibrium velocity is equivalent to that obtained in Ref.[15] with a *dc* bias. Thus it can be concluded that in semiannular LJJ, the magnetic field exerts a driving force on trapped fluxons and produces a transitory motion in the junction.

The effects of a *dc* current on the fluxon dynamics in the presence of the external field is studied using Eq. (4.11). Even in the forward biased state, ZVS

exists in the junction (flux-free state) when the driving force due to the field ($\gamma_b(x)$) and that of the dc current (γ) are nearly equal and is in opposite direction. By variation of the soliton position x'_0 , from Eq. 4.21, we find the largest possible bias current of ZVS ($u = 0$) to be [90]

$$\gamma_1 = b \sec h \left(\frac{\pi^2}{2l} \right) \quad (4.22)$$

This is the threshold value of the applied bias, below which flux propagation is not possible in the junction. This threshold value depends on the magnetic field and is directly proportional to the field.

4.3 General properties of the junction

4.3.1 Properties of the junction under a dc bias

Fig.4.3 shows the average velocity (equivalently average voltage) attained by the fluxon-antifluxon pair $\langle \uparrow \downarrow \rangle$ as a function of the dc bias in the junction in the forward biased (positive values of γ) state and in the reverse biased state (negative values of γ). We have considered a junction of length $l = 34$ and dissipation parameter $\alpha = 0.1$. The field strength is fixed at $b = 0.1$. The system is started with $\varphi = 0$ and $\frac{\partial \varphi}{\partial t} = 0$. For positive values of the sweeping dc current, flux penetration is possible in the junction. ZVS corresponding to flux-free state exists in the junction upto a bias value of $\gamma = 0.32$. At this threshold value, a fluxon enter the junction from the left end and an antifluxon enter from the right end simultaneously and they move in opposite directions in the junction under the influence of the dc bias. This fluxon-antifluxon pair is found to be stable for sufficiently larger bias values. Dynamics of the pair $\langle \uparrow \downarrow \rangle$ in the junction gives an average normalized maximum velocity of $u \simeq 2$. This pair executes highly stable motion upto a bias value of $\gamma = 0.58$. On increasing the bias values further, large number of fluxons and antifluxons enter into the junction and they make successive reflections at the boundaries which result in a switching of the IVC to

high voltage states. We have not pursued the high voltage states of the junction as the number of fluxons taking part in the dynamics is not fixed. In the reverse sweep of the bias, *i.e.*, on decreasing the bias uniformly in very small steps, we observed hysteresis in the dynamics and finite voltage is observed upto $\gamma = 0.22$. In the inset of the figure the spatial derivative of the phase (φ_x) in the state $\langle \uparrow \downarrow \rangle$ along the junction is plotted. A fluxon on entering from the left end moves towards the right end and an antifluxon on entering from the right end moves towards the left end. For negative values of the *dc* bias, flux penetration is not possible and ZVS (flux-free state) exists for all values of the negative *dc* bias. In this region the junction behaves as a reverse biased diode.

4.3.2 Properties of the junction under a static field

It is important in practical applications to know the behavior of the junction under a static magnetic field especially the dependance of critical current (I_c) on the applied field (H)[3]. In weak static magnetic fields, LJJs behave like weak superconductors and show the Meissner effect. In this regime the critical current decreases linearly with the external field. This behavior exists up to a critical field H_c . At this critical field, magnetic flux in the form of fluxons can overcome the edge barrier effects and can penetrate the junction[94]. For LJJs the first critical field is $H_c = \frac{\Phi_0}{\pi \Lambda \lambda_J}$, where Λ is the effective magnetic thickness of the junction. The dependance of I_c (normalized to maximum Josephson current I_0) on a static magnetic field (H / H_c) applied to a semiannular LJJ of $l = 10$ is shown in Fig.4.4 (solid circles). For comparison, critical current versus magnetic field pattern of a standard rectangular LJJ is presented (open circles). In positive magnetic fields, $I_c(H)$ pattern in semiannular LJJ shows that static fluxons can exist in the junction and a minimum critical current is required to induce flux motion in the junction. In negative fields, the junction behaves differently and the critical current pattern is displaced and indicates that higher critical currents

are required to induce flux motion in the junction.

The threshold values of the *dc* bias (γ_1) allowing propagation of a single fluxon in the junction at various values of the field is shown in Fig.4.5. The threshold value increases on increasing the magnetic field. To determine the threshold values, we have considered the dynamics of a single trapped fluxon in the junction. Below the threshold value propagation is not possible in the junction and the trapped fluxon is annihilated. A small magnetic field applied to the junction can damp the motion of a trapped fluxon. On increasing the field, the fluxon slows down and finally annihilated in the junction. In Fig.4.6, the damping effects of a small field is shown for a trapped fluxon moving under different values of the *dc* bias.

4.4 Demonstration as a fluxon diode

Recently, fluxon based voltage rectifiers[95, 96, 89] have attracted much attention due to the fact that they can find important applications in Josephson digital devices[97]. Various geometries and external conditions are investigated towards this end. The influence of an artificially created ratchet potential on fluxon dynamics in nonuniform LJJ have been studied and voltage rectification properties of these LJJs are demonstrated in recent papers[95, 96]. The net unidirectional motion exhibited by a particle in a ratchet potential is the key factor which is also employed in magnetic flux cleaning applications[98] and in Abrikosov vortex diodes[99]. Ratchet voltage rectifiers based on three junction device[100], asymmetric SQUIDs[101] and on specially engineered arrays[102] have also been investigated in the past. However, working of all these voltage rectifiers critically depend on the ratchet potential and we cannot expect stable performance from these devices as ratchet potentials are highly sensitive to external perturbations. In addition, amplitude ranges of rectification is also limited in these devices and the rectified output does not have a linear relationship with the input.

Detailed analysis shows that the semiannular LJJ embedded with the static magnetic field has the characteristics of a diode. Thus fluxon based diodes can be implemented using this geometry. To demonstrate the rectification effects, we use the pair $\langle \uparrow \downarrow \rangle$ dynamics in the junction. The IVC of the junction shows that fluxons and antfluxons can enter the junction only if the junction is forward biased and fluxon dynamics is not possible in the reverse biased state. Fig.4.3 demonstrate the forward biased state and reverse biased state of the junction. In the forward biased state (positive values of γ in Eq. (4.11), the pair $\langle \uparrow \downarrow \rangle$ is highly stable against perturbations. This pair exists for sufficiently higher values of the dc bias. In the reverse biased state (negative values of γ), fluxons cannot exist in the junction and ZVS exists for all values of the negative bias. We have considered different parameters of the junction and found **that** the pair executes symmetric motion in the junction under the influence of the dc bias.

4.4.1 Rectification of a square wave

To demonstrate rectification effects of an ac current we used a square wave $\gamma(t) = - \left\{ \begin{array}{l} A, \quad 0 \leq t < \frac{T}{2} \\ -A, \quad \frac{T}{2} \leq t < T \end{array} \right\}$ in Eq. (4.11). The period of the square wave is taken much larger than the typical response time of the system (~ 1 ns) so that it is in the adiabatic regime. The amplitude of the ac signal should be sufficiently large to induce flux motion in the junction. In the first half cycle of the square wave, fluxon penetration is not possible and zero voltage exists in the junction. In the second half cycle, one fluxon enter from the left end and one antfluxon enter from the right end and the pair $\langle \uparrow \downarrow \rangle$ moves in opposite directions. The strength of the external field is adjusted in such a way that no more fluxons can enter into the junction. Rectification process is demonstrated in the time domain snapshots of Fig.4.7, where we plot the instantaneous voltage ($V(t)$) across the junction as a function of time. If the amplitude of the ac signal is below a threshold value, ZVS exists in the junction as it can be seen in the left panel of Fig.4.7. In Fig.4.8, we

plot the average voltage (averaged over a period of the input signal) as a function of the amplitude of the square wave. Average voltage increases on increasing the amplitude of the input signal. ZVS exists if the amplitude is below 0.56 (peak to peak, $A = 0.26$) and the output voltage increases linearly in the range 0.6 to 0.7 of the square wave amplitude. At higher values, additional fluxons enter into the junction so that the output is no longer proportional to the input current. We have considered different frequencies of the input signal and found that the pair $\langle \uparrow \downarrow \rangle$ gives stable and reliable results.

4.4.2 Rectification of a sine wave

To study the rectification properties of sinusoidal *ac* currents, we used a sine wave $\gamma(t) = -A \sin(\omega t)$ in Eq. (4.11). The period of the signal is taken much higher than the typical response time of the system. The frequency of the signal used is $\omega = 0.02$. The dynamics of the pair $\langle \uparrow \downarrow \rangle$ is studied under a magnetic field of strength $b = 0.21$ on a junction of length $l = 25$ and dissipation parameter $\alpha = 0.1$. Fig.4.9 shows the time domain voltage pulses in the junction. In Fig.4.10, we plot the average voltage as a function of the amplitude of the sine wave. Average voltage increases on increasing the amplitude of the input signal. We have considered different amplitudes and frequencies of the input signal and could get best results using the pair $\langle \uparrow \downarrow \rangle$.

4.5 Flux-flow state - demonstration as a bidirectional flux-flow oscillator

A FFO[103] is a LJJ in which an applied *dc* magnetic field and a uniformly distributed *dc* bias current drive a unidirectional motion of fluxons. The external static magnetic field required for the FFO operation is generated using a *dc* current in an external coil and is applied perpendicular to the FFO. The magnetic field penetrates the junction in the form of fluxons and their motion through

the junction leads to an electromagnetic radiation. According to the Josephson relation, a FFO biased at voltage V oscillates with frequency $f = (2\pi/\Phi_0) V$ (at about 483.6 GHz/mV)[1]. Due to the losses in the superconducting electrodes, the maximum operational frequency is about $f = \Delta/(e \Phi_0)$ corresponding to the superconducting energy gap Δ . Typically, for Niobium, the gap frequency f is in the range of 650 – 700 GHz. The radiation frequency, which is also related to the fluxon velocity u , by $f = u/d_{fl}$, is determined by the spacing between the moving fluxons d_{fl} . The velocity and density of the fluxons, and thus the power and frequency of the emitted radiation can be controlled by controlling the bias current and the strength of the applied field. The wide-band tunability and narrow line-width of a Josephson FFO make them a perfect on-chip local oscillator for integrated submm-wave receivers [45]. Various geometries [37, 85, 104, 105, 106, 107] and superconducting materials are employed to make high performance oscillators. Using conventional superconducting junctions like $Nb - AlO_x - Nb$, FFOs have been successfully tested and these devices are found to be capable of delivering sufficient power ($\approx 1\mu W$) in the frequency range 120 – 700 GHz.

To study the feasibility of making this device as a FFO[108, 109, 110], we have done a preliminary study and investigated the flux dynamics of a group of fluxons under a large magnetic field. In the proposed oscillator, fluxons enter the junction from the left end and move towards the right end due to the applied bias (in the forward biased state) and on reaching the right end, they are selectively terminated (a passive load of impedance z in series with a diode is connected at the ends of the junction). In a similar way, antfluxons enter the junction from the right end and move towards the left end where they are terminated. In implementing the device, we used a special technique by which fluxons are absorbed selectively at the right end of the junction and antfluxons are absorbed at the left end of the junction. In experiment, this can be realized by using

a load resistor in series with a diode. At the right end, the diode should be placed in such a way that it allows the screening currents associated with the fluxons to go through the load (termination of fluxons) and disallows the screening currents associated with the antfluxons. Similarly at the left end, the diode should allow the screening currents of the antfluxons to go through the load (termination of antfluxons). Thus selective absorption of the fluxons can be achieved at the ends. Fig.4.11(a) shows the snapshots of the spatial profile (φ_x) of a group of fluxons entering from left end and antfluxons from the right end in the junction. Fig.4.11(b) shows the snapshots (φ_x) of the resonant motion of fluxons and antfluxons in the opposite directions in a coherent state. This resonant motion is highly stable and can be a mechanism for constructing the bidirectional oscillators. This resonant, coherent motion also helps to avoid any stray fluxons in the junction thus making the junction a highly tunable device. Fig.4.12(a) shows the corresponding time dependence of the voltage pulse form in the middle of the junction. All the voltage pulses are equally spaced showing spatial coherence in the junction. The calculated frequency spectrum using fast Fourier transform (FFT) of the voltage pulses is shown in Fig.4.12(b). The figure shows the dominant first harmonic of the oscillations at frequency $f = 0.181$ (in normalized units) and the second harmonic at frequency at $f = 0.362$. It is important for practical applications to know the influence of the load (z) on the average output power of the device, in particular to see how it behaves at larger loads. Fig.4.13 shows the dependency of the average output power ($P = VI \equiv \frac{\varphi_x^2}{z}$) obtained from both ends as a function of the load for the values of the junction $l = 20$, $\alpha = 0.1$, $\gamma = 0.4$ and $b = 0.4$. The output power increases and becomes maximum at the impedance matching condition and then decreases slightly on increasing the load. At larger values of the load the output becomes practically independent of the load, which is a desirable feature for using these devices as oscillators.

The main characteristics of this flux-flow oscillator is that both fluxons and antfluxons take part in the dynamics and because of that output can be obtained from both ends. Only in the resonant state we get output from the junction and the resonant state avoids any stray fluxons inside the junction. The oscillator can be tuned by tuning the dissipative junction parameters, applied dc bias currents and the external magnetic field values.

4.6 *rf* field rectification

In this section, a novel method for rectifying alternating magnetic fields is demonstrated using fluxons in semiannular LJJs. An external magnetic field applied parallel to the dielectric barrier of the semiannular junction has opposite polarities at the ends of the junction and supports penetration of opposite polarity fluxons into the junction in the presence of a constant dc bias. When the direction of the field is reversed, flux penetration is not possible and flux-free state exists in the junction. Thus effective rectification of an alternating magnetic field can be achieved in semiannular LJJs. This unique phenomenon is specific to this geometry and can be employed in *rf* SQUID magnetometers.

4.6.1 Introduction

When a LJJ is irradiated with a microwave of frequency f , quantized voltages, $V_n = nhf / 2e$, are observed in the junction [1], where n is an integer and h is the Planck's constant. In IVC, this effects manifests itself as constant voltage steps crossing the zero current axis. The occurrence of these voltage steps is a direct consequence of the ac Josephson effect and the phase coherent pair tunneling in response to an external electromagnetic excitation. Since no voltage other than the quantized values V_n are present, for zero current bias, Josephson tunnel junctions are ideal as voltage standards which require constant voltage output independent of any external perturbations.

In all the previous works on Josephson diodes, rectification properties are studied using alternating bias currents and effective means of rectification of alternating magnetic fields are not discussed. In this section, we demonstrate a novel method to construct fluxon based diodes for rectifying harmonically oscillating magnetic fields. Investigations on a dc biased semiannular LJJ placed in an alternating magnetic field applied parallel to the plane of the dielectric barrier shows that the junction supports flux-flow only in alternate half cycles of the field. The flux linked with the edges of the junction has opposite polarities and support penetration of fluxons and antfluxons simultaneously from opposite ends of the junction under a constant dc bias. When the direction of the field is reversed, flux penetration is not possible and flux-free state exists in the junction. Thus, with this geometry, effective rectification of oscillating fields can be achieved. This is a unique phenomenon associated with the semiannular junctions.

4.6.2 Theoretical model

A LJJ with a semiannular geometry is considered with an external harmonically varying magnetic field applied parallel to the dielectric barrier of uniform thickness[111]. The corresponding dynamical equation is

$$\varphi_{tt} - \varphi_{xx} + \sin \varphi = -\alpha\varphi_t + b \sin(\omega t) \sin(kx) - \gamma \quad (4.23)$$

The boundary conditions of the junction can be obtained from the induced current term $\frac{d\varphi(x)}{dx} = \varepsilon H \sin(\omega t) \cos(kx)$ as

$$\varphi_x(0, t) = \frac{b}{k} \sin(\omega t); \quad \varphi_x(l, t) = -\frac{b}{k} \sin(\omega t) \quad (4.24)$$

These boundary conditions are consistent with the fact that the effective field linked with the junction has opposite polarities at the ends. For sufficiently higher positive values of γ in Eq. (4.23), fluxons can enter the junction from $x = 0$ and antfluxons can enter the junction from $x = l$ (right-end) and they can move in opposite directions. As the boundary conditions are not reflective, after

a transitory motion, fluxons and antfluxons are exited from the junction. When the direction of the field is reversed, fluxon (or antfluxon) penetration becomes impossible and flux-free state exists in the junction. To get some information on the fluxon dynamics, we first determine the potential induced by the external field inside the junction and then find energy change associated with a moving fluxon in the junction. Lagrangian density of Eq. (4.23) with $\alpha = \gamma = 0$ is

$$\mathbf{L} = \left\{ \frac{\varphi_t^2}{2} - \frac{1}{2} \left(\varphi_x - \frac{b}{k} \sin(\omega t) \cos(kx) \right)^2 - (1 - \cos \varphi) \right\} \quad (4.25)$$

Therefore the corresponding potential energy density is (second term of the above equation)

$$\mathbf{U}(x, t) = \frac{1}{2} \left\{ \varphi_x^2 - \frac{2b}{k} \sin(\omega t) \cos(kx) \varphi_x + \left(\frac{b}{k} \sin(\omega t) \cos(kx) \right)^2 \right\} \quad (4.26)$$

The first term is independent of the applied field and the third term is independent of the flux motion in the junction. Therefore the change in the potential due to the combined effect of the applied field and the flux motion in the junction can be determined from the second term as :

$$U(x, t) = - \frac{b}{k} \int_{-\infty}^{+\infty} \varphi_x \sin(\omega t) \cos(kx) dx \quad (4.27)$$

Substituting Eq. (1.38) in (4.28) and integrating, we get

$$U(x_0, t) = - 2 b l \operatorname{sech} \left(\frac{\pi^2}{2 l} \sqrt{1 - u^2} \right) \sin(\omega t) \cos(k x_0) \quad (4.28)$$

For long junctions and at relativistic velocities, $u \sim 1$, Eq. (4.28) becomes

$$U(x_0, t) = - C \sin(\omega t) \cos(k x_0) \quad (4.29)$$

where $C = 2 b l$ is a constant. Eq. (4.29) shows that the potential is oscillating at the frequency of the applied field. This oscillating potential controls the flux flow inside the junction and helps in the rectification of the field.

Energy of the unperturbed sG system is given by Eq. (1.37). Perturbational parameters modulate the velocity of the solitons and may cause to dissipate energy. The rate of dissipation is calculated by computing

$$\frac{d}{dt}(H^P) = [\varphi_x \varphi_t]_0^l + \int_0^l [-\alpha \varphi_t^2 + (b \sin(\omega t) \sin(kx) - \gamma) \varphi_t] dx \quad (4.30)$$

where the first term on the right side account for the boundary conditions. From Eq. (1.38), we get $\varphi_t = -u \varphi_x$ and from Eq. (4.25), we get $\varphi_x^2(0, t) = \varphi_x^2(l, t)$ (symmetric boundary conditions). Substituting these expressions, we find that the first term in the right hand side of the above equation vanishes - a symmetric boundary condition does not change average energy value of a fluxon. Inserting Eq. (1.38) in Eq. (4.30) and following perturbative analysis[15], we get

$$(1 - u^2)^{-3/2} \frac{du}{dt} = -\alpha \frac{u}{\sqrt{1 - u^2}} - \frac{\pi}{4} \{ b \operatorname{sech} \left[\frac{\pi^2 \sqrt{1 - u^2}}{2l} \right] \sin(\omega t) \sin(kx_0) - \gamma \} \quad (4.31)$$

This expression describes the effect of perturbations on the fluxon velocity. In the above equation, the first term in the right-hand side represents the energy dissipation due to internal damping, second term account for the energy change associated with the external field and the third term represents the input power from the bias current.

The effects of a *dc* current on the fluxon dynamics in the presence of the external field is studied using Eq. (4.31). ZVS exists in the junction (flux-free state) when the *dc* bias is below a threshold value. By variation of the soliton position x_0 , from Eq. (4.31), we find the largest possible bias current of zero-voltage state ($u = 0$) to be[90]

$$\gamma_1 = b \operatorname{sech} \left(\frac{\pi^2}{2l} \right) \quad (4.32)$$

This is the threshold value of the applied bias, below which flux propagation is

not possible in the junction. This threshold value depends on the magnetic field and is directly proportional to the field.

4.6.3 IVC in *rf* fields

An oscillating magnetic field is applied parallel to the dielectric barrier of the junction with a constant *dc* bias. In the positive half cycles of the applied field, flux penetration and propagation is possible and finite voltages are observed across the junction. In the negative half cycles of the field, fluxons (or antfluxons) cannot enter the junction due to the repulsive Lorentz force, and zero voltage exists in the junction. Simulations are started with $\varphi = 0$ on a junction of $l = 10$. Time period of the *ac* signals are taken much larger than the typical response time of the system. In the following simulations we assumed the dissipation parameter $\alpha = 0.1$. Fig.4.14 shows the IVC of the junction for different values of the oscillating field amplitudes and at a constant frequency ($\omega = 0.1$). In the figure, applied magnetic field is increasing from the top to the bottom curve in the range 0.50 to 1.50 in steps of 0.1. At lower magnetic fields, critical currents for fluxon penetration is large and the critical current gradually decreases on increasing the field strength.

4.6.4 Rectification of alternating fields

To demonstrate the rectification properties of the junction, we show a series of plots showing the time domain snapshots of voltage pulse forms $v(t)$ as a function of time t . The magnitude of the field should be sufficiently large to introduce fluxons into the junction. At small magnetic fields, fluxons cannot enter the junction and zero voltage exists. For sufficiently higher amplitudes (e.g. $b = 1.0$), fluxon penetration is possible in the positive half cycles and we get finite voltage in the junction. This is shown in Fig.4.15. Rectification takes place in the following way. In the first half (positive part) of the alternating

field, fluxons enter from the left-end and antfluxons enter from the right-end and they move in opposite directions under the influence of the dc bias. The motion of fluxons in opposite directions produces a finite voltage across the junction. During the second half (negative part) of the magnetic field, antfluxon (or fluxon) penetration is not possible due to the repulsive Lorentz force and zero voltage (flux-free state) exists in the junction. Thus effective rectification of the field can be achieved in semiannular Josephson junctions. The number of fluxons taking part in the dynamics (and therefore the output voltage) can be controlled by controlling the strength of the magnetic field.

In Fig.4.16 we plot the average velocity (averaged over a period of the field) as a function of the magnitude of the field for different length of the junctions. A constant dc bias is applied to the junction in order to maintain flux motion in alternate half cycles. In the figure average voltage increases from zero and then increases linearly at higher values of the external field. Thus this device gives output which is linearly proportional to the input.

By reversing the dc bias (*i.e.*, γ to $-\gamma$), positive part of the alternating field can be suppressed. Fig.4.17 represents this rectification and shows negative pulses. In this case, fluxons cannot enter the junction during positive half cycles of the field due to the repulsive Lorentz force while flux penetration and propagation is possible in the negative half cycles.

4.7 Conclusions

In conclusion, we have studied flux-quantum dynamics in a semiannular geometry and the results suggest that this geometry can be used for fabrication of fluxon based diodes for rectification of ac signals, rectification of alternating magnetic fields and for implementing bidirectional flux-flow oscillators. The magnetic field driven transit of a trapped flux quantum under static conditions can find applications in digital transmission lines and in flux cleaning in stacked junctions.

Using vertically stacked junctions, the power associated with the bidirectional flux-flow oscillator can be increased considerably. The *rf* field rectification properties of this device may find important applications in sub-millimeter radio wave astronomy, SQUID magnetometers, SIS mixers, etc. The main advantages of the proposed diodes are (i) very simple to fabricate, (ii) output of the device is linearly proportional to the applied field, (iii) flux motion takes place only in alternate half cycles so that heating and energy losses associated with flux motion can be reduced and (iv) independent of external perturbations. In the proposed LJJ diode, velocity of a fluxon is proportional to the voltage and a nonzero average velocity over a period of the *rf* field means rectification of the field. By properly selecting junction parameters and the *dc* bias, it is possible to rectify fields in different amplitude and frequency ranges.

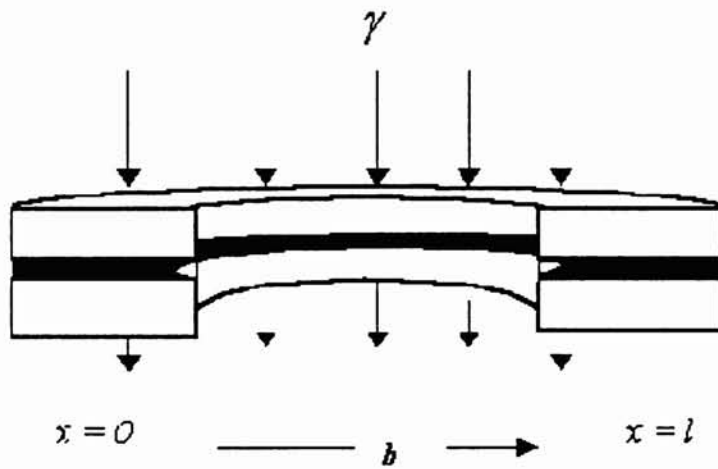


Fig.4.1a Geometry of the semiannular LJJ with the applied field b .

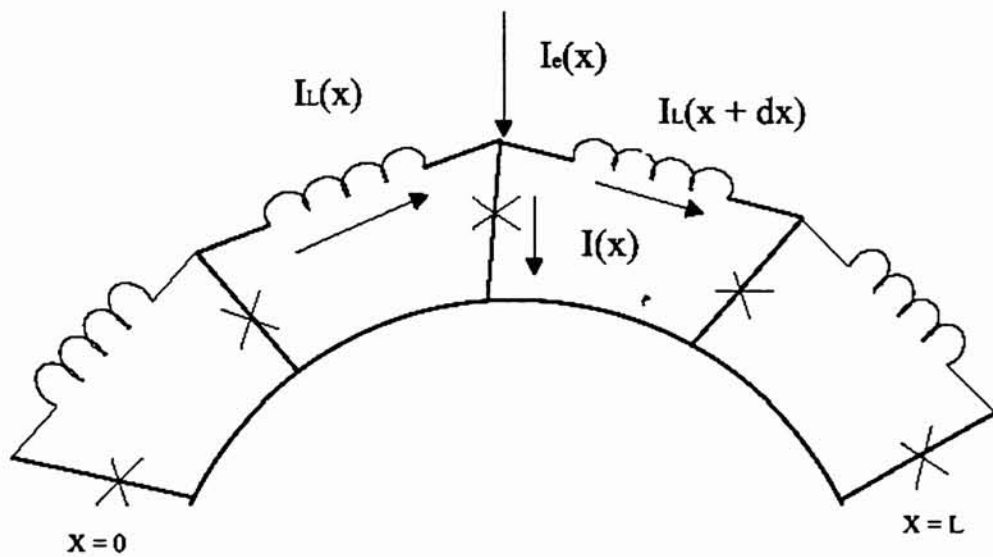


Fig.4.1b Schematic representation of the junction using discrete elements.

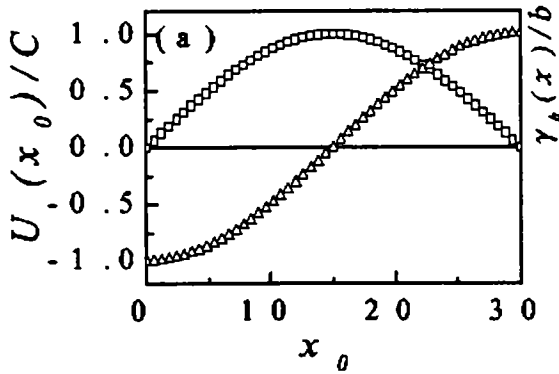


Fig.4.2 Tilted potential $U(x_0)/C$ along the junction as a function of the fluxon coordinate x_0 (triangles) and the field induced term $\gamma_b(x)/b$ (squares) for a junction of $l=30$.

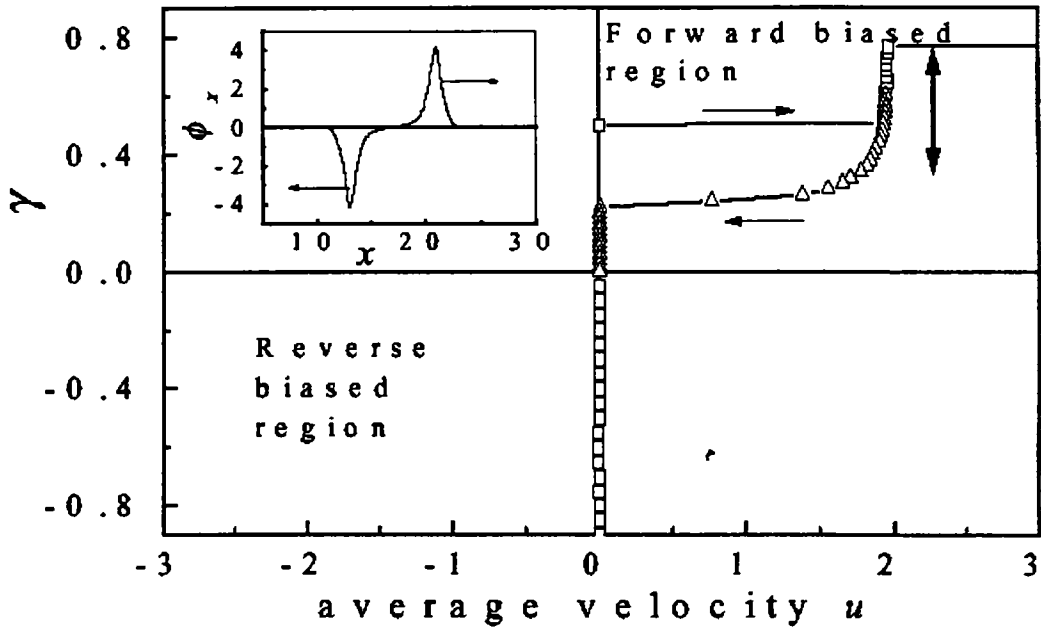


Fig.4.3 Applied dc bias γ versus the average velocity $u=V/(l/2\pi)$ in the junction in the forward-biased state and in the reverse-biased state. Arrows indicate the direction of current sweep. The parameters are $l=34$, $\alpha = 0.1$ and $b=0.1$. Inset in the figure shows the spatial profile (ϕ_x) of the fluxon-antifluxon pair $\langle \uparrow \downarrow \rangle$ in the junction. Parameters are $l=20$, $\alpha = 0.1$ and $b=0.1$.

Chapter 4. Figures

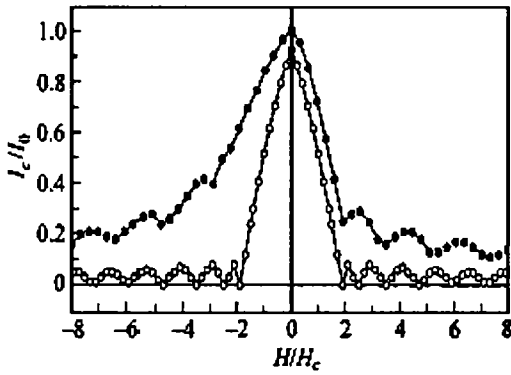


Fig.4.4 Normalized critical current (I_c/I_0) vs. static magnetic field b of a semicircular (\bullet) and rectangular (\dagger) JJ.

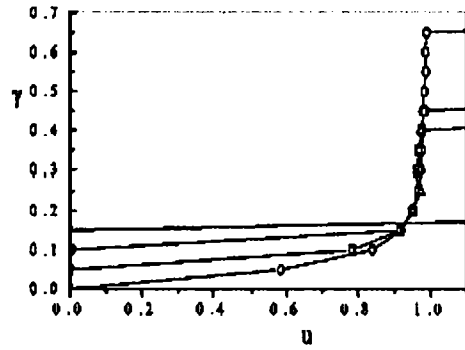


Fig.4.5 IVC of a single trapped fluxon showing threshold value of the bias current at different magnetic field values. ZVS exists below the threshold value. The parameters are $l=20$, $\alpha = 0.05$, $b=0.0$ (circles), $b=0.1$ (squares), $b=0.12$ (up triangles) and $b=0.15$ (down triangles).

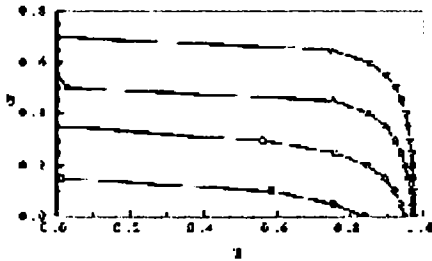


Fig.4.6 Damping effects of the magnetic field on a single fluxon trapped in the junction. Parameters are $l=20$, $\alpha = 0.05$, $\gamma = 0.1$, $b=0.2$ (circles), $b=0.1$ (squares), $b=0.3$ (up triangles) and $b=0.4$ (down triangles).

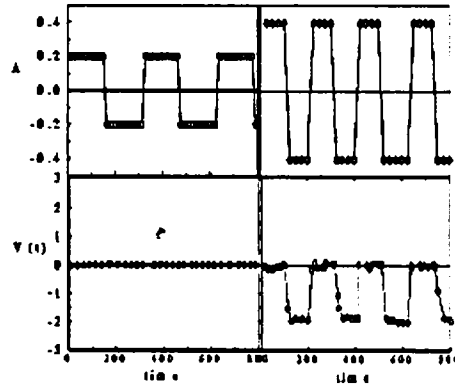


Fig.4.7 Rectification of a square wave. Left panel shows zero output voltage for the input amplitude $A=0.20$. Right panel shows rectified voltage pulses for input amplitude $A=0.32$. Frequency of the signal is $\omega = 0.02$. Parameters are $l=34$, $\alpha = 0.1$, $b=0.11$

Chapter 4. Figures

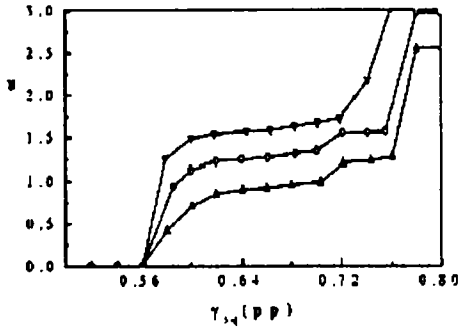


Fig.4.8 Square wave amplitude vs. average velocity in the junction for different input signal frequency. Parameters are $l=34$, $\alpha = 0.1$, $b=0.1$, $A=0.4$, $\omega = 0.02$ (down triangle), $\omega = 0.04$ (up triangle) and $\omega = 0.03$ (circles).

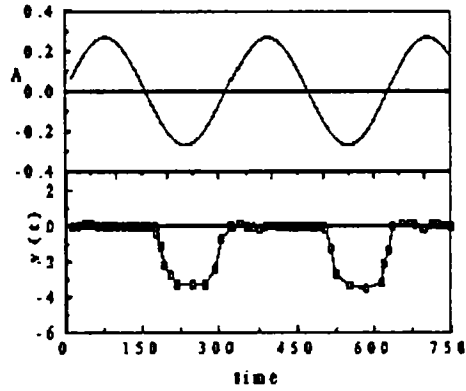


Fig.4.9 Voltage pulses across the junction as a function of time showing rectification of a sine wave. Parameters are $l=25$, $\alpha = 0.1$, $b=0.21$, $A=0.27$ and $\omega = 0.02$.

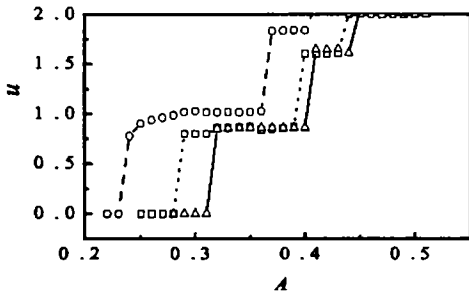


Fig.4.10 Sine wave amplitude vs. average velocity in the junction for different input signal frequency. Parameters are $l=30$, $\alpha = 0.1$, $b=0.1$, $A=0.4$, $\omega = 0.02$ (circles), $\omega = 0.03$ (squares) and $\omega = 0.04$ (triangles).

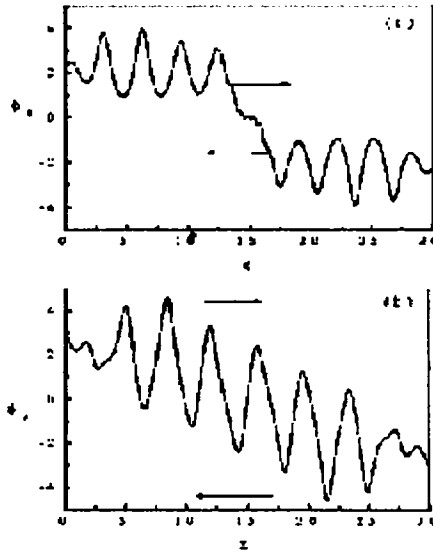


Fig.4.11 (a) Spatial profile (ϕ_x) showing a train of fluxons entering the junction from the left end and a train of antfluxons entering from the right end. (b) Spatial profile showing resonant propagation of fluxons towards the right end and antfluxons towards the left end.

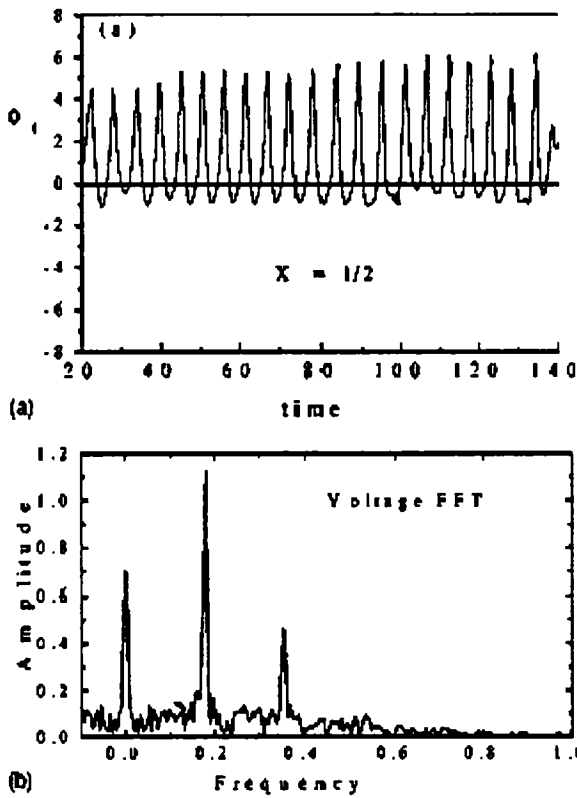


Fig.4.12 (a) Voltage pulses in the middle of the junction. Parameters are $l=20$, $\alpha = 0.1$, $b=0.4$, $\gamma = 0.4$ and $z=0.02$. (b) The corresponding Fourier power spectrum of the voltage pulses. Spectrum has been computed from 4250 data points.

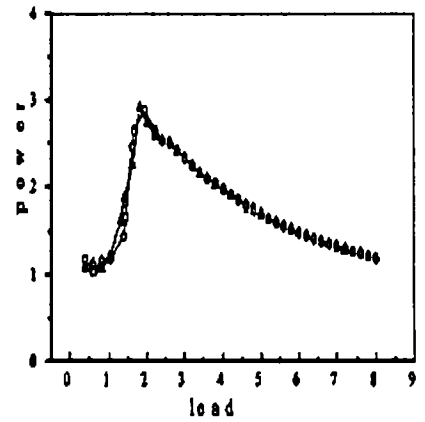


Fig. 4.13 Average output power vs. load z on the left end of the junction (circles) and on the right end of the junction (triangles). Parameters are same as in Fig.4.12.

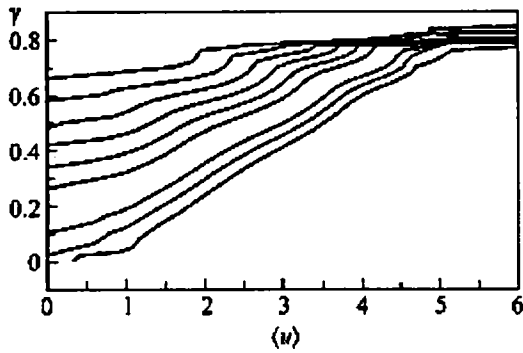


Fig.4.14 Applied *dc* bias vs. average velocity for different values of the applied *rf* field. The parameters are $l=10$ and $\omega = 0.1$. The field strength increases from the top to the bottom curve from 0.5 to 1.50 in steps of 0.1.

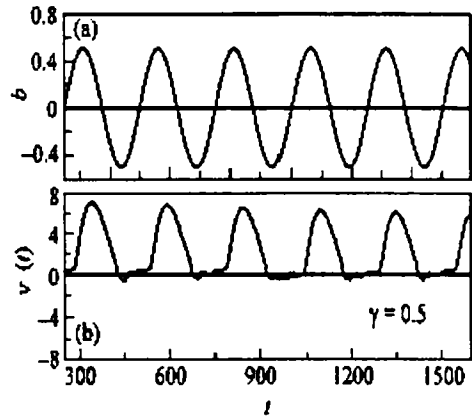


Fig.4.15 Rectification of a *rf* field with $\gamma = 0.5$ on a junction of $l=10$. (a) Applied field of amplitude $b=1.0$ (pp) and frequency $\omega = 0.05$. (b) Output pulse form $v(t)$ as a function of time t .

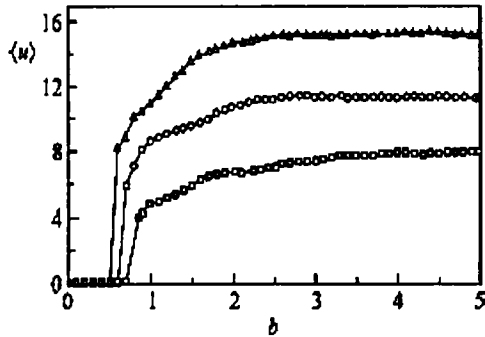


Fig.4.16 Magnetic field amplitude b vs. average velocity for different junctions. The parameters are $\omega = 0.1$, $\gamma = 0.5$, $l=10$ (squares), $l=15$ (circles) and $l=20$ (triangles)

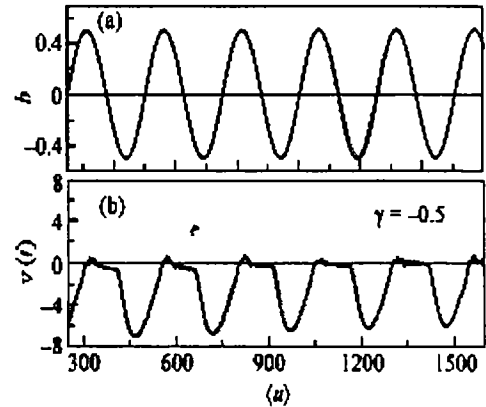


Fig.4.17 Rectification on a junction of $l=10$ with $\gamma = -0.5$. (a) Applied field of amplitude $b=1.0$ (pp) and frequency $\omega = 0.05$. (b) Output pulse form $v(t)$ as a function of time t showing negative pulses.

Chapter 5

Quarter annular Josephson junctions

A new geometry is proposed for Josephson junctions to construct fluxon based diodes. A Josephson junction with a quarter annular geometry terminated with a load resistor at one end exhibits the characteristics of a diode under a homogeneous static magnetic field applied parallel to the plane of the dielectric barrier. The external field interacts with the edges of the junction and make asymmetric boundary conditions that support penetration of fluxons from one end of the junction in the forward biased state and stops fluxon penetration in the reverse biased state. This unique phenomenon is specific to this geometry and can be exploited for making Josephson diodes.

5.1 Theoretical model

A LJJ with a quarter annular geometry is considered with an external static magnetic field applied parallel to the dielectric barrier of uniform thickness. A sketch of the geometry is shown in Fig.5.1. The external field is applied in such a way that it is directed radially at one end of the junction. The external field interacts with the interior as well as through the boundaries of the junction and the flux linked with the junction can be expressed as $d\varphi(x) = \varepsilon (\bar{B} \cdot \bar{n}) = \varepsilon B \cos(kx) dx$ [90, 91, 112, 113], where \bar{B} is the strength of the applied magnetic

field, \bar{n} is a unit vector normal to the direction of propagation and in the plane of the junction, ε is the coupling factor which links the external field with the junction, $k = \frac{\pi}{2l}$ is the spatial periodicity of the magnetic field inside the quarter annular junction. Therefore the induced current in the junction due to the applied field is $\frac{d\varphi(x)}{dx} = \varepsilon B \cos(kx)$. This current term gives a net positive value over the length of the junction and indicates that the induced current does not flow in closed form across the junction. This means that the external field cannot have any influence on the interior part of the junction. Thus a quarter annular LJJ under a static magnetic field with a *dc* bias is modelled with the general perturbed sine-Gordon (sG) partial differential equation[15, 12, 90]

$$\varphi_{tt} - \varphi_{xx} + \sin \varphi = -\alpha\varphi_t - \gamma \quad (5.1)$$

where $\varphi(x, t)$ is the superconducting phase difference between the electrodes of the junction. The boundary conditions of the junction in an external field with a passive load of impedance z , connected at $x = l$ (right end) of the junction are

$$\varphi_x(0, t) = \varepsilon B = b; \quad \varphi_x(l, t) = -\frac{\varphi_t}{z} \quad (5.2)$$

These boundary conditions are consistent with the fact that the effective field linked with the junction makes asymmetric boundary conditions with maximum field value at $x = 0$ (left end) and zero value at the right end of the junction. Due to these boundary conditions, fluxon penetration is possible only from the left end of the junction. For positive values of γ in Eq. (5.1), fluxon penetration is possible (forward biased state) and for negative values, fluxon penetration is not possible and flux-free (Meissner state) exists in the junction (reverse biased state). The passive load (z) connected at the right end can be used to absorb the fluxon chain entering the junction in the forward biased state.

Eq. (5.1) with boundary conditions given by Eq. (5.2) represents the quarter annular LJJ in a magnetic field. To solve these equations, we use an implicit

method. In the following simulations we assumed the dissipation parameter $\alpha = 0.1$ and the load impedance $z = 0.5$.

5.2 General Properties of the junction

5.2.1 *dc* current voltage characteristics

In the absence of the external field ($b = 0$), fluxon dynamics in quarter annular LJJ is same as that in any ordinary rectangular junction. When the field is applied, fluxons enter the junction from the left end in the forward biased state and they move unidirectionally to the right end where they are absorbed by the load. The fluxon-fluxon repulsive force makes the fluxon chain to be uniformly distributed over the length of the junction. The transit of the fluxon chain in the junction produces a nonzero voltage at the load. In the reverse biased state fluxon penetration is not possible and the junction exists in the zero voltage state. Simulations are started with $\varphi = 0$ on a junction of $l = 20$. Fig.5.2 demonstrates the forward biased state and reverse biased state on the IVC of the junction. The applied magnetic field is increasing from the top to the bottom curve in the range 1.0 to 5.0 in steps of 0.4. At low magnetic fields, critical currents for fluxon penetration is large and the critical current gradually decreases on increasing the field strength. Almost all the IV curves are linear which implies that the device gives output that is linearly proportional to the input. Absence of any constant voltage steps in the IVC increases the tunability of the device. At higher fields, unusual zero crossing flux flow steps (ZCFFS) are observed in the IVC[87]. This phenomenon consists in the fact that the IVC of a nonuniform LJJ can cross the $\gamma = 0$ axis at a nonzero voltage. This is due to a preferential direction for fluxon motion contributed by the external field in the junction. In all IVCs, voltage increases linearly with the bias which is an essential characteristics required for making ideal diodes. The spatial derivative of the phase (φ_x) of the fluxons entering the junction from the left end in the forward biased state is shown in

the inset. For negative values of the dc bias, flux penetration is not possible and flux-free state exists for all values of γ . In this region the junction behaves as a reverse biased diode.

5.2.2 Critical current versus magnetic field

It is important in practical applications to know the behavior of the junction in a static magnetic field especially the dependance of critical current (I_c) on the applied field (H) (*cf.* Sec.4.3.2). The dependance of I_c (normalized to maximum Josephson current I_0) on a static magnetic field (H/H_c) applied to a quarter annular LJJ of $l = 10$ is shown in Fig.5.3 (solid circles). For comparison, critical current versus magnetic field pattern of a standard rectangular LJJ is presented (open circles). For positive values of the magnetic fields, $I_c(H)$ pattern in quarter annular LJJ follows exactly with that of the rectangular junction up to the first critical field. At higher fields, critical current crosses the zero current axis and becomes negative indicating the existence of ZCFFS in the junction[87]. ZCFFS is a manifestation of flux-flow in the absence of a bias current. Thus in quarter annular junctions, there is a preferential direction for flux motion under a static parallel magnetic field. For negative values of the magnetic field, the critical current does not decrease on increasing the field and is an indication that flux penetration is not possible in the junction and the junction remains in flux-free state. This typical characteristics - allowing flux penetration in positive fields and preventing flux penetration in negative fields - exhibited by the junction is specific to quarter annular geometry. Thus the quarter annular LJJ supports flux-flow only in one direction and strictly prohibits flux-flow in other direction which is an essential characteristics required for making diodes.

5.3 *ac* bias - demonstration as a diode

In this section, a novel method to construct fluxon based diodes is demonstrated using the quarter annular LJJ geometry. Investigations on a quarter annular LJJ terminated with a load resistor at one end placed in a magnetic field applied parallel to the dielectric barrier shows that the junction supports flux flow in the forward biased state and prevents flux flow in the reverse biased state. The external field make a preferential direction for fluxon motion in the junction and the junction exhibits the characteristics of a diode. This unique phenomenon is specific to this geometry. In the following sections, the rectification properties of the junction using semi-adiabatic sine waves and *ac* square waves are demonstrated.

5.3.1 Rectification of a sine wave

To study the rectification properties of sinusoidal currents, a sine wave $\gamma \equiv \gamma(t) = A \sin(\omega t)$ is used in Eq. (5.1). A signal of frequency $\omega = 0.05$ and amplitude $A = 0.4$ is considered. The amplitude of the *ac* signal should be sufficiently large to induce flux motion in the junction. Fig.5.4 shows the input sine wave and the time domain output voltage pulses $v(t)$, in the junction as a function of time t . Rectification takes place in the following way. During the positive pulse (first half) of the input sine wave, fluxons enter from the left end and they move towards right end where they get terminated by the load resistor. The number of fluxons taking part in the dynamics (and therefore the output voltage) can be controlled by controlling the external magnetic field. In the second half (negative pulse) of the input cycle, fluxon penetration is not possible and zero voltage (flux-free state) exists in the junction. In Fig.5.5, we plot the average velocity (averaged over a period of the input signal) as a function of the amplitude of the sine wave for different length junctions. Average velocity increases linearly on increasing the amplitude of the input signal which is an essential feature required for rectification of the signals. Amplitude ranges of rectification can be improved

by tuning the system and selecting appropriate impedance matching load z .

5.3.2 Rectification of a square wave

To demonstrate rectification of a square wave, we assumed $\gamma \equiv \gamma(t) =$

$-\left\{ \begin{array}{l} A, 0 \leq t < \frac{T}{2} \\ -A, \frac{T}{2} \leq t < T \end{array} \right\}$ in Eq. (5.1) (*cf* Sec. 4.4). Fig.5.6 shows the average voltage as a function of the amplitude of the square wave for different length junctions. Average voltage increases linearly with the input signal amplitude.

5.4 Rectification of *rf* fields

A novel method for rectifying harmonically varying magnetic fields is demonstrated using fluxons in quarter annular Josephson junctions. A Josephson junction with a quarter annular geometry terminated with a load resistor at one end is found to be capable of rectifying alternating fields when biased with a constant *dc* current. The asymmetric boundary conditions facilitate fluxon penetration under a *dc* bias from one end of the junction in alternate half cycles of the applied field. Thus effective rectification of the field can be achieved using quarter annular Josephson junctions. This proposed device is expected to have important applications in millimeter and sub-millimeter radio wave astronomy.

In Chapter 4, a semiannular LJJ geometry is proposed and demonstrated a novel mechanism for fluxon based *rf* field rectifiers[113]. In this section, we demonstrate another method to construct fluxon based diodes for rectifying harmonically oscillating magnetic fields.

5.4.1 Theoretical model

A LJJ with a quarter annular geometry is considered with an external harmonically varying magnetic field applied parallel to the dielectric barrier of uniform thickness. The external field is applied in such a way that it is directed radially at the left end ($x = 0$) of the junction. The field interacts with the interior as well

as through the boundaries of the junction and the flux linked with the junction can be expressed as $d\varphi(x) = \varepsilon (\bar{H} \cdot \bar{n}) = \varepsilon H \sin(\omega t) \cos(kx) dx$ [90, 91, 111, 112]. Where ω is normalized frequency of the oscillating field. Therefore the induced current in the junction due to the applied field is $\frac{d\varphi(x)}{dx} = \varepsilon H \sin(\omega t) \cos(kx)$. This current term gives a net positive value over the length of the junction and therefore cannot circulate in closed form across the junction. It means that the external field does not have any influence on the interior part of the junction. Thus a quarter annular LJJ under a time varying magnetic field with a *dc* bias is modelled with the general perturbed sG partial differential equation

$$\varphi_{tt} - \varphi_{xx} + \sin \varphi = -\alpha \varphi_t - \gamma \quad (5.3)$$

The boundary conditions of the junction in an external field with a passive load of impedance z , connected at $x = l$ (right end) of the junction are

$$\varphi_x(0, t) = \varepsilon H \sin(\omega t) = b \sin(\omega t); \quad \varphi_x(l, t) = -\frac{\varphi_t}{z} \quad (5.4)$$

These boundary conditions shows that the effective field linked with the junction make asymmetric boundary conditions with alternating field values at $x = 0$ and zero value at $x = l$ of the junction. Due to this boundary conditions, flux penetration is possible only from the left end of the junction. For positive values of γ in Eq. (5.3), fluxon penetration is possible as long as the magnetic field linked with the left end of the junction is positive. The transit of the fluxon chain from one end to the other end in the junction produce a nonzero voltage at the load. The passive load (z) connected at the right end can be used to absorb the fluxon chain entering the junction in the positive half cycles of the field. For negative values of the field, fluxon (or antfluxon) penetration is not possible and flux-free state exists in the junction. Eqs. (5.3) and (5.4) represent a quarter annular LJJ in an alternating magnetic field.

To get some information on the fluxon dynamics, we consider the energy

change associated with a moving fluxon in the junction. The energy of the unperturbed sG system is given by Eq. (1.37). Perturbational parameters modulate the velocity of the solitons and may cause to dissipate energy. The rate of dissipation is calculated by computing

$$\frac{d}{dt}(H^P) = [\varphi_x \varphi_t]_0^l - \int_0^l [\alpha \varphi_t^2 + \gamma \varphi_t] dx \quad (5.5)$$

where the first term on the right side account for the boundary conditions. From Eq. (1.38), we get $\varphi_t = -u \varphi_x$. Inserting Eq. (1.38) in Eqs. (1.37) and in (5.5) and following perturbative analysis [15], we get

$$(1 - u^2)^{-3/2} \frac{du}{dt} = \frac{1}{8} \varphi_x(0, t) b \sin(\omega t) - \frac{1}{8z} u \varphi_x^2(l, t) - \alpha \frac{u}{\sqrt{1 - u^2}} + \frac{\pi \gamma}{4} \quad (5.6)$$

In the above equation, the first term in the right-hand side represents the energy input from the field, the second term represents the power transferred to the load, the third term accounts for the energy dissipation due to internal damping and the fourth term represents the input power from the bias current. Substituting a single fluxon solution (Eq. (1.38)) into Eq. (5.6) we obtain the modulation of the velocity by the perturbation as

$$\frac{du}{dt} = \frac{1}{4} \pi \gamma (1 - u^2)^{\frac{3}{2}} - \alpha u (1 - u^2) \quad (5.7)$$

The first term accelerates fluxons and the second term decelerates fluxons in the junction. For sufficiently higher values of the dc bias, this equation shows that fluxons will always be accelerated towards the limiting velocity $u = 1$. Thus maximum velocity that can be attained by fluxons in a LJJ is equal to the Swihart velocity (\bar{c}).

In the numerical simulation, the time period of the ac signals are taken much larger than the typical response time of the system. In the following, we assumed the dissipation parameter $\alpha = 0.1$ and the load impedance $z = 0.5$.

5.4.2 Current voltage characteristics

When external magnetic field is applied, the asymmetric boundary conditions created by the field causes fluxons to enter the junction from the left end under a positive dc bias in the positive half cycles of the oscillating field. These fluxons move unidirectionally to the right end where they are absorbed by the load. In the negative half cycles of the field, fluxons (or antfluxons) cannot enter the junction and zero voltage exists. Simulations are started with $\varphi = 0$ on a junction of $l = 10$. Fig.5.7 shows the IVC of the junction for different values of the field magnitudes and at a constant frequency. In the figure, applied magnetic field is increasing from the top to the bottom curve in the range 1.50 to 3.30 in steps of 0.2. At lower magnetic fields, critical currents for fluxon penetration is large and the critical current gradually decreases on increasing the field strength. Constant voltage steps V_n at integer values of n are observed in all the IV curves. This constant voltage steps corresponds to integer number of fluxons taking part in the dynamics. Fig.5.8 shows IVC of the junction at a constant magnitude of the field and at different frequencies. Constant voltage steps are observed in all the curves.

5.5 Rectification of alternating fields

To demonstrate the rectification properties of the device, we show a series of plots showing the time domain snapshots of voltage pulse forms $v(t)$ as a function of time. The magnitude of the field should be sufficiently large to introduce fluxons into the junction. At small magnetic fields, fluxons cannot enter the junction and zero voltage exists. To show this, we have considered a field of frequency $\omega = 0.05$ and amplitude $b = 0.4$. For sufficiently higher amplitudes (*e.g.* $b = 1.5$), fluxon penetration is possible in the positive half cycles and we get finite voltage in the junction. Fig.5.9 represents this process. The number of fluxons taking part in the dynamics (and therefore the output voltage) can be controlled by controlling

the strength of the magnetic field. At higher values of the field (higher than H_c and at smaller values of the dc bias), flux penetration takes place in both half cycles of the field and therefore we get a mean nonzero voltage in the junction.

In Fig.5.10 we plot the average velocity (averaged over a period of the field) as a function of the magnitude of the field for different length junctions. Discrete steps are observed in all the plots which corresponds to integer number of fluxons taking part in the dynamics. Three typical regions are clearly seen in all the plots. Zero voltage exists in the first region (I) where flux penetration and propagation is not possible in the junction (flux-free state). In the second region (II), fluxons penetrate the junction and move unidirectionally to the other end constituting a finite voltage (active region). The switch to a different voltage state (jumps) is due to additional fluxons taking part in the dynamics. In the third region (III), the magnitude of the external field is very large and fluxons enter the junction in the positive half of the field and antfluxons enter in the negative half of the field. So both fluxons and antfluxons take part in the dynamics over a period of the field so that positive and negative voltages are observed in a cycle making average zero voltage (overdriven region). Amplitude ranges of rectification can be improved by tuning the system and selecting appropriate impedance matching load z .

By reversing the dc bias (*i.e.*, γ to $-\gamma$), positive part of the alternating field can be suppressed. In this case, fluxons cannot enter the junction due to the repulsive Lorentz force while antfluxons will be accelerated to the interior of the junction. Therefore antfluxons take part in the dynamics and we get negative voltage pulses.

5.6 Conclusions

In conclusion, this chapter contains theoretical predictions of rectification of ac signals using fluxons in quarter annular LJJ's by applying an external homoge-

neous magnetic field and rectification of rf fields by applying a constant dc bias across the junction. This diode may find important roles in telecommunications, signal processing circuits, SQUID magnetometers, SIS mixers, RSFQ logic circuits, in the detection of rf fields, in sub-millimeter radio wave astronomy and in many other digital applications of LJJ devices. The mechanism of rectification discussed is entirely different from that of the ratchet potential based diodes. By properly selecting junction parameters and the applied field strength, it is possible to rectify signals in different amplitude ranges. The junction is expected to give very good results for adiabatic ac signals.

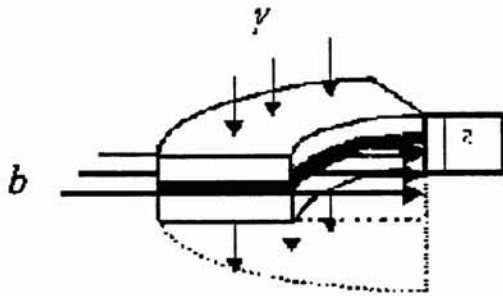


Fig. 5.1 Geometry of the quarter annular LJJ in a parallel magnetic field b .

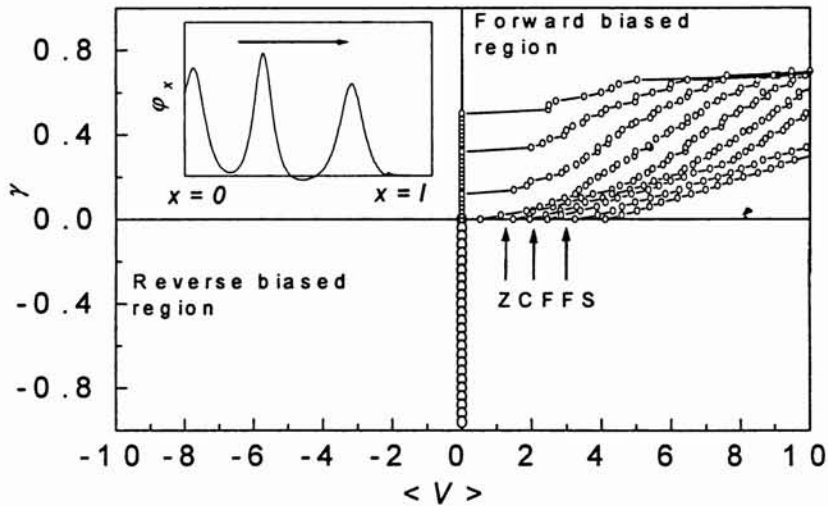


Fig.5.2 IVC of the quarter annular junction showing forward-biased region and reverse-biased region. The applied field, b , is increasing from the top to bottom curve in the range 1.0 to 5.0 in steps of 0.4. The parameters are $l=20$, $\alpha = 0.05$ and $z=0.5$. Inset in the figure shows spatial profile of the fluxons moving in the junction.

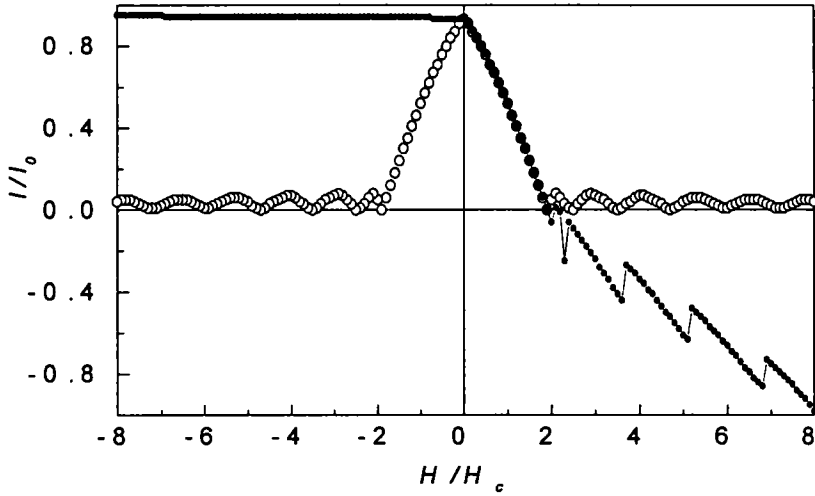


Fig. 5.3 The dependence of the normalized current I_c on the static magnetic field H applied to a quarter annular LJJ (solid symbols) and critical current pattern of a rectangular junction (open symbols).

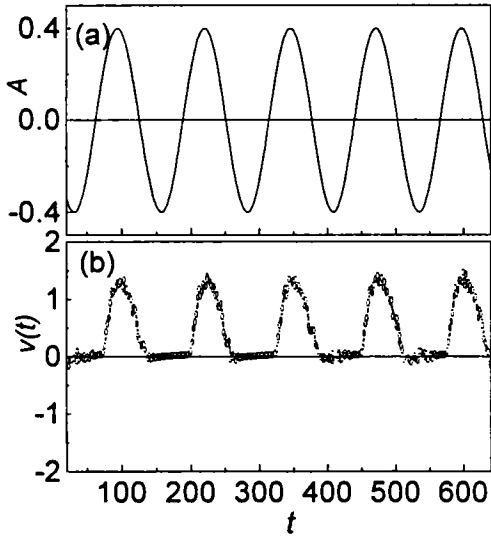


Fig.5.4 Rectification of a sine wave. (a) Input sine wave of amplitude $A=0.4$ and frequency $\omega =0.05$. (b) Output voltage pulse form across the junction with parameters $l=10$, $\alpha =0.05$ and $z=0.5$.

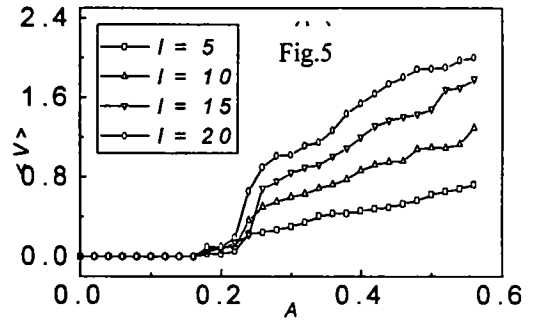
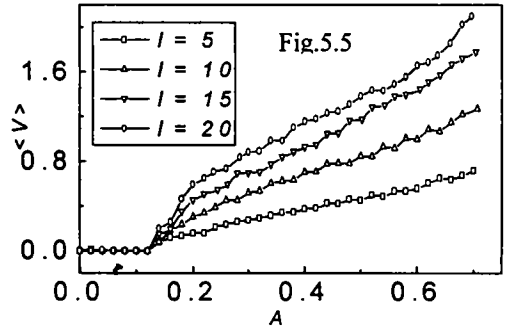


Fig.5.5 Sine wave amplitude (A) vs. average velocity in different length junctions. Parameters are same as in Fig.5.4.

Fig.5.6 Square wave amplitude (A) vs. average velocity in different length junctions.

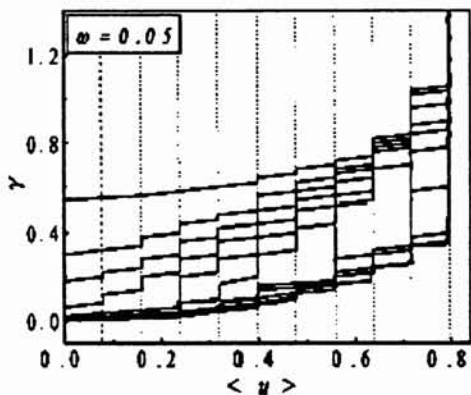


Fig.5.7 Applied dc bias vs. average normalized velocity for different values of the field. The field strength increases from top to the bottom curve from 1.5 to 3.3 in steps of 0.2. Parameters are $l=10$, $\alpha = 0.05$ and $z = 0.5$

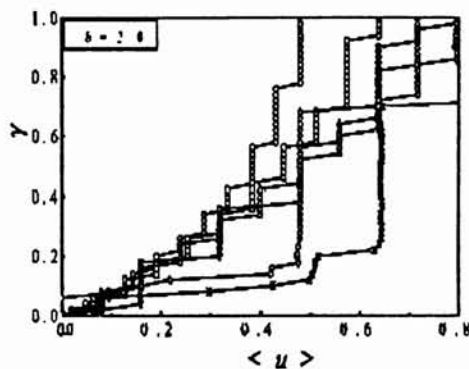


Fig.5.8 Applied dc bias vs. average normalized velocity for different frequencies of the field. Frequency increases from left to right from 0.03 to 0.4.

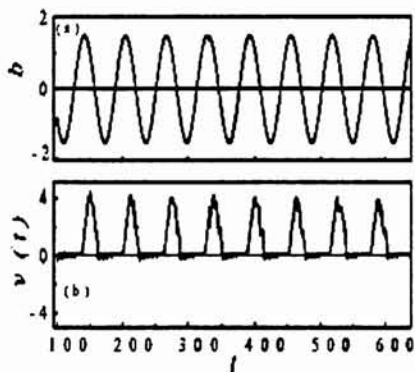


Fig. 5.9 Rectification of a rf field with $\gamma = 0.5$ on a junction of length $l=10$. (a) Applied field of amplitude $b=1.5$ and frequency $\omega = 0.1$. (b) Output voltage form showing positive pulses.

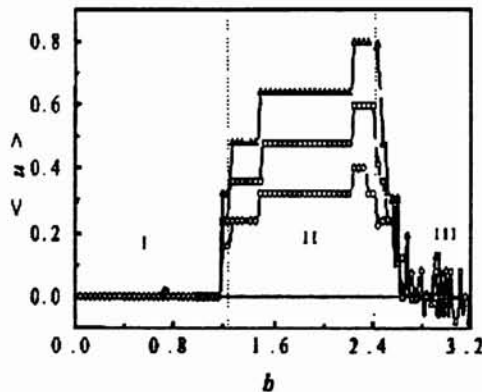


Fig.5.10 Magnetic field amplitude b vs. average velocity for different junctions. Parameters are $\omega = 0.05$, $\alpha = 0.05$, $z = 0.5$, $l=10$ (circles), $l=15$ (squares), and $l=20$ (triangles).

Chapter 6

Quarter annular Josephson flux-flow oscillator

Using quarter annular geometry a Josephson flux-flow oscillator is constructed and found that the quarter annular geometry provides several advantages for making Josephson flux-flow oscillators over a rectangular geometry. An external static magnetic field applied parallel to the dielectric barrier of a quarter annular junction has asymmetric boundary conditions that makes a preferential direction for flux-flow even in the absence of a dc bias. When the applied field is increased above a threshold level, static field distribution become unstable and gives rise to a train of fluxons moving unidirectionally from one end to the other end of the junction. The speed and density of the flux-flow can be controlled by controlling the field or using a small dc bias transverse to the junction. The output power of the oscillator is found to be directly proportional to the applied field. Low power consumption, increased output power, higher tunability and decreased line-width are some of the advantages of the proposed oscillator compared to a standard rectangular flux-flow oscillator. This proposed device will be useful in millimeter and sub-millimeter wave experiments.

6.1 Introduction

The spectral line-width of a FFO can be due to junction inhomogeneities, perturbations caused by trapped flux-quanta and chaos in the dynamical behavior of the fluxon chain. The internal degrees of freedom in the moving fluxon chain may give a significant contribution to the line-width. Thus any local variations of the fluxon spacing in the flux-flow mode will change the radiation frequency of the FFO. In general, the line-width Δf of the Josephson radiation is determined by thermal fluctuations of the current passing through the junction. Assuming a Nyquist noise spectrum for a current-biased short Josephson tunnel junction, the full line-width at half power is given by $\Delta f = (4\pi k_B T R_D^2) / (\Phi_0^2 R_s)$, where k_B is the Boltzmann's constant and T is the temperature[114]. The line-width depends on the differential resistance $R_D = dV/dI$ at the junction bias point and the static resistance $R_s = V/I$, where I is the bias current through the junction. A free running FFO with line-width considerably below 1 MHz has been constructed and measured near 450GHz [115]. Currently available possibilities for reducing the line-width are to mix two such devices or to drive on by an external oscillator. Recently, the feasibility of phased locking of the FFO to an external oscillator was demonstrated experimentally [116].

Investigations on a quarter annular LJJ under a static magnetic field show that the flux linked with the junction has asymmetric boundary conditions and make a preferential direction for flux motion in the junction. The preferential direction in the flux-flow due to the external field decreases the internal degrees of freedom of the fluxons and make a highly coherent and steady flux-flow in the junction. It is observed that above a threshold value of the applied field, static solution becomes unstable and gives rise to a train of fluxons moving unidirectionally from one end to the other end of the junction. The repulsive fluxon-fluxon interactive force pushes the fluxons in the chain to flow from one end to the other end of the junction. The flux motion is accelerated when a small *dc* bias is applied

transverse to the junction. Extensive numerical results with analytical predictions are presented to demonstrate that quarter annular geometry reduces the small current instability region present in the rectangular junction and leads to a laminar flow regime where the voltage wave form is periodic giving the oscillator minimal spectral width. The low electrical power requirements of the proposed device make them suitable in on-chip applications.

6.2 Theoretical aspects

A LJJ with a quarter annular geometry proposed in Chapter 5 is considered with an external static magnetic field applied parallel to the dielectric barrier of uniform thickness. The external field is applied in such a way that it is directed radially at the left-end ($x = 0$) of the junction. A quarter annular LJJ under a static magnetic field with a dc bias is modelled with the Eqs. (5.1) and (5.2) (*cf.* Sec.5.1).

At higher values of the applied field, continuous flow of fluxons takes place and a moving dense fluxon chain corresponds to the so-called flux-flow regime. If the distance between fluxons is order ~ 1 , then the soliton solution is not relevant and the corresponding solution of the unperturbed sG equation is a cnoidal wave[117]

$$\varphi_{cn} = \pi - 2 \operatorname{am} \left(\frac{x - \xi(t)}{k\sqrt{1 - u^2}} \right) \quad (6.1)$$

where $\operatorname{am}()$ is the elliptic amplitude function, u is the velocity of the fluxon chain and k is the elliptic modulus $0 < k < 1$.

6.2.1 Static and dynamic solutions

For small values of b , no voltage is observed in the junction (at $\gamma = 0$) and the corresponding solution of Eq. (5.1) is a time independent value of φ . In this case, time derivatives of the sG equation disappear so we obtain the modified pendulum equation

$$\frac{d^2\varphi}{dx^2} = \sin \varphi \quad (6.2)$$

together with the boundary conditions, $\frac{\partial\varphi}{\partial x} |_{x=0} = b$ and $\frac{\partial\varphi}{\partial x} |_{x=l} = 0$. This equation can be integrated to obtain the solution[105]

$$\varphi(x) = -2 \arctan \left(\frac{1}{\sinh(x - x_1)} \right) \quad (6.3)$$

where $x_1 = \ln \left(\frac{2}{b} - \sqrt{\frac{4}{b^2} - 1} \right)$. This static solution has a half fluxon content and exists up to the critical value $b_c = 2$. Above this value, static solution changes to a full fluxon. The fluxon penetration into the junction is shown in Fig.6.1. For values $b > b_c$, fluxons penetrate the junction and the generated fluxons can move towards the load if their velocity exceeds the critical value $u_{cr} = \alpha \ln |b|^{-1}$ [53].

6.2.2 Fluxon-fluxon repulsive force

As it is well known, fluxons with like polarities repel each other and if they are nonrelativistic, they stay at a distance much larger than their proper size (which is ~ 1 in the notation adopted). In this case the effective fluxon-fluxon repulsive interaction potential is $U_{ff}(X) \propto e^{-X}$, where X is distance between the fluxons [118]. Due this repulsive interaction, fluxons will be separated by a distance which can be calculated by considering fluxons as a particle and using the equation of motion

$$\frac{d^2X}{dt^2} + \alpha \frac{dX}{dt} - 2 e^{-X} = 0 \quad (6.4)$$

if the fluxons move at a steady velocity, the above equation can be approximated as

$$\alpha \frac{dX}{dt} - 2 e^{-X} = 0 \quad (6.5)$$

which can be solved to get $X = \ln\left(\frac{2t}{\alpha}\right)$. Thus the distance between fluxons increases with time. So in a fluxon chain, individual fluxons will be separated by a

constant distance.

6.2.3 Laminar flux-flow - Energetic analysis

In this section simple analytical models describing a smooth phase flow of the fluxon chain is introduced which is referred to as laminar flow [106] for which temporal behavior is periodic. We approximate the laminar flow by taking the variational approach and consider the high voltage limit in which the small changes in the instantaneous voltage due to the changes in the parameters x and t are neglected to a first approximation. The variational analysis is made on the basis of conservation of energy by the sG Hamiltonian. The energy of the unperturbed sG system is Eq. (1.37). Perturbational parameters modulate the velocity of the solitons and may cause to dissipate energy. The rate of dissipation is calculated by computing

$$\frac{d}{dt}(H) = [\varphi_x \varphi_t]_0^l - \int_0^l [\alpha \varphi_t^2 + \gamma \varphi_t] dx \quad (6.6)$$

where the first term on the right side account for the boundary conditions. From Eq. (1.38), we get $\varphi_t = -u \varphi_x$. Inserting Eq. (1.38) in Eqs. (6.6) and following perturbative analysis [15], we get

$$\frac{d}{dt}(H) = -b \varphi_t(0, t) - \frac{1}{z} \varphi_t^2(l, t) - \alpha \int_0^l \varphi_t^2 dx - \gamma \int_0^l \varphi_t dx \quad (6.7)$$

In the above equation, the first term in the right-hand side represents the energy input from the field at the left-end of the junction, the second term represents the power transferred to the load, the third term accounts for the energy dissipation due to internal damping and the fourth term represents the input power from the bias current. In the steady state, the average rate of change of the Hamiltonian is zero, $\left\langle \frac{dH}{dt} \right\rangle = 0$, so the above equation becomes

$$b \langle \varphi_t(0, t) \rangle + \frac{1}{z} \langle \varphi_t^2(l, t) \rangle + \alpha \left\langle \int_0^l \varphi_t^2 dx \right\rangle + \gamma \left\langle \int_0^l \varphi_t dx \right\rangle = 0 \quad (6.8)$$

The average voltage is given by the formula

$$V = \langle \varphi_t \rangle = \frac{1}{T} \int_0^T \varphi_t(x, t) \quad (6.9)$$

For sufficiently large values of b , we assume $\langle \varphi_t^2 \rangle = \langle \varphi_t \rangle^2 \equiv V$, thus the Eq. (6.9) can be written as

$$bV + \frac{V^2}{z} + \alpha V^2 l + \gamma l V = 0 \quad (6.10)$$

giving the mean voltage

$$V = -\frac{z(b + \gamma l)}{(1 + \alpha l z)} \quad (6.11)$$

the negative sign indicates that fluxons are accelerated towards the right-end. Thus the ZCFFS voltage ($\gamma = 0$) can be obtained from the above equation as $V_{ZCFFS} = -\frac{z b}{(1 + \alpha l z)}$. The power is calculated as

$$P = VI = \frac{V^2}{z} = \frac{z(b + \gamma l)^2}{(1 + \alpha l z)^2} \quad (6.12)$$

Thus in a quarter annular junction output power depends on the external field.

6.3 General properties of the junction

The dependance of critical current (I_c) on the applied field (H) of the quarter annular junction is shown in Fig.5.3. The quarter annular LJJ supports flux-flow only in one direction and strictly prohibits flux-flow in other direction which is an essential characteristics required for making FFOs.

6.3.1 *dc* IVC of the oscillator

When the applied external magnetic field is increased above the threshold value b_c , fluxons penetrate the junction from the left-end and these fluxons move uni-

directionally to the right-end due to the fluxon-fluxon repulsive interaction. The continuous unidirectional fluxon transit produce voltage pulses at the load which can be averaged over a time. To get a detailed account of the internal fluxon dynamics, we numerically simulated the FFO using the sG equation. Simulations are started with $\varphi = 0$ on a junction of $l = 10$. IVC can reveal the details of the flux dynamics in the junction and to plot the IVC, we calculate the required data from the simulation. Fig.6.2 shows the IVC of the quarter annular junction at different values of the magnetic field. In the figure, applied magnetic field is increasing from the top to the bottom curve in the range 1.0 to 5.0 in steps of 0.5. At lower magnetic fields, critical current for fluxon penetration is found to be large and the critical current gradually decreases on increasing the field strength. In all curves, average voltage increases linearly with the bias and absence of any constant voltage steps in the IVC indicate the high tunability of the device. At higher magnetic fields, finite voltage is observed at zero bias current indicating the existence of ZCFFS. This is a manifestation that even in the absence of a bias current fluxons can move unidirectionally from one end to the other end of the junction. The voltage values calculated from Eq. (6.11) along with numerically simulated values are shown in Fig.6.1a. Both values agree exactly in the high voltage limit.

6.3.2 Magnetic field - voltage characteristics

The influences of an external field on the dynamical properties of the junction are studied in the absence of a dc bias ($\gamma = 0$). At low magnetic fields, the static solution in the junction has only a half-fluxon content. This static solution exists up to a critical value of the magnetic field $b_c = 2.0$, Above this value, static solution become unstable and gives rise to a train of fluxons moving in the junction. In Fig.6.1, static distribution of the flux profile in the junction at $b = 1.9$ (circles) and dynamic distribution of the fluxons at $b = 2.1$ (solid line)

are presented. This figure illustrates the process of fluxon penetration into the junction at a high magnetic field. The data were obtained by numerical solution of Eqs. (6.1) and (6.2) which automatically takes into account the fluxon interaction with the edges and with each other. The unidirectional flow of fluxons produce an average voltage across the junction. The magnetic field (b) versus average voltage ($\langle u \rangle$) in a quarter annular junction is presented in Fig.6.3a. For generality, different lengths of the junctions are considered. Average voltage is zero below the critical value b_c and linearly increases with the applied field above the critical value.

In Fig.6.3b, the magnetic field versus average velocity on a junction of length $l = 10$ at different values of the dissipation parameter α , are plotted. These graphs demonstrates that in quarter annular junctions, due to the asymmetrically linked magnetic field, unidirectional flux-flow takes place even in the absence of a dc bias. This peculiar property of the quarter annular junctions make them superior in performance as a FFO. A quarter annular LJJ when fabricated as FFO require less power and will be suitable for on-chip integration with other devices. Rectangular junctions require much higher power for operation and the heating effects associated will have a negative influence on the performance in integrated devices.

6.4 Flux-flow characteristics

6.4.1 Spatial and temporal behavior

Spatial coherence of the fluxon chain in flux-flow oscillators can reduce the line-width of the radiation considerably. To demonstrate spatial coherence of the flux-flow in quarter annular junctions, we present a series of plots. In Fig.6.4, we present the spatial coherence in terms of the fluxon profiles φ_x and in terms of the voltage pulses φ_t along the length of the junction (solid lines). For comparison, the spatial profiles with the corresponding parameters in a rectangular

oscillator is presented (dotted lines). The uniformly increasing amplitude of the pulses shows that fluxons are uniformly accelerated in quarter annular junctions. The spatial behavior in a quarter annular junction is found to be regular and highly periodic. In rectangular junction, there is a gradual decrease in the amplitude of the fluxons as they reach the load. This means that fluxons are slightly decelerated in a rectangular junction as they reach the load. This is due to the repulsive interaction of the fluxons with the external field linked with the right-end of the junction. In quarter annular junctions, there is no flux linked at the right-end and therefore there is no deceleration of the fluxons as they reach the load. The well defined profiles in the quarter annular junction represent highly ordered and regular flux-flow. Irregular behavior is observed in the rectangular junctions which is a manifestation that some form of chaos is present in the rectangular junctions. Thus a quarter annular junction is expected to give minimum spectral width compared to a rectangular junction. The time dependence of voltage pulse forms in the load is shown in Fig.6.5. The voltage pulses are periodic with well defined pulse peaks. These pulse forms indicate the ordered smooth flow of fluxons in the junction with constant spacing between the individual fluxons. The periodic nature indicates that flux-flow takes place in a highly coherent form. A highly rigid fluxon chain is transported through the junction and is stable against perturbations. The calculated frequency spectrum using fast Fourier transform (FFT) of the voltage pulses is shown in Fig.6.5a. The dominant first harmonic is seen along with the small second and third harmonic contents. Absence of any noise signals in the spectrum proves the assumption that in quarter annular junctions flux-flow takes place in a highly coherent and ordered form.

6.4.2 Output power

It is found that the output power, $P(t) = z (\partial\varphi/\partial x)^2(l, t)$, on the load z as function of time t is periodic. The periodic nature of pulse forms and the periodic

distribution of the power intensity in the load is also a manifestation of the coherence and tunability of the oscillator. The periodic nature of the power content on the load have important contribution in increasing the average output power of the device. It is important in practical applications to know the influence of load z on the average output power of the oscillator. Impedance matching load can increase the output power of the oscillator. Fig.6.6 shows the dependency of the average output power as a function of the load at the bias point $\gamma = 0.3$ and at the magnetic field $b = 2.0$. Output power is calculated as $P = (\partial\varphi(l)/\partial t)^2/z$. Quarter annular and rectangular junctions of different lengths are studied. It is observed that fine impedance matching can be achieved in quarter annular junctions. Higher output power is obtained at the impedance matching load. In rectangular junctions, exact impedance matching cannot be achieved. At larger loads, output power becomes practically independent of the load which is a desirable feature of these devices as oscillators. In all cases, average output power in a quarter annular junction is clearly larger than that of a rectangular junction.

6.5 Two coupled flux-flow oscillator

In recent years, a great deal of attention has been attracted to different kinds of solid-state multilayered systems. Multilayers are attractive because it is often possible to multiply a physical effect achieved in one layer by N times (N is the number of layers). This can be exploited in the fabrication of solid-state devices. Also, multilayered solid-state systems show a variety of physical phenomena which result from the interaction between individual layers. In this section, two vertically stacked inductively coupled quarter annular junctions are studied. Analysis shows that in-phase flux-flow mode in coupled junctions increases the output power and stability of the oscillator.

6.5.1 Theoretical model

LJJ operated in the flux-flow mode were found to be attractive in the sub-mm wave-band tunable local oscillators. The performance of such an oscillator is limited by the rf power available for pumping a nonlinear detector. It is well known that higher radiation power can be achieved by using an array of coherently operating devices. It has been shown that in a stack of magnetically coupled LJJ, chains of fluxons moving in different layers can be mutually phase locked. In a two-fold stack, both in-phase and out-of-phase locked modes can be obtained[36, 119]. It has been predicted that the in-phase flux-flow mode multiplies the power of flux-flow oscillator whereas the out-of-phase mode doubles the main radiation frequency of the oscillator. Fluxon dynamics in a two coupled stack is described by the equations[41, 107, 120]

$$\begin{aligned}\varphi_{tt} - \frac{1}{1-S^2}\varphi_{xx} + \sin \varphi &= -\alpha\varphi_t - \gamma - \frac{S}{1-S^2}\psi_{xx} \\ \psi_{tt} - \frac{1}{1-S^2}\psi_{xx} + \sin \psi &= -\alpha\psi_t - \gamma - \frac{S}{1-S^2}\varphi_{xx}\end{aligned}\tag{6.13}$$

where S ($-1 < S < 0$) is a dimensionless coupling constant. The boundary conditions of the stack in an external field with a passive load of impedance z , connected at $x = l$ (right end) of the junction are

$$\begin{aligned}\varphi_x(0, t) &= \varepsilon H = b; & \varphi_x(l, t) &= -\frac{\varphi_t}{2z} \\ \psi_x(0, t) &= \varepsilon H = b; & \psi_x(l, t) &= -\frac{\psi_t}{2z}\end{aligned}\tag{6.14}$$

These boundary conditions are consistent with the fact that the effective field linked with the junction make asymmetric boundary conditions with maximum field value at $x = 0$ (left end) and zero value at the right end of the junction. Due to these boundary conditions, fluxon penetration is possible only from the left end of the junction. For positive values of γ in Eq. (6.13), fluxon penetration is possible (forward biased state) and for negative values, fluxon penetration is not possible and flux-free (Meissner state) exists in the junction (reverse biased state). The passive load (z) connected at the right end across the two junction

can be used to absorb the fluxon chain entering the junction in the forward biased state.

6.5.2 Numerical results

Eq. (6.13) with boundary conditions given by Eq. (6.14) represents the two coupled quarter annular LJJ in a magnetic field. To solve these equations, we use an implicit method. In the following simulations we assumed the dissipation parameter $\alpha = 0.1$ and the load impedance $z = 0.5$. The output power of the LJJ stack operating in the in-phase mode is investigated. Detailed analysis shows that in-phase flow of fluxons decreases the noise in the junction and make highly ordered coherent flow of fluxons. The in-phase flow of fluxons can be achieved using highly homogeneous junctions under uniform boundary conditions. The characteristic propagation velocity in the in-phase mode is given by the expression $\bar{c}_+ = \frac{\bar{c}_0}{\sqrt{1+S}} > \bar{c}_0$ and the characteristic propagation velocity in the out-of-phase mode is given by the expression $\bar{c}_- = \frac{\bar{c}_0}{\sqrt{1-S}} < \bar{c}_0$. The power of a flux-flow oscillator is expected to be proportional to the square of the amplitude of the voltage at the edge of the junction facing the load. In the numerical experiment the coupling parameter was chosen as $S = -0.5$. The output power of the oscillator is calculated across the two stacks of the junction. The increased output voltage obtained from the oscillator is presented in Fig.6.7. This shows how the coupling of different junction increases the average output power of the oscillator.

6.6 Conclusions

A simple and reliable geometry is proposed for constructing a Josephson FFO. This geometry is found to be advantageous over standard rectangular geometry in power consumption, spectral purity and in output power. In quarter annular FFOs, as opposed to rectangular FFOs, output power depends directly on the

applied field. In rectangular junctions, output power depends on the field only at small values and is independent of the applied field at larger values. The asymmetric boundary conditions created by the external field make a highly coherent and regular flux-flow even at zero current bias. This new results indicate that quarter annular geometry will substantially improve the performance of a FFO. Using an exponentially tapered dielectric barrier, as suggested and demonstrated in [105, 106], the performance and tunability of the device can be increased considerably. Using vertically stacked junctions, power of the oscillator can be increased further. Flux-flow in the absence of an applied bias can be utilized in the construction of a field to voltage transducer which can be used to detect magnetic fields higher than the first critical field of the junction.

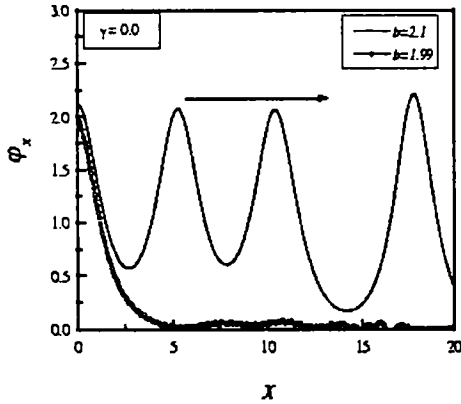


Fig. 6.1 Fluxon penetration into the quarter annular junction at zero dc bias. Fluxons enter from the left end. Static solution (circles) and dynamic solution (line) in a junction of length $l=10$ with parameters $\alpha=0.05$, $\gamma=0.0$ and $z=0.5$.

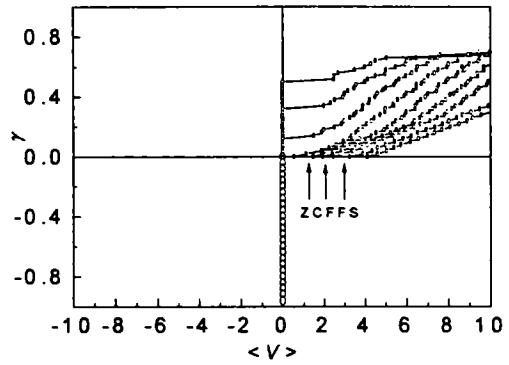


Fig. 6.2 IVC of the quarter annular LJJ showing ZCFFS. The parameters are $l=10$, $\alpha=0.1$ and $z=0.5$. Applied field increases from top to the bottom curve from 1.0 to 5.0 in steps of 1.0

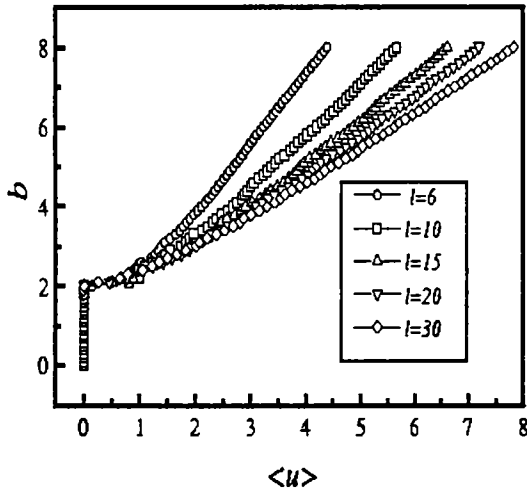


Fig. 6.3a Magnetic field b vs. average velocity for different length junctions. The parameters are $\alpha=0.1$ and $z=0.5$.

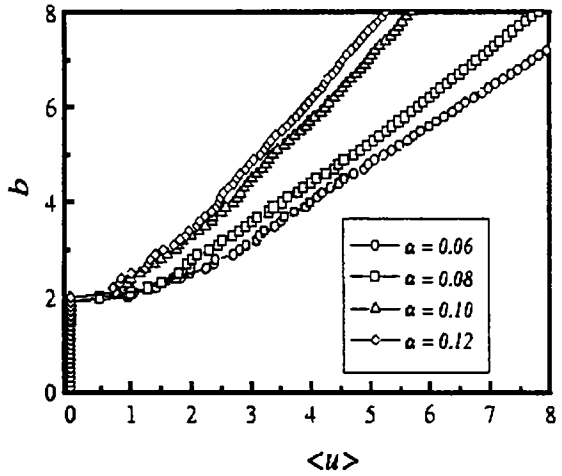


Fig. 6.3b Magnetic field b vs. average velocity for different dissipation parameters. The parameters are $l=10$ and $z=0.5$.

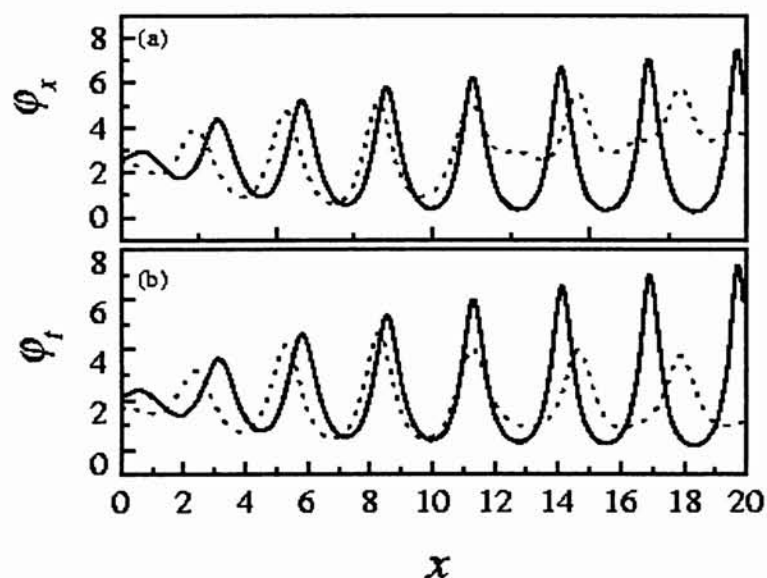


Fig.6.4 (a) Spatial profiles of the fluxons (ϕ_x) showing coherent flow of fluxons in quarter annular junctions (solid lines). The dotted lines shows flux-flow in a rectangular junction. (b) Voltage pulse forms (ϕ_t) along the junction showing coherent flux-flow in quarter annular junction (solid line) and in rectangular junction (dotted line). The parameters are $l=20$, $\alpha=0.05$, $\gamma=0.3$, $b=2.5$ and $z=0.5$.

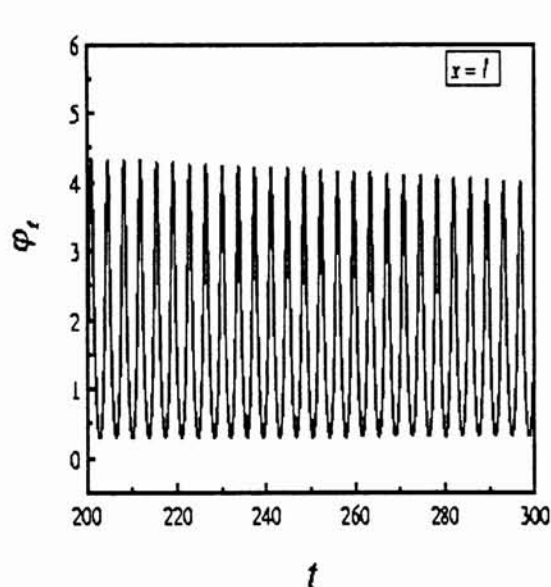


Fig.6.5 Voltage pulse forms at the load as a function of time t . Parameters are $l=30$, $\alpha=0.1$, $\gamma=0.3$, $b=2.5$ and $z=1.0$.

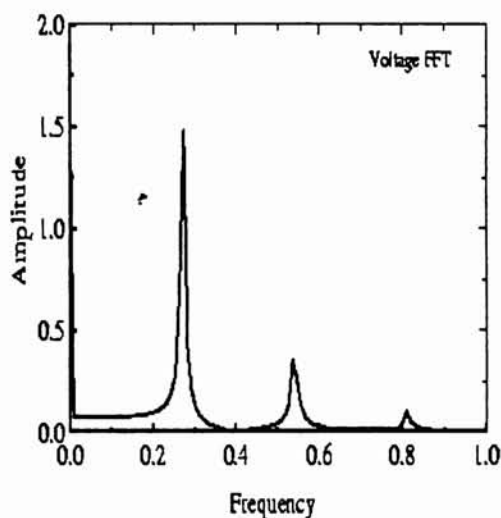


Fig. 6.5a Fourier transform of the voltage pulse form shown in Fig.6.5

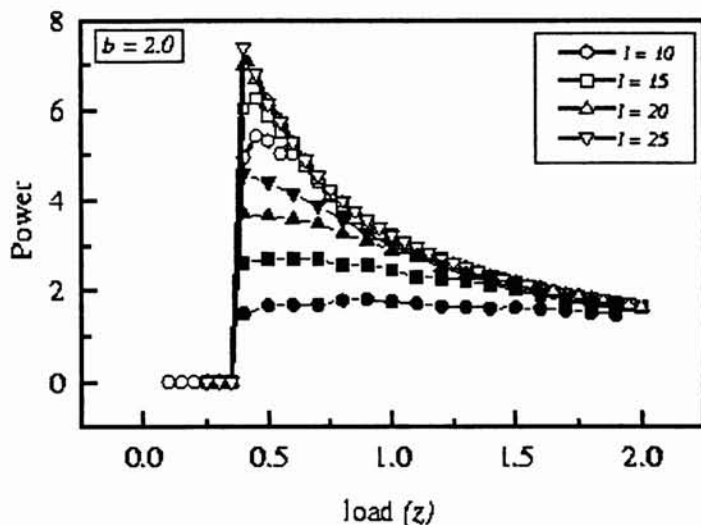


Fig.6.6 Power vs. load for different length junctions of quarter annular geometry (open symbols) and in rectangular geometry (solid symbols). Parameters are $l=10, \alpha=0.1, \gamma=0.3$ and $b=2.5$

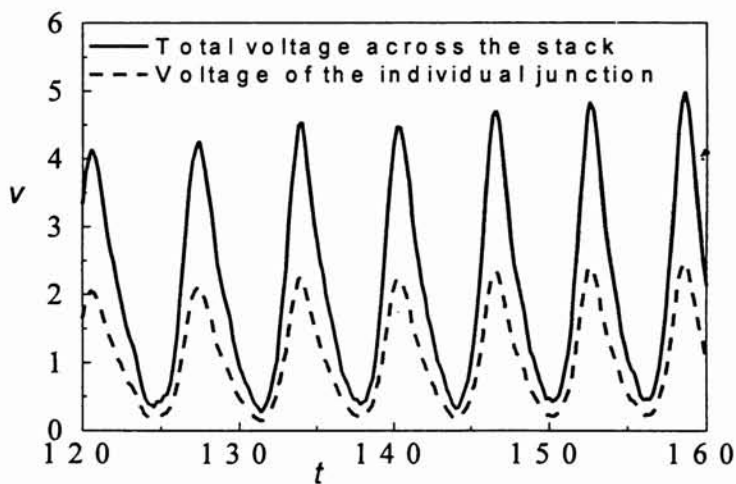


Fig.6.7 Output voltage across the two junctions showing sum of the individual voltages.

Chapter 7

Magnetic field sensors using exponentially tapered quarter annular Josephson junctions

A novel fluxon based magnetic field sensor is proposed using an exponentially tapered quarter annular Josephson junction geometry. Theoretical studies shows that quarter annular geometry provides asymmetric boundary conditions in a parallel magnetic field and exponentially tapered width of the dielectric barrier provides a geometrical driving force for the fluxons facilitating unidirectional flow of fluxons from one end to the other end in the junction when a magnetic field parallel to the dielectric barrier is applied to the junction. The proposed device acts as a field to voltage transducer and does not require electric power for its operation.

7.1 Introduction

Josephson junctions are best transducers which can convert magnetic energy into electrical energy. They are widely used in SQUID magnetometers[121], SIS mixers[122] and in voltage standard applications[123]. SQUIDs are used for an extremely sensitive measurement of the magnetic fields. They can detect even the magnetic fields of the biological cells. In many applications, the extraordinary

sensitivity of the SQUID based sensors are not required. For such applications, we can make use of some simple LJJ devices to fabricate sensors with less sensitiveness than SQUID sensors but exhibiting better performance compared to other commercially available magnetic field sensors.

Detection of both static and *rf* magnetic field signals for nondestructive testing and evaluation needs a wide range of different sensor types depending on spatial resolution and field sensitivity. In this chapter, an exponentially tapered quarter annular LJJ terminated with a load resistor at one end is studied and demonstrates that the device can be effectively used as a magnetic field to voltage transducer. Quarter annular geometry provides non-uniform boundary conditions to a parallel magnetic field. Exponential tapering in LJJ was introduced in Ref.[105, 106] as a means to produce coherent unidirectional flow of fluxons in a flux-flow oscillator. Exponential tapering provides a geometrical force for the fluxons and avoids the presence of trapped fluxons and gives perfect impedance matching to an external load. The load resistor connected at one end of the junction can be used to terminate the fluxon chain moving in the junction. This is a unique device in which fluxons enter the junction from one end and move unidirectionally to the other end of the junction under the influence of the geometrical driving force and also due to the fluxon-fluxon repulsive interaction.

7.2 Theoretical model

A LJJ with a quarter annular geometry is considered with an external magnetic field applied parallel to the dielectric barrier of uniform thickness. A sketch of the quarter annular geometry is shown in Fig.7.1a. The width of the junction is exponentially tapered (*i.e.*, $w(x) = w_0 e^{-\lambda x}$), decreasing towards the load as represented schematically in Fig.7.1(b). The external field is applied in such a way that it is directed radially at the left end ($x = 0$) of the junction. The magnetic flux linked with the junction can be expressed as $d\varphi(x) = \varepsilon (\vec{H} \cdot \vec{n}) =$

$\varepsilon H \cos(kx) dx$ [90, 91, 112] The effects of an applied magnetic field is to induce currents in closed form across the junction. The induced current in the junction due to the applied field is $\frac{d\varphi(x)}{dx} = \varepsilon H \cos(kx)$. This current term gives a net positive value over the length of the junction and therefore cannot circulate in closed form across the junction. This means that the external field cannot have any influence in the interior part of the junction. Thus an exponentially tapered quarter annular LJJ under a static magnetic field is modelled with the general perturbed sG partial differential equation[105, 12]

$$\varphi_{tt} - \varphi_{xx} + \sin \varphi = -\alpha\varphi_t - \lambda\varphi_x \quad (7.1)$$

Where λ is the tapering factor. The boundary conditions of the junction in an external field with a passive load of impedance z (representing a connection to a microwave circuit) connected at $x = l$ (right-end of the junction) are

$$\varphi_x(0, t) = \varepsilon H = b; \quad \varphi_x(l, t) = -\frac{\varphi_t}{z} \quad (7.2)$$

These boundary conditions are consistent with the fact that the effective field linked with the junction has asymmetric boundary conditions. Due to this boundary conditions, flux penetration is possible only from the left-end of the junction. The penetrated fluxons are pushed towards right-end due to the geometrical driving force. The fluxon-fluxon repulsive interaction maintain constant distance between the fluxons. The transit of the fluxons from the left-end to the right-end in the junction produce periodic voltage pulses in the load which can be averaged over a time. The passive load (z) connected at the right-end absorbs the fluxon chain in the junction.

In nonuniform junctions, a static field can produce a preferential direction for the flux-flow even in the absence of an external dc bias. This effect gives rise to ZCFFS in the current voltage characteristics of the junction [87, 49]. ZCFFS is a manifestation of flux-flow in the absence of a dc current. Thus, in nonuniform

junctions or junctions with asymmetric boundary conditions, it is possible to extract work from a constant magnetic field.

Eq. (7.1) with boundary conditions, Eq. (7.2), represents an exponentially tapered quarter annular LJJ in a static magnetic field. Eqs. (7.1) and (7.2) are mathematically equivalent to Eqs. (11), (12) and (13) in Ref.[105] and therefore all the results obtained in that work is applicable to the present model. In Ref.[105], a coherent unidirectional flow of fluxons was achieved by feeding a *dc* bias from one end of a rectangular junction. In the present work, the same phenomenon is achieved by considering an exponentially tapered quarter annular junction and applying a magnetic field parallel to the dielectric barrier.

In the case of exponentially tapered junctions, impedance can be exactly matched. From Eq. (7.1), we can see that any travelling wave (*i.e.*, $\phi(x, t) = f(x - ut)$), has a solution with the velocity $u = \lambda/\alpha$. The condition for impedance matching can be obtained by equating this limiting velocity to $-\varphi_t/\varphi_x$. Therefore the impedance matching load can be calculated as $z = \lambda/\alpha$.

In the case, $0 < \lambda \leq 1$, the maximum value of b , for a static solution to exist is $b_c = 2 - 2\lambda$ (*cf.* Sec. 6.2.1). This expression shows that exponential tapering decreases critical magnetic field value.

To determine the dynamical properties of the device, we introduce simple analytical models describing a smooth phase flow of the fluxons through the junction which is referred as laminar flow[106]. We approximate the laminar flow by taking the variational approach and consider the high voltage limit in which small changes in the instantaneous voltage due to the changes in the parameters x and t are neglected to a first approximation. The variational analysis is made on the basis of conservation of energy by the sG Hamiltonian. The energy of the unperturbed sG system is given by Eq. (1.37). Perturbational parameters modulate the velocity of the solitons and may cause to dissipate energy. The rate of dissipation is calculated by computing

$$\frac{d}{dt}(H) = [\varphi_x \varphi_t]_0^l - \int_0^l [\alpha \varphi_t^2 + \lambda \varphi_x \varphi_t] dx \quad (7.3)$$

where the first term on the right side account for the boundary conditions. From Eq. (1.38), we get $\varphi_t = -u \varphi_x$. Inserting Eq. (1.38) in Eq. (7.4) and following perturbative analysis[105, 106], we get

$$\frac{du}{dt} = (1 - u^2)(\lambda - \alpha u) \quad (7.4)$$

This equation shows that for $\lambda > \alpha$, fluxon will always be accelerated towards the limiting value $u = 1$. When $\lambda < \alpha$, the fixed point $u = \lambda/\alpha$ is linearly stable. Assuming a linear flow of the fluxons, we get the average voltage across the load as[105]

$$V = -\frac{(2 + \lambda l)zb}{2 + 2\alpha lz - \lambda l} \quad (7.5)$$

and the travelling wave speed of the fluxon as

$$u = \frac{(1 + \lambda l/2)z}{(\lambda - \alpha z) + 1 + \alpha lz - \lambda l/2} \quad (7.6)$$

7.3 Static field detection properties

The influences of an external static magnetic field on the dynamical properties of an exponentially tapered junction is studied and seen that at low magnetic fields, the static solution in the junction has only a half-fluxon content. This static solution exists up to a critical value of the magnetic field b_c , above this value, static solution becomes unstable and gives rise to a train of fluxons moving in the junction. In Fig.7.2, static distribution of the flux profile (φ_x) in the junction at $b = 1.9$ (solid line) and dynamic distribution of the fluxons at $b = 2.0$ (circles) are presented. This figure illustrates the process of fluxon penetration into the junction at higher magnetic fields. The data were obtained by numerical solution of Eqs. (7.1) and (7.2) which automatically takes into account the fluxon interaction with the edges and with each other. The unidirectional flow of fluxons

produces an average voltage across the junction. The magnetic field (b) versus average voltage ($\langle u \rangle$) is presented in Fig.7.3. For generality, different tapering factors are considered. It is found that as the tapering factor increases, the critical field required for flux penetration decreases. Average voltage is zero below the critical value b_c and linearly increases with the applied field above the critical value. These graphs demonstrates that in exponentially tapered quarter annular junctions, due to the geometrical driving force and due to the asymmetrically linked magnetic field, unidirectional flux-flow takes place even in the absence of a dc bias. This peculiar property of the exponentially tapered quarter annular junctions make them superior in the design of the magnetic field sensors.

7.4 rf field detection

To determine the rf field detection capabilities of the device, we have considered a harmonically varying rf field parallel to the dielectric barrier of the junction. Theoretical model suggests that the corresponding boundary conditions of the junction become:

$$\varphi_x(0, t) = \varepsilon H \sin(\omega t) = b \sin(\omega t) ; \quad \varphi_x(l, t) = -\frac{\varphi_t}{z} \quad (7.7)$$

These boundary conditions show that the flux linked with the junction at every alternate half cycles of the field changes in sign. Thus in the first half cycle of the field, fluxons enter the junction while in the second half cycle antfluxons enter the junction. Thus this device support fluxon and antfluxon propagation in the same direction one after another. In Fig.7.4, we plot the spatial profiles (φ_x) of the fluxons and antfluxons moving in the same direction along the junction. Fluxons on reaching the load produce positive voltage pulses while antfluxons produce negative voltage pulses. Thus the rf field produces an alternating voltage across the load. The amplitude of the induced ac voltage will be proportional to the rf field intensity.

7.5 Conclusions

The proposed device is very simple to fabricate and can be operated as a static device as this device does not require electric power for its operation. Absence of an electric bias current minimizes the heating effect and decreases the degradation of the device and therefore make them suitable in space applications. The device gives output voltage which is linearly proportional to the applied field. Both static and time varying magnetic fields can be detected using this device. One limitation of the device is that it can detect only fields of strength higher than the first critical field of the LJJ and that is parallel to the dielectric barrier. Junctions of large λ_J will give lower critical field and therefore can be preferred in making the device. As it can be seen from Eq. (7.6), low dissipative junctions give higher voltages and are suitable for making the sensor. The transit time of the fluxons can be reduced using shorter junctions and therefore the delay in the detection can be minimized. A static magnetic field produces a proportional *dc* voltage across the load and a *rf* field produces a proportional alternating voltage across the load. Using vertically stacked junctions output voltage can be increased. Instead of the exponential tapering, a properly chosen *dc* bias can be used to drive the fluxons. This device is extremely useful in detecting comparatively higher fields with less precision. Experimental realization of the device will create potential market in the superconducting electronic industry.



Fig.7.1a A sketch of the quarter annular LJJ geometry with the applied field parallel to the dielectric barrier.

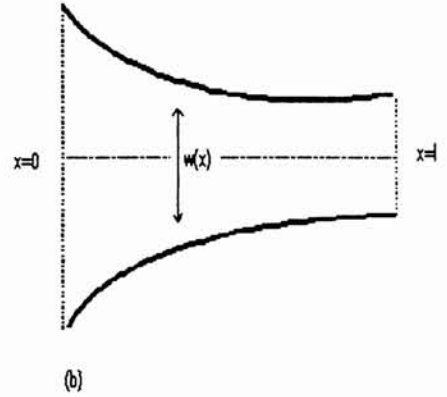


Fig.7.1b Schematic representation of the top view of the exponentially tapered width of the junction.

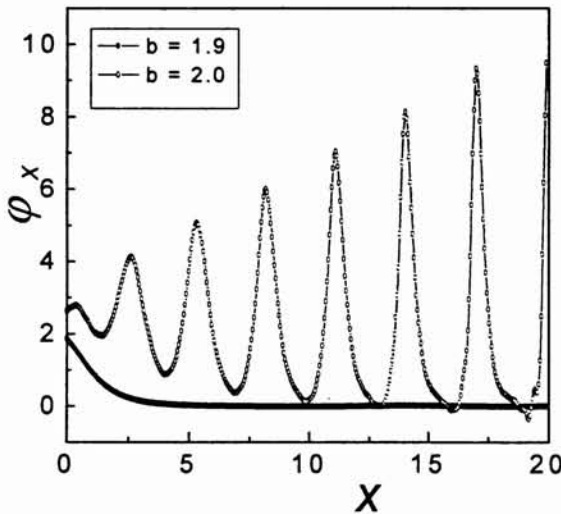


Fig.7.2 Fluxon penetration into an exponentially tapered quarter annular junction at a constant magnetic field. Static solution (solid circles) and dynamic solution (open circles) in a junction of length $l=20$ with parameters $z=1.0$, $\alpha=0.1$ and $\lambda=0.02$.

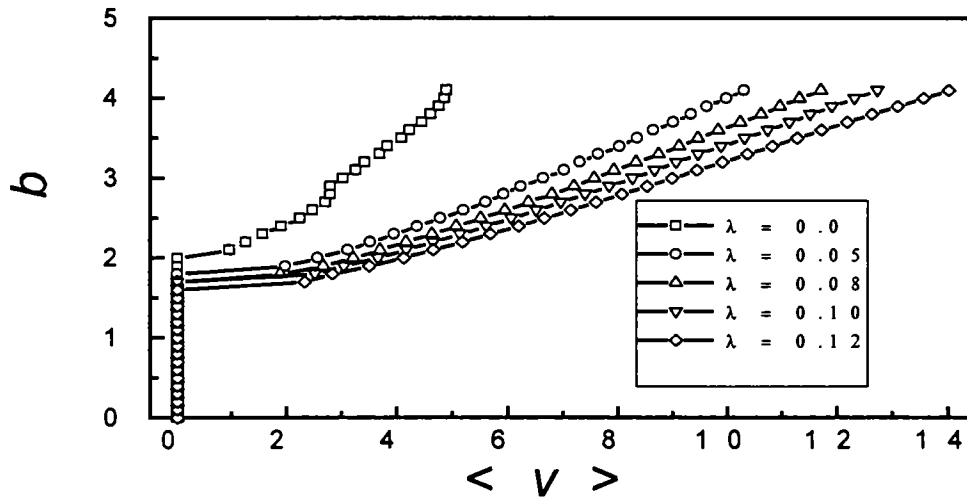


Fig.7.3 Applied static magnetic field b versus the average normalized velocity $\langle u \rangle$ computed at different tapering factors. The parameters of the junctions are $l=20$, $\alpha=1.0$ and $z=0.05$.

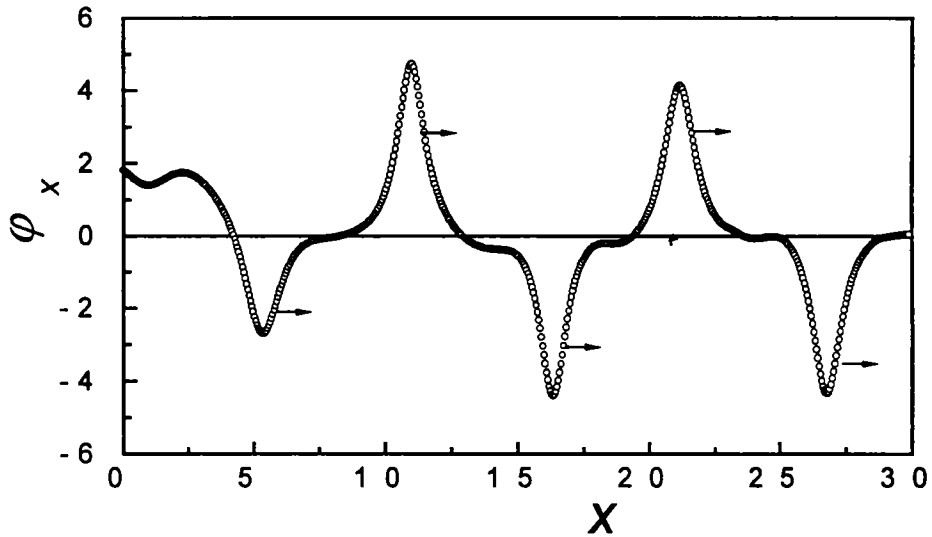


Fig. 7.4 The spatial profiles along the junction showing fluxons and antfluxons moving in the same direction towards the load when an rf field is applied to the junction. The parameters are $l=30$, $z=1.0$, $\alpha=0.05$, $b=2.0$, $\omega=0.5$ and $\lambda=0.05$.

Chapter 8

Results and conclusions

The static and dynamic properties of various one-dimensional single and coupled superconducting junctions are studied by making use of the fundamental properties of flux-quantization and the associated nonlinear supercurrent in these junctions. It is found that the stable dynamics exhibited by the fluxons in these junctions are extremely useful in the fabrication of various devices like logic gates, diodes, magnetic field rectifiers, flux-flow oscillators, magnetic field sensors, etc.

Coupled Josephson junctions with many layers exhibit very complex dynamics. Therefore it is important at first to understand in detail the dynamics in single and in two or three coupled junctions. In this thesis, fluxon dynamics in various LJJ geometries are modelled theoretically and studied using the perturbed sine-Gordon partial differential equation. The fluxon dynamics is artificially simulated by solving the perturbed sine-Gordon equation using finite-difference method. Some new geometries like the semiannular and quarter annular geometries are proposed to implement some novel devices. Both single and vertically stacked junctions under various internal and external conditions are studied to predict the complicated fluxon dynamical properties. It is found that coupled junctions offer an extremely rich spectrum of dynamical properties which can be advantageously employed in implementing various fluxon based devices.

In short, the thesis contains theoretical analysis of fluxon dynamics in vari-

ous LJJ geometries under various internal and external conditions. In particular studies include (1) fluxon dynamics in long linear LJJ with spatially periodic perturbation to understand the soliton creation and annihilation properties and to know the bunching properties of the fluxons (2) interaction of fluxons in two and three vertically coupled junctions to implement logic gates (3) fluxon dynamics in semiannular geometry under an external magnetic field to make fluxon based diodes for rectification of *ac* signals and harmonically oscillating magnetic fields and also to implement a novel bidirectional flux-flow oscillator with a distinct operational characteristics (4) dynamics in quarter annular junctions for construction of fluxon based diodes for rectification of *ac* signals and *rf* magnetic fields (5) fluxon dynamics in quarter annular junctions for constructing magnetic field based flux-flow oscillator with superior performance compared to the conventional standard rectangular flux-flow oscillator and in two vertically coupled junctions to get increased output power (6) theoretical analysis of an exponentially tapered quarter annular LJJ to determine the feasibility of making fluxon based magnetic field sensors for detecting high intensity fields with extreme precision.

In this thesis, Josephson junctions of three types of geometries, *viz*, rectangular, semiannular and quarter annular geometries in single and in coupled format are studied to implement various fluxon based devices. Rectangular geometries are considered for studying fluxon creation and annihilation phenomena and to construct logic gates of two different geometrical structures. Semiannular and quarter annular geometries are considered with an embedded parallel magnetic field applied to the system. The major difference between fluxon dynamics in semiannular junctions and in quarter annular junctions is in the fact that in semiannular junctions, the external magnetic field has influence both in the interior as well as on both boundaries of the junction while in quarter annular junctions, the external field has influence only at one boundary of the junction.

Thus in quarter annular junctions, external field produces asymmetric boundary conditions which helps fluxon penetration from one end of the junction even in the absence of a bias current. There is a preferential direction for fluxon motion in quarter annular junction that makes the performance of quarter annular junction better than that of the semiannular junction.

Studies presented in this thesis reveal that multistacked junctions are extremely useful in the fabrication of various superconducting electronic devices. The stability of the dynamical mode and therefore the operational stability of the proposed devices depends on parameters such as coupling strength, external magnetic fields, damping parameters etc. Stacked junctions offer a promising way to construct high- T_c superconducting electronic components. Exploring the complex dynamics of fluxons in coupled junctions is a challenging and important task for the future experimental and theoretical investigations.

Bibliography

- [1] B. D. Josephson, *Phys. Lett.* **1**, 251 (1962)
- [2] B. D. Josephson, *Rev. Mod. Phys.* **36**, 216 (1964)
- [3] A. Barone and G. Paternó, *Physics and applications of the Josephson effect* (Wiley, New York, 1982)
- [4] C. P. Poole, Jr. Horacio, A. Farah and R. J. Creswick, *Superconductivity* (Academic press, USA, 1995)
- [5] I. Giaever, *Phys. Rev. Lett.* **5**, 464 (1960)
- [6] L. Solymer, *Superconductive tunneling and applications* (Chapman and Hall, London, 1972)
- [7] P. W. Anderson and J. M. Rowell, *Phys. Rev. Lett.* **10**, 230 (1963)
- [8] V. Ambegaokar and B. Baratoff, *Phys. Rev. Lett.* **10**, 486 (1963)
- [9] S. Shapiro, *Phys. Rev. Lett.* **11**, 80 (1963)
- [10] N. F. Pedersen, *Physica D* **68**, 27 (1993)
- [11] A. V. Ustinov, *Physica D* **123**, 315 (1998)
- [12] P. S. Lomdahl, O. H. Sorensen and P. L. Christiansen, *Phy. Rev. B* **25**, 5737 (1982)

- [13] A. C. Scott, F. Y. F. Chu and D.W. McLaughlin, Proc. IEEE Trans. Magn. **MAG-61**, 1443 (1973)
- [14] J. C. Swihart, J. Appl. Phys. **32**, 461 (1961)
- [15] D. W. McLaughlin and A. C. Scott, Phys. Rev. A **18**, 1652 (1978)
- [16] J. Weiss, M. Tabor and G. Carnevale, J. Math. Phys. **24**, 1522 (1983)
- [17] C. S. Gardner, J. M. Green, M. D. Kruskal and K. M. Miura, Phys. Rev. Lett. **19**, 1095 (1967)
- [18] P. D. Lax, Commun. Pure Appl. Math. **21**, 467 (1968)
- [19] V. E. Zabusky and A. B. Shabat, Sov. Phys. JETP **34**, 62 (1972)
- [20] M. J. Ablowitz, D. J. Kaup, A. C. Newell and H. Segur, Phys. Rev. Lett. **30**, 1462 (1973)
- [21] M. J. Ablowitz, D. J. Kaup, A. C. Newell and H. Segur, Stud. Appl. Math. **53**, 249 (1974)
- [22] M. J. Ablowitz, D. J. Kaup, A. C. Newell and H. Segur, Phys. Rev. Lett. **31**, 125 (1973)
- [23] G. L. Lamb, *Elements of soliton theory* (Wiely, NY, 1980)
- [24] V. E. Zakharov *et al.*, *Theory of soliton* (Consultant bureau, NY, 1980)
- [25] M. J. Ablowitz and H. Segur, *Soliton and inverse scattering transform* (SIAM, NY, 1981)
- [26] J. Wiess, J. Math. Phys. **24**, 1405 (1983)
- [27] R. Hirota, J. Phys. Soc. Jpn. **35**, 1566 (1973)
- [28] J. Rubinstein, J. Math. Phys. **11**, 258 (1970)

- [29] J. Weiss, *J. Math. Phys.* **25**, 2226 (1984)
- [30] A. Davidson, B. Dueholm, B. Kryger and N. F. Pedersen, *Phys. Rev. Lett.* **55**, 2059 (1985)
- [31] S. L. Miller, K. R. Biagi, J. R. Clem and D. K. Finnemore, *Phys. Rev. B* **31**, 2684 (1985)
- [32] Yu. S. Kivshar and B. A. Malomed, *Rev. Mod. Phys.* **61**, 763 (1989)
- [33] P. Barbara, A. B. Cawthorne, S. V. Shitov and C. J. Lobb, *Phys. Rev. Lett.* **82**, 1963 (1999)
- [34] T. Yamashita, *Physica C* **362**, 58 (2001)
- [35] A. V. Ustinov, H. Kohlstedt *et al.*, *Phys. Rev. B* **48**, 10614 (1993)
- [36] S. Sakai, A. V. Ustinov, *et al.*, *Phys. Rev. B* **50**, 12905 (1994)
- [37] S. Sakai, A. V. Ustinov, N. Thyssen and H. Kohlstedt, *Phys. Rev. B* **58**, 5777 (1998)
- [38] S. Sakai and Y. Yamamori, *Physica C* **362**, 1 (2001)
- [39] V. M. Krasnov and D. Winkler, *Phys. Rev. B* **56**, 9106 (1997)
- [40] S. Sakai, N. F. Pedersen, *Phys. Rev. B* **60**, 9810 (1999)
- [41] S. Sakai, P. Bodin and N. F. Pedersen, *J. Appl. Phys.* **73**, 2411(1993)
- [42] T. A. Fulton and R. C. Dynes, *Solid State Commun.* **12**, 57 (1973)
- [43] K. Nakajima, T. Yamashita and Y. Onodera, *J. Appl. Phys.* **45**, 3141 (1974)
- [44] M. D. Fiske, *Rev. Mod. Phys.* **36**, 221 (1964)
- [45] V. P. Koshelets, S. V. Shitov, A. M. Baryshev, *et al.*, *IEEE Trans. Appl. Supercond.* **5**, 3057 (1995)

- [46] A. V. Ustinov, T. Doderer, B. Mayer, *et al.*, *Physica D* **68**, 41 (1993)
- [47] S. Keil, I. V. Vernik, *et al.*, *Phys. Rev. B* **54**, 14948 (1996)
- [48] I. V. Vernik, V. A. Oboznov and A. V. Ustinov, *Phys. Lett. A* **168**, 319 (1992)
- [49] Yu. S. Kivshar and B. A. Malomed, *Phys. Rev. B* **37**, 9325 (1988)
- [50] G. Filatrella, B. A. Malomed, R. D. Parmentier and M. Salerno, *Phys. Lett. A* **228**, 250 (1997)
- [51] B. A. Malomed, *Phys. Rev. B* **38**, 9242 (1998)
- [52] B. A. Malomed and A. V. Ustinov, *Phys. Rev. B* **41**, 254 (1990)
- [53] Yu. S. Kivshar and B. A. Malomed, *Zh. Eksp. Theor. Fiz.* **95**, 742 (1989) (*Sov. Phys. JETP*)
- [54] S. Sakai and M. R. Samuelsen, *Appl. Phys. Lett.* **50**, 1107 (1987)
- [55] T. A. Fulton, R. C. Dynes and P. W. Anderson, *Proc. IEEE* **61**, 28 (1973)
- [56] D. D. Coon and M. D. Fiske, *Phys. Rev. A* **138**, 744 (1965)
- [57] A. V. Ustinov, T. Doderer, *et al.*, *Phys. Rev. Lett.* **69**, 1815 (1992)
- [58] S. Pagano, M. P. Soerensen, P. L. Christiansen and R. D. Parmentier, *Phys. Rev. B* **38**, 4677 (1988)
- [59] B. A. Malomed, *Phys. Rev. B* **47**, 1111 (1993)
- [60] M. P. Soerensen, B. A. Malomed, A. V. Ustinov and N. F. Pedersen, *Physica D* **68**, 38 (1993)
- [61] N. Grønbech-Jensen, D. Cai, *et al.*, *Phys. Rev. B* **48**, 16160 (1993)

- [62] N. Grønbech-Jensen, D. Cai, *et al.*, Phys. Rev. B **50**, 6352 (1994)
- [63] A. V. Ustinov, B. A. Malomed and S. Sakai, Phys. Rev. B **57**, 11691 (1998)
- [64] W. F. Ames, *Numerical Methods for Partial Differential Equations* (Academic, NY, 1977)
- [65] A. A. Golubov and A. V. Ustinov, IEEE Trans. Magn. **MAG-23**, 781 (1987)
- [66] W. E. Lawrence and S. Doniach, Proc. Twelfth Int. Conf. on Low Temp. Physics, ed. E. Kanda (Academic Press of Japan, Kyoto, 1971)
- [67] S. Trillo, S. Wabnitz *et al.*, Opt. Lett **13**, 672 (1988)
- [68] M. H. Jakubowski, K. Steiglitz and R. Squier, Phys. Rev. E **56** 7267 (1997)
- [69] D. B. Mortimore and J. W. Arkwright, Appl. Opt. **30**, 650 (1991)
- [70] G. Cancellieri, F. Chiaraluce, E. Gambi and P. Pierleoni, J. Opt. Soc. Am. B **12**, 1300 (1995)
- [71] M. Sakai, A. Odagawa, H. Adachi and K. Setsune, Physica C **299**, 31 (1998)
- [72] M. Albrecht and W. Kessel, *Superconducting Quantum Electronics*, ed. Volkmar Kose (Springer Verlag 1989)
- [73] P. Barbara, A. V. Ustinov and G. Costabile, Phys. Lett. A **191**, 443 (1994)
- [74] S. A. Hattel, A. Grunnet-Jepsen and M. R. Samuelsen, Phys. Lett. A **221**, 115 (1996)
- [75] P. Gueret, IEEE Trans. Magn. **MAG-11**, 751 (1975)
- [76] K. Nakajima, Y. Onodera and Y. Ogawa, J. Appl. Phys. **47**, 1620 (1976)
- [77] Y. Nakamura, Y. A. Pashkin and J. S. Tsai, Nature **398**, 786 (1999)

- [78] P. D. Shaju and V. C. Kuriakose, *Mod. Phys. Lett. B* **12** 1217 (1998)
- [79] N. Grønbech-Jensen, O. H. Olson and M. R. Samuelsen, *Phys. Lett. A* **179**, 27 (1993)
- [80] A. C. Scott and A. Petraglia, *Phys. Lett. A* **211**, 161 (1996)
- [81] N. Grønbech-Jensen, M. R. Samuelsen, P. S. Lomdahl and J. A. Blackburn, *Phys. Rev. B* **42**, 3976 (1990)
- [82] M. B. Mineev, G. S. Mkrtchyan and V. V. Schmidt, *J. Low. Temp. Phys.* **45**, 497 (1981)
- [83] P. D. Shaju and V. C. Kuriakose, *Physica C* **322**, 163 (1999)
- [84] P. D. Shaju and V. C. Kuriakose, *Phys. Lett. A* **267**, 420 (2000)
- [85] J. H. Thompson, M. A. Ketkar, J. B. Beyer and J. E. Nordman, *IEEE Trans. Appl. Supercond.* **3**, 2543 (1993)
- [86] S. A. Vasenko, K. K. Likharev and V. K. Semenov, *Zh. Eksp. Theor. Phys.* **4**, 1444 (1981)
- [87] V. M. Krasnov, V. A. Oboznov and N. F. Pedersen, *Phys. Rev. B* **55**, 14486 (1997)
- [88] E. Goldobin, A. Wallraff, N. Thyssen and A. V. Ustinov, *Phys. Rev. B* **57**, 130 (1998)
- [89] E. Goldobin, A. Sterck and D. Koelle, *Phys. Rev. E* **63**, 031111 (2001)
- [90] N. Grønbech-Jensen, P. S. Lomdahl and M. R. Samuelsen, *Phys. Lett. A* **154**, 14 (1991)
- [91] A. V. Ustinov and B. A. Malomed, *Phys. Rev. B* **64**, 020302 (2001)

- [92] A. V. Ustinov , B. A. Malomed and N. Thyssen, Phys. Lett. A **233**, 239 (1997)
- [93] N. F. Pedersen and A. Davidson, Phys. Rev. B **41**, 178 (1990)
- [94] C. S. Owen and D. J. Scalapino, Phys. Rev. **164**, 538 (1967)
- [95] G. Carapella and G. Costabile, Phys. Rev. Lett. **87**, 077002 (2001)
- [96] G. Carapella, Phys. Rev. B **63**, 054515 (2001)
- [97] K. K. Likharev and V. K. Semenov, IEEE Trans. Appl. Supercond. **1**, 3 (1991)
- [98] C. S. Lee, B. Janko, I. Derenyi and A. L. Barabasi, Nature, **400**, 337 (1999)
- [99] J. F. Wambaugh, C. Reichhardt, C. J. Olson, F. Marchesoni and F. Nori, Phys. Rev. Lett. **83**, 5106 (1999)
- [100] I. Zapata, R. Bartussek, F. Sols and P. Hänggi, Phys. Rev. Lett. **77**, 2292 (1996)
- [101] S. Weiss, D. Koelle, J. Muller, R. Gross and K. Barthel, Europhys. Lett. **51**, 499 (2000)
- [102] E. Trias, J. J. Mazo, F. Falo and T. P. Orlando, Phys. Rev. E **61**, 2257 (2000)
- [103] T. Nagatsuma, K. Enpuku, F. Irie and K. Yoshida, J. Appl. Phys. **63**, 1130 (1983)
- [104] A. V. Ustinov and S. Sakai, Appl. Phys. Lett. **73**, 686 (1998)
- [105] A. Benabdallah, J. G. Caputo and A. C. Scott, Phys. Rev B **54**, 16139 (1996)

- [106] A. Benabdallah, J. G. Caputo and A. C. Scott, *J. Appl. Phys.* **88**, 3527 (2000)
- [107] A. Wallaraf, G. Goldobin and A. V. Ustinov, *J. Appl. Phys.* **80**, 6523 (1996)
- [108] Y. Makhlin, G. Schön and A. Shnirman, *Rev. Mod. Phys.* **73**, 357 (2001)
- [109] *Nonlinear Superconducting Devices and High-Tc Materials*, edited by R. D. Parmentier and N. F. Pedersen (World Scientific, Singapore,1995)
- [110] A. V. Ustinov, H. Kohlstedt and P. Henne, *Phys. Rev. Lett.* **77**, 3617 (1996)
- [111] M. Salerno, M. R. Samuelsen, G. Filatrella, S. Pagano and R. D. Parmentier, *Phys. Lett. A* **137**, 75 (1989)
- [112] M. Salerno, M. R. Samuelsen, G. Filatrella, S. Pagano and R. D. Parmentier, *Phys. Rev. B* **41**, 6641 (1990)
- [113] P. D. Shaju and V. C. Kuriakose, *Phys. Rev. B* **65**, 214508 (2002)
- [114] M. J. Stephen, *Phys. Rev. Lett.* **21**, 1629 (1968)
- [115] V. P. Koshelets, S. V. Shitov, A. V. Shchukin, L. V. Flippenko and J. Mygind, *Appl. Phys. Lett.* **69**, 699 (1996)
- [116] V. P. Koshelets, S. V. Shitov, L. V. Flippenko, *et al.*, *Rev. Sci. Instr.* **71**, 289 (2000)
- [117] P. M. Marcus and Y. Imry, *Solid State Communi.* **33**, 345 (1980)
- [118] B. A. Malomed and A. A. Nepomnyashchy, *Phys. Rev. B* **45**, 12435 (1992)
- [119] A. Petraglia, A. V. Ustinov, N. F. Pedersen and S. Sakai, *J. Appl. Phys.* **77**, 1171 (1995)
- [120] E. Goldobin, B. A. Malomed and A. V. Ustinov, *Phys. Rev. B* **62**,1414 (2000)

- [121] J. Clarke, *The New Superconducting Electronics*, ed. H. Weinstock and R. W. Ralston (Kluwer, Dordrecht, 1993)
- [122] J. R. Tucker and M. J. Feldman, *Rev. Mod. Phys.* **57**, 1055 (1985)
- [123] M. T. Levinsen, R. Y. Chiao, M. J. Feldman and B. A. Tucker, *Appl. Phys. Lett.* **31**, 776 (1977)
- [124] W. H. Press, S. A. Teukolsky, W. T. Vetterling and B. P. Flannery, *Numerical recipes in C* (Cambridge University press, UK) 1992

G 8514